GENETIC MECHANISM OF SKELETAL MYOGENESIS

by

RENJIE SHANG

(Under the Direction of PENGPENG BI)

ABSTRACT

This research investigates the genetic aspects of skeletal myogenesis in *Mus musculus*, intending to broaden our comprehension of the matter. Skeletal muscle, a major tissue type in mammals, relies heavily on muscle stem cells for efficient regeneration and homeostasis. Commonly referred to as satellite cells, these stem cells are located between the basal lamina and myofibers' plasma membrane in adult muscle tissue, reminiscent of a satellite's positioning. They typically remain quiescent in healthy tissues but can quickly activate in response to injury, proceeding through cell cycles, proliferating, and differentiating. A subset returns to a quiescent state, reserving themselves for future tissue regeneration.

Maintenance of the stem cell pool under aging or disease conditions necessitates strict regulation of these cells' stemness. In-depth study of in vivo molecular mechanisms of muscle development and regeneration involves specific gene deletion from muscle stem cells. A powerful tool for this is the Cre/loxP system, facilitating precise, controlled gene deletion. Despite its robustness, creating each conditional knockout model requires substantial effort and faces technical challenges.

We propose an alternative approach using a unique CRISPR donor design combined with the *i*-GONAD technique. Demonstrating its potential and simplicity, we created floxed alleles for

five genes (*Fosl1, Plagl1, Ak040954, Clcf1,* and *Gm44386*) in a single attempt with reduced costs and minimal equipment. Alongside the conditional alleles, we also obtained constitutive knockout alleles.

Fosl1 is of particular interest, an AP-1 family member, with enriched mRNA in fresh-isolated SCs. Other AP-1 family members like *Fos*, *ATF3*, and *Fosl2* have been revealed to play vital roles in muscle regeneration. *Fosl1*'s function in muscle development and regeneration is, however, yet to be understood. Thus, we chose to study *Fosl1* and created a specific *Fosl1* gene deletion mouse model, Fosl1-cKO. After tamoxifen treatment and regeneration assay, we found that Fosl1 loss in muscle satellite cells significantly disrupted muscle regeneration. Furthermore, we found its induction rapidly when satellite cells are activated by injury or dissociations. Interestingly, loss or over-expression of Fosl1 doesn't influence human myoblast proliferation, differentiation, or fusion. However, RNA-seq analysis showed significant downregulations of muscle stem cell markers and myogenic differentiation markers in the Fosl1-cKO group. This study thus reveals Fosl1's critical role in muscle stem cell activation and tissue regeneration.

INDEX WORDS: CRISPR/Cas9, Mus. musculus, genome editing, conditional knockout, Cre-loxP, Fosl1, Fos family, AP-1 family, muscle satellite cell, activation, proliferation, muscle regeneration

GENETIC MECHANISM OF SKELETAL MYOGENESIS

by

RENJIE SHANG

B.Sc., Ocean University of China, 2018

A Dissertation Submitted to the Graduate Faculty of The University of Georgia in Partial Fulfillment of the Requirements for the Degree

DOCTOR OF PHILOSOPHY

ATHENS, GEORGIA

2023

GENETIC MECHANISM OF SKELETAL MYOGENESIS

by

RENJIE SHANG

Major Professor:	Pengpeng Bi
Committee:	Jonathan Eggenschwiler
	Kaixiong Ye
	Yao Yao

Electronic Version Approved:

Ron Walcott
Vice Provost for Graduate Education and Dean of the Graduate School
The University of Georgia
August 2023

DEDICATION

I dedicate this work to all the mice who contributed to this quest for knowledge.

ACKNOWLEDGEMENTS

This thesis holds great significance as it was completed during a truly exceptional period in my life. Firstly, I want to express my deepest gratitude to my soulmate and unwavering supporter, MSc. Jianli Zhang. Throughout our five-year journey in the United States, Jianli has been my pillar of strength, both physically and emotionally. We first crossed paths in 2015 at Ocean University of China, where we obtained our bachelor's degrees, and our love for each other has only grown stronger over the past seven years. The moment I discovered that Jianli had also received a PhD offer from the College of Engineering at UGA, I felt an overwhelming sense of excitement. Since 2019, we have embarked on a new chapter of our lives in Athens, Georgia, standing by each other's side as cherished partners. Without her unwavering support, dedication, and companionship, I doubt I would have made it to this very moment of writing these words. It is with a tinge of regret that I acknowledge not having proposed to her before, but I am resolved to rectify this delay without further hesitation.

Secondly, I want to express my heartfelt appreciation to my family. Since my arrival in the United States in 2019, circumstances, such as my research commitments and the pandemic, have prevented me from returning home. Our family is not rich, with a modest barbershop being our sole asset—a place where I learned to read and write, and where I spent my formative years. Despite neither of my parents having attended college, their circumstances did not hinder my path to becoming a PhD candidate. I am particularly grateful to my mother, who instilled in me the importance of being a decent person long before I learned how to navigate the world. My father, as the sole laborer in the barbershop, tirelessly worked from 9 AM to 9 PM, making three

decades feel like mere moments, all to support our family. As the most educated individual in our neighborhood, I am proud to have made them proud, but I am equally proud of them for shielding me from hunger and fostering a peaceful and harmonious family environment. No matter how far or for how long their son has traveled, rest assured that he will eventually return home, with heartfelt apologies and gratitude.

Thirdly, I wish to extend my gratitude to the Bi Lab, which has provided invaluable support and nurtured my growth as a scientist. I am deeply thankful to my major advisor, Dr. Pengpeng Bi, who recruited me from my college in China to join the Bi Lab. Starting as a post-bac researcher, I received comprehensive and rigorous training directly from Dr. Bi, which laid the foundation for my proficiency in experimental techniques. During my initial two years as a graduate student, he consistently encouraged me to embrace challenges outside of my comfort zone. From basic molecular cloning to animal experiments, from cell culture to bioinformatic analysis, I have remained on the right trajectory, constantly evolving into a skilled and sophisticated scientist. Beyond the essential research training, the most valuable lesson I learned from Dr. Bi is the art of conducting science with meticulous rigor, fueled by critical thinking and advanced hypothesis development. In the Bi Lab, I also want to express my gratitude to Dr. Haifeng Zhang, a postdoctoral fellow who generously imparted his cell culture expertise, provided invaluable suggestions for my experimental plans, and worked in tandem with Dr. Bi to foster an environment conducive to my future career. I am equally grateful to the current and past members of the lab, including technicians and undergraduate trainees such as Zheng Zhang, Xinran Zhu, Yanqing Cai, Yanran Zhao, Ashlynn Kim, Hannah Jean Namgoong, Aaryahi Deshmukh, Alina Baiju, Jiachen Chen, Junfei Wen, and many others, who have assisted me throughout my projects.

Lastly, I extend my heartfelt thanks to my committee members and the Department of Genetics. The seminars, classes, and committee meetings have played a pivotal role in shaping and completing my PhD work. My department has provided an exceptional research environment, and I genuinely hope to maintain connections with this remarkable family that has witnessed my growth during these unforgettable five years of my youth.

TABLE OF CONTENTS

Page

LIST OF TABLES

Page

LIST OF FIGURES

Page

CHAPTER 1

INTRODUCTION AND LITERATURE REVIEW

Cre-loxP system

Advances in genetic engineering have revolutionized biomedical research and allowed scientists to unravel the intricate complexities of biological systems. Among the various methods employed for precise genetic modifications *in vivo*, the Cre-loxP system has emerged as one of the most powerful tools. The Cre-loxP system enables controlled DNA recombination, allowing researcher to selectively manipulate specific genes in various organisms(Hubbard, 2014; Kim et al., 2018; Pan et al., 2005; Siegal & Hartl, 1996).

Cre recombinase, along with flipase (Flp) and D6 specific recombinase (Dre), belongs to the family of tyrosine site-specific recombinases (T-SSRs)(Meinke et al., 2016; Nagy, 2000). Originating from the cre (cyclization recombinase) gene of bacteriophage P1, Cre is a 38-kDa DNA recombinase(Sauer, 1998; Sternberg et al., 1978). It recognizes a specific DNA fragment sequences known as loxP (locus of x-over, P1) sites and facilitating site-specific alteration of DNA sequences situated between two loxP sites(Sauer & Henderson, 1988). The structure of the loxP site comprises a 34-bp sequence (ATAACTTCGTATAATGTATGCTATACGAAGTTAT), which includes two 13-bp inverted and palindromic repeats (ATAACTTCGTATA) along with an 8-bp core sequence (ATGTATGC)(Metzger & Feil, 1999). The orientation and position of loxP sites dictate the outcome of the recombination event. The presence of two loxP sites in the same orientation (or

strand) results in excision of the DNA segment between them, while loxP sites in opposite orientations lead to DNA inversion or translocation(Meinke et al., 2016; Nagy, 2000).

The Cre-loxP system has widespread applications in various fields of biological research. It enables precise control for gene expression, tissue-specific gene manipulation and inducible gene knockout. By utilizing tissue-specific promoters to drive Cre recombinase expression, researchers can apply genetic modifications to specific cell types or tissues, allowing the study of gene function in a spatially and temporally controlled manner(Indra et al., 1999; Kim et al., 2018; Monvoisin et al., 2006). Moreover, conditional gene knockout can be achieved by flanking target genes with loxP sites, enabling the deletion of specific genes at desired developmental stages or in specific tissues. Over the years, the Cre-loxP system has undergone several modifications to enhance its utility and specificity(Kim et al., 2018). Various strategies have been devised to achieve temporal control over Cre recombinase activity, such as the use of tamoxifen inducible CreER(T) fusion proteins or Cre variants that respond to specific stimuli(Indra et al., 1999; Meinke et al., 2016). Additionally, novel variants of the loxP sequence, such as engineered or mutant loxP sites, have been developed to enable precise recombination events with improved efficiency or altered specificity(Karimova et al., 2013; Langer et al., 2002). These advancements have expanded the capabilities of the Cre-loxP system, allowing for more sophisticated genetic manipulations.

The versatility of the Cre-loxP system has made it a great tool in model organisms, including mice, zebrafish, Drosophila, and Caenorhabditis elegans(Hubbard, 2014; Kim et al., 2018; Pan et al., 2005; Siegal & Hartl, 1996). In mice, the Cre-loxP system has revolutionized the field of mouse genetics, facilitating tissue-specific gene ablation, inducible gene expression, and cell lineage tracing(Clausen et al., 1999; Kim et al., 2018). The availability of a vast

collection of Cre driver lines has enabled researchers to investigate the function of specific genes in a tissue-specific manner. Similarly, the Cre-loxP system has been extensively employed in other model organisms, enabling precise genetic modifications for gene function studies.

Generation of floxed alleles in mice *in vivo*

The DNA sequences flanked by two loxP sites were commonly referred as floxed alleles. The utilization of floxed alleles is crucial in genetic studies for achieving precise control over gene expression *in vivo*, allowing for the temporal and spatial controls of gene deletions. Traditionally, the floxed alleles were generated by a tedious process that involves manipulations of embryonic stem (ES) cells, clonal isolation and transplantations of correctly targeted clones to the developing mouse embryos(Mansour et al., 1988; Riele et al., 1992; Thomas & Capecchi, 1987a). The large collections of floxed mice have firmly established the mouse as a fundamental model organism in research(Skarnes et al., 2011). Generating floxed alleles using ES cells involves a multi-step process: first, targeting vector is designed to contain the loxP sites flanking a specific region of gene with homology arms. It typically includes a selection marker, such as neomycin resistance element (neo), to enable positive selection of targeted ES cells. Then the targeting vector is introduced into ES cells through electroporation or other transfection methods (e.g., microinjection). Following transfection, ES cells are subjected to selection with a drug, which allows only cells containing the targeting vector to survive and form colonies. Surviving ES cell clones are genotyped to identify correct homologous recombination and integrations of the targeting vector at the desired genomic location(Hall et al., 2009). The common genotyping approaches include PCR and Southern blotting. Then correctly targeted ES cells are injected into blastocysts of recipient mice, and the resulting chimeric embryos are transferred into surrogate females. The chimeric embryos develop into mice, commonly referred as F0 generation, with a

mixture of cells derived from the injected ES cells and the recipient blastocyst. The mutants from F0 generation are then crossed with wild-type mice to allow germ line transmission of the floxed allele. The pups carrying the floxed allele from F1 generation can be identified through genotyping and authenticated by sequencing analysis.

The generation of floxed alleles using embryonic stem (ES) cells has several disadvantages. It requires specialized techniques and resources, making it time-consuming and technically challenging. The efficiency of homologous recombination in ES cells can be low, and off-target effects can arise, complicating the interpretation of results. Germline transmission and animal breeding are necessary, involving significant time and effort.

CRISPR technology has emerged as a powerful tool for genetic manipulations and the generations of engineered mouse models(Fujii et al., 2013; Harms et al., 2014; Heckl et al., 2014; Maddalo et al., 2014). For gene editing experiments that require homology directed repair (HDR), single-stranded oligodeoxynucleotides (ssODNs) appeared to be more efficient donors, compared with double stranded DNA templates(Miura et al., 2015; Richardson et al., 2016; Yoshimi et al., 2016). Thus, we decided to test the efficiency of using a pair of ssODNs, each contains a homology arm and loxP site, to simultaneously insert two loxP sites and the floxed allele. Notably, this method will presumably allow the targeting of genes where the loxP integration sites span a large region of DNA for which it is entirely impossible to generate a single-piece HDR donor. Yang et al. initially demonstrated the high success rate of floxing by microinjecting two ssODNs along with in vitro transcripts of Cas9 and two gRNAs(Yang et al., 2013). However, a subsequent large-scale study conducted across multiple centers worldwide reported inconsistent results with the original approach, achieving successful floxing in only 11 out of 56 targeted loci(Gurumurthy O'Brien, et al., 2019). These discrepancies may stem from

technical variations compared to Yang et al.'s methodology. Meanwhile, smaller-scale studies have reported the generation of multiple floxed models using microinjection of two gRNAs and two ssODNs, employing either Cas9 as IVT(Bishop et al., 2016; Hai et al., 2019; Qin et al., 2016) or protein(Nakagawa et al., 2016), as well as the electroporation of gRNA/Cas9 ribonucleoproteins (RNPs) alongside ssODNs into embryos(Chen et al., 2021).

A study of the interactions between the Cas9 protein with its DNA substrate revealed that the design of ssODN affected the exogenous DNA insertion efficiency(Richardson et al., 2016). Specifically, comparing with symmetric design, asymmetric target-strand ssODNs had higher efficiency in introducing point mutations. More recently, Sentmanat et al. employed electroporation to introduce two CRISPR RNPs and two ssODNs into single-cell embryos to generate floxed alleles. They achieved a success rate of 85% in the first round of targeting four genes and 100% rate when supplementing a second round of targeting(Sentmanat et al., 2022).

improved-Genome editing via Oviductal Nucleic Acids Delivery (*i*-GONAD)

All these previous strategies for generating loxP alleles *in vivo* require three essential steps: mating of super-ovulated females, isolation of zygotes, microinjection of genome editing cocktail into the zygotes, and transferring the microinjected zygotes into the oviducts of pseudopregnant females. These procedures require sophisticated technical expertise and expensive equipment such as micromanipulators. Due to the complexity of this protocol, animal genome engineering experiments are often challenging to conduct in individual laboratories and are typically centralized in core facilities with highly trained personnel. Recently, Ohtsuka et al. reported a simplified yet robust method known as improved-Genome editing via Oviductal Nucleic Acids Delivery (*i*-GONAD) that allows the efficient delivery of CRISPR RNPs to E0.7 (~16 hpf, hours post fertilization) mouse embryos through in situ electroporation(Ohtsuka et al.,

2018). This procedure saves the time from mouse embryo isolation, microinjection, and subsequent transfer to recipient females.

i-GONAD is a procedure performed on pregnant mouse females carrying E0.7 (1-cell stage) embryos. Briefly, one needs to surgically expose the oviducts by making an incision at a dorsolateral position. Genome editing reagents are then injected into the oviductal lumen using a glass capillary pipette. Immediately after the injection, electroporation is applied to the entire oviduct using tweezer-type electrodes. Following electroporation, the ovaries and oviducts are repositioned, and the incision is sutured. Within 3 weeks, the offspring will be genotyped to identify mutants.

By applying *i*-GONAD method for *Foxe3* gene editing, Ohtsuka et al. demonstrated that nearly all E13.5 or E17.5 embryos had indel mutations within the Foxe3 target sequence (35/36, 97%) through sequencing. In addition to generate indels, *i*-GONAD can also be used for precision gene editing mediated by HDR. For instance, Ohtsuka et al. corrected a point mutation on *Tyr* gene using a gRNA and a ssODN. The reported efficiency for this gene targeting experiment is around 47% (14/32). Ohtsuka et al. also reported that the *i*-GONAD method can be applied to generate large genomic deletions (67%) and knock-in long ssDNA(15% and 36%) in mice.

Of note, the *i*-GONAD method is developed from an earlier electroporation protocol with the following improvements to further improve the CRISPR editing efficiency(Takahashi et al., 2015a). Firstly, day 0.7 of pregnancy is determined to be the optimal time for CRISPR targeting, allowing for effective introduction of the solution into the ampulla. Secondly, Cas9 mRNA was replaced by Cas9 protein. Thirdly, synthesized gRNA composed of crRNA and tracrRNA was used in place of *in vitro* transcribed sgRNA. Fourthly, electroporation parameters were

optimized for gene targeting using embryos of various mouse strains. Fifthly, the female mice treated by the *i*-GONAD retains their full reproductive capability. Lastly, *i*-GONAD can be performed using different commercially available electroporators, which are significantly less expensive than microinjection setups and do not require specialized personnel. Overall, the *i*-GONAD method presents a cost-effective and easily accessible alternative for genome editing experiments.

Myogenesis of skeletal muscle

Skeletal muscle is one of the largest tissues for mammals, accounting for around 40% of body weight in human and contains 50–75% of all body proteins, and responsible for maintaining necessary complex life activities, such as breathing and voluntary locomotion(Frontera & Ochala, 2015). As a key metabolic organ, muscle is also responsible for 80–90% of postprandial insulin-stimulated glucose uptake(Merz & Thurmond, 2020). Thus, proper muscle function is important for human health and life quality. The basic function unit consists skeletal muscle is myofiber, which is multinucleated because of the myoblast fusion. Myofibers are composed of numerous myofibrils, arranged in regular sarcomeres, and contain contractile proteins such as myosin and actin. When muscle affiliated nerve activates, myofiber membrane will depolarize and initialize the action potential spreads rest of the local membrane. This triggers the release of calcium ions from the sarcoplasmic reticulum, which, in conjunction with ATP and troponin, facilitates the binding of myosin to actin, resulting in muscle contraction(Cretoiu et al., 2018).

Different from cardiac muscle that is derived from lateral plate mesoderm(Tirosh-Finkel et al., 2006), skeletal muscle originates from somites originated from paraxial mesoderm, which can be voluntarily controlled by somatic nervous system(Pu et al., 2015). During early stages of

embryonic development, the mesoderm is created by gastrulation lays between endoderm and ectoderm and later continuing develop to tail bud. Lying along the neural tube, the mesoderm divides into three subtypes: paraxial mesoderm, intermediate mesoderm, and lateral plate mesoderm(Tani et al., 2020). The paraxial mesoderm consists of two bilateral streaks of tissue adjacent to the notochord. Paraxial mesoderm will exit from the progenitor zone and differentiate to the posterior presomitic mesoderm, which is controlled by the Wnt and fibroblast growth factor (FGF) signaling pathways(Takada et al., 1994; Yamaguchi et al., 1994). Marker genes in presomitic mesoderm specification, such as Brachyury (*T*), *Tbx6*, and Mesogenin1 (*Msgn1*), are known downstream factors of Wnt signaling(Chalamalasetty et al., 2011; Lou et al., 2006; Turner et al., 2014; Yasuhiko et al., 2006). Followed by segmentation clock, the posterior presomitic mesoderm undergo transcriptional profile changes and enter the anterior presomitic mesoderm, with the activation of *Mesp2, Pax3, Foxc1/2* and *Meox1/2*(Goulding et al., 1991; Kume et al., 2001; Mankoo et al., 2003). Later, somites forms from anterior presomitic mesoderm and eventually differentiate to epithelial dermomyotome and a ventral sclerotome. The dermomyotome will become skeletal muscle, brown adipose tissue, and dermis of the back, while the ventral sclerotome will become the axial skeleton and tendons(Brent & Tabin, 2002). Study in the chicken revealed that in the sclerotome, *Pax3* and *Pax7* expression is reduced, but in the dermomyotome they are both maintained(Otto et al., 2006). Then muscle progenitor cells (myoblast) delaminate from the dermomyotome and have reduced expression of *Pax3* but have higher expression of Mrfs (myogenic regulatory factors), such as *Mrf5, Myf4, MyoD*, and *MyoG*(Pownall et al., 2002; Rudnicki et al., 1993). This will lead to the cell fate determination and fusion of the muscle progenitor cells, which triggers the formation of the myotome, which is a crucial step for skeletal muscle formation. Given that the myotome is already progressively

differentiated and post-mitotic that is composed of primary myocytes, however, this primary structure cannot account for the massive amount of muscle in early embryo.

Two phases of myogenesis are chronically appeared during development after the formation of early myotome: a primary or early embryonic phase (E10.5-E12.5 in mouse, E3-7 in chicken) and a secondary or later fetal phase (E14.5-17.5 in mouse, E8+ in chicken)(Biressi et al., 2007; Stockdale, 1992). The first phase results in the production of the primary myofibers, which derive from Pax3+ dermomyotomal progenitors through fusion. These primary myofibers migrate to form body wall and limb buds, and more importantly, provide the scaffolds for which mature muscles will be built. Known markers at this stage are slow MyHC and myosin light chain 1 (MyLC1, *Myl1*). During the second phase of myogenesis in mouse, Pax7+ myogenic precursors either fuse themselves or fuse to the primary myofibers formed in first phase and give rise to secondary or fetal fibers that specifically express markers such as MyLC3 (*Myl3*) and fast MyHC isoforms. During secondary myogenesis, Pax7+ progenitors contribute to the massive muscle development and later become most of the adult muscle satellite cells laying between sarcolemma and basal laminal of myofibers(Olguin & Pisconti, 2012; Rodriguez-Outeirino et al., 2021).

Regeneration of skeletal muscle

The process of skeletal muscle regeneration is highly organized and involving the activation of diverse cellular and molecular activities. Muscle satellite cells, which are specific stem cells for skeletal muscle, play a crucial role in this regenerative process. These cells originate from Pax7+ myogenic progenitors located in the dermomyotome(Kassar-Duchossoy et al., 2005; Schmidt et al., 2019). The functionality of satellite cells is regulated by signaling pathways such as Notch and Wnt, as well as the extrinsic cues from the niche where stem cells

reside(Laumonier & Menetrey, 2016; Yin et al., 2013). In general, when adult skeletal muscle is injured, the regeneration process can be chronologically divided into three phases: the inflammation phase, the phase of satellite cell activation and differentiation, and the phase of tissue formation(Charge & Rudnicki, 2004).

After muscle injury, an influx of extracellular calcium is released due to the disruption of the myofiber plasma membrane, leading to the proteolysis and degeneration of the damaged tissue. Consequently, the necrosis and degeneration of the affected myofibers trigger the infiltration of inflammatory cells(Laumonier & Menetrey, 2016). Factors released during necrosis accumulate in the injured area, attracting more inflammatory cells. Neutrophils are the first inflammatory cells recruited to the injury site, followed by the arrival of macrophages that initiate the phagocytosis of muscle debris(Dort et al., 2019). Interestingly, macrophages not only fulfill immune functions but also play a role in promoting satellite cell differentiation and tissue revascularization(Latroche et al., 2017). Recent studies have highlighted the metabolic crosstalk between macrophages and satellite cells, wherein macrophage-derived glutamine sustains the enhancement of satellite cells and muscle regeneration(Shang et al., 2020). Furthermore, the depletion of macrophages can impair the regenerative capacity of muscle tissue(Shang et al., 2020; Summan et al., 2006). In conclusion, macrophages are crucial not only for their positive involvement in inflammation but also for their contribution to muscle regeneration in the inflammation phase.

The activation and differentiation of satellite cells constitute the second phase of skeletal muscle regeneration, involving precise cellular morphological changes(Charge & Rudnicki, 2004). Quiescent satellite cells reside between the sarcolemma and basal lamina of the myofiber. They specifically express *Pax7* while lacking *MyoD* expression(Yin et al., 2013). Upon injury,

satellite cells transition from their quiescent state to the activation state and enter cell cycle, leading to the upregulation of *MyoD* and *Myf5*. In this stage, activated satellite cells initially migrate to the injury site, where they either fuse with damaged myofibers or undergo proliferation to become myogenic progenitor cells, also known as myoblasts(Schultz et al., 1985; Snow, 1977). The downregulation of *Pax3* and *Pax7*, coupled with the upregulation of *MyoG*, drives the differentiation of satellite cells into elongated myocytes. These myocytes subsequently fuse together under the control of *Myomaker* and *Myomixer* proteins, forming multinucleated myotubes that eventually mature into myofibers(Bi et al., 2017; Millay et al., 2013; Zhang et al., 2020). The newly formed myofibers exhibit small size, central-nucleation, and express developmental myosin heavy chain (devMHC). These myofibers undergo maturation, characterized by hypertrophy and the migration of nuclei towards the periphery, to become fully functional muscle fibers(Collins et al., 2005; Yablonkareuveni & Rivera, 1994).

To ensure the preservation of satellite cell populations and prevent potential loss resulting from repetitive muscle injury, the capacity for self-renewal is a vital characteristic of satellite cells, as it is for all stem cells. Currently, two mechanisms are recognized for satellite cell maintenance. Asymmetric division of a satellite cell produces two daughter cells, one of which becomes a new satellite cell while the other becomes a myogenic progenitor. Alternatively, symmetric division generates two daughter cells that both become myogenic progenitors. Consequently, when most satellite cells downregulate *Pax7* and initiate differentiation and proliferation to generate new myofibers, a small number of cells maintain *Pax7* expression and return to a quiescent state, thus replenishing the satellite cell pool(Feige et al., 2018). During the skeletal muscle regeneration process described earlier, the maintenance of satellite cell populations involves the activation of Wnt and Notch signaling pathways(Brack et al., 2008). In

mammals, there are currently known to be four Notch receptors and five ligands. Binding of extracellular ligands to receptors triggers sequential cleavage of the Notch extracellular domain, leading to the liberation of the Notch intracellular domain (NICD). The NICD translocates to the nucleus, where it binds with *RBP-Jκ* (also known as *CBF1*), activating the transcription of specific target genes, including those of the *Hes* and *Hey* family(Bray, 2016). After asymmetric division of satellite cells, the apical cell expresses *Notch1* and the Notch ligand *Dll1*. Dll1 is concentrated at the cell-cell interface with the basal cell, potentially binding to Notch3 in the basal cell to initiate self-renewal. Asymmetric distribution of Dll1 and the specific expression of the Notch inhibitor Numb in the committed daughter cell repress Notch activity, leading to myogenic commitment. The Notch effector genes are highly expressed to maintain satellite cells in a quiescent state and are downregulated during terminal differentiation(Sun et al., 2008; Yartseva et al., 2020). In adult skeletal muscle, canonical Wnt signaling primarily triggers satellite cell differentiation through the ligand Wnt3a, while non-canonical Wnt signaling promotes symmetric division, migration, and myofiber growth through the ligand Wnt7a(Bentzinger et al., 2014; Brack et al., 2008; Le Grand et al., 2009; Otto et al., 2006; von Maltzahn et al., 2012). In conclusion, the Notch signaling pathway is responsible for maintaining the quiescent state and self-renewal of muscle satellite cells, while the Wnt signaling pathway is responsible for their migration, symmetric division, and differentiation upon injury. This intricate transition from Notch to Wnt signaling pathways represents a crucial aspect of effective muscle regeneration.

The determination of skeletal muscle fate relies on the expression of myogenic transcription factors *Pax3/7*, *Myf5*, and *MyoD* in the dermomyotome, followed by the expression of muscle-specific genes that contribute to the formation of mature muscle tissue. The transition

from mononucleated myoblasts to multinucleated myofibers is crucial for the proper functioning of skeletal muscles, enabling contraction and locomotion. Recent research has unveiled two muscle-specific membrane proteins: Myomaker (*MymK*) and Myomixer (*MymX*), also known as *Myomerger* or *Minion*(Bi et al., 2017; Millay et al., 2013; Quinn et al., 2017; Zhang et al., 2017). These proteins play indispensable roles in myoblast fusion during embryonic development. Myomaker, a transmembrane protein with seven passes, is essential for fusion, as genetic deletion of Myomaker completely blocks myoblast fusion and prevents the formation of multinucleated muscle fibers in embryogenesis. On the other hand, Myomixer, a micropeptide, acts as a booster for Myomaker but cannot induce fusion on its own. Knockout of Myomixer in mice results in the failure of multinucleation and leads to postnatal death. Interestingly, coexpression of Myomaker and Myomixer is sufficient to induce fusion even in non-fusogenic cells such as fibroblasts(Bi et al., 2017; Millay et al., 2013; Zhang et al., 2020).

During muscle regeneration, both Myomaker and Myomixer are upregulated in satellite cells (SC). Additionally, specific deletion of either protein in adult satellite cells does not impact the initial response to muscle injury. However, a significant absence of regenerative myofibers is observed at 9 days post-injury for Myomaker-SCKO and 7 days post-injury for Myomixer-SCKO(Bi et al., 2018; Millay et al., 2014). A recent study proposed a fusion regulation model for human myoblasts, where Myomaker alone induces low-grade fusion, and Myomixer enhances fusion efficiency to generate large myotubes, a process regulated by MyoD(Zhang et al., 2020). While the MyoD–MymX/MymK regulatory axis provides insights into fusion regulation, there are likely other unidentified muscle-specific factors responsible for activating the cell fusion program that remain to be discovered(Zhang et al., 2020).

Activator Protein-1 (AP-1) family members and muscle regeneration

The activation of muscle satellite cell from quiescence stage marks the second phase of muscle regeneration which is essential for the transition from stem cell to myoblast. Recent studies have documented numerous disparities in the gene expression patterns of freshly isolated satellite cells when compared to their quiescent counterparts *in vivo*. These findings suggest that the process of isolating satellite cells is perceived as a signal of damage by the cells, resulting in the swift inhibition of genes associated with quiescence and the activation of other genes, potentially including crucial regulators of muscle stem cell function(Machado et al., 2017; van den Brink et al., 2017; van Velthoven et al., 2017). By comparing activated satellite cells and quiescent satellite cells, these studies noted that satellite cells undergo significant transcriptional changes and transition into an early activation stage during the isolation process(Machado et al., 2017; van den Brink et al., 2017; van Velthoven et al., 2017). Among these differentially expressed genes, AP-1 family members showed rapid induction in activated satellite cells.

The AP-1 family is a group of transcription factors that play crucial roles in various cellular processes, including proliferation, differentiation, apoptosis, and quick response to external stimuli(Shaulian & Karin, 2002). The AP-1 family consists of a collection of protein dimers composed of members from the Jun (*c-Jun, JunB, JunD*) and Fos (*Fos, c-Fos, FosB, Fosl1, Fosl2*) protein families, along with other related proteins such as ATF and MAF sub-families(Glover & Harrison, 1995). The AP-1 family of transcription factors is highly responsive to various stress signals. AP-1 activation can be induced by a wide range of stressors, including oxidative stress, DNA damage, ultraviolet radiation, heat shock, inflammatory cytokines, and growth factors(Eferl & Wagner, 2003; Jochum et al., 2001; Shaulian & Karin, 2002). The sensitivity of the AP-1 family to stress signals allows them to act as important regulators of

cellular stress responses. Under stress conditions, AP-1 members, such as *c-Fos*, *c-Jun*, *JunB*, and *JunD*, can be rapidly induced and activated. They form heterodimers or homodimers, which bind to specific DNA sequences in the promoters of target genes. This binding leads to the transcriptional regulation of genes involved in stress adaptation, cell survival, inflammation, and tissue repair. AP-1 transcription factors all possess basic leucine-zipper (bZIP) domains and regulate gene expression by binding to specific DNA sequences (TGA(C/G)TCA) known as AP-1 binding sites in the promoters or enhancer regions of target genes(Glover & Harrison, 1995).

The AP-1 family members play crucial roles in muscle development and regeneration. As a key regulator in myogenesis, MyoD was abundantly studied for its association with AP-1 complex. By in vivo and in vitro studies, c-Jun and MyoD was shown to physically interact through the binding of LZ domain and HLH domain respectively and inhibit the function of each other(Bengal et al., 1992). AP-1 was also shown to negatively regulate MyoD expression in proliferating myoblasts by binding to the CRE (cAMP-responsive element)-like element identified in MyoD promoter region(Pedrazaalva et al., 1994). In differentiating myoblasts, Fosl2 was identified as the major component in AP-1 complex and heterodimerized with c-Jun and JunD to transactivate MyoD expression(Andreucci et al., 2002). Recently, Almada et. al. reported that Fos functioned as earliest regulators for muscle satellite cell activation by targeting Art1 to initiate satellite cell expansion and muscle regeneration(Almada et al., 2021). Another AP-1 family member, AFT3, was demonstrated to preserve the premature activation of satellite cell by directly activating Histon 2B expression to enhance genome stability and inhibit replicative senescence (Zhang et al., 2022. bioRxiv). These studies converge on AP-1family to fine-tune gene expression and ensure proper muscle function and regeneration.

CHAPTER 2

GENERATION OF MOUSE CONDITIONAL KNOCKOUT ALLELES IN ONE STEP USING THE *i*-GONAD METHOD[1]

[1] Shang, R., Zhang, H., & Bi, P. (2021). Generation of mouse conditional knockout alleles in one step using the i-GONAD method. Genome research, 31(1), 121-130.
Reprinted here with permission.

Introduction

Our understanding of the genetic mechanisms of human diseases has been largely expanded by loss-of-function studies using engineered mouse models. Two types of gene knockout mouse models are commonly used: global and conditional, each with unique advantages. Ubiquitous deletion of a gene from all tissues in a global knockout model can mimic the genetic condition of human disease, thus permitting a quick and thorough evaluation of gene function in vivo(Amoasii et al., 2017; Cheon & Orsulic, 2011; Doyle et al., 2012; Gurumurthy & Lloyd, 2019; Wang et al., 2013). Given the flexible design of gene inactivation, for example, frame shift mutation caused by a small insertion or deletion (indel) or targeted removal of exon(s), the design and creation of a global knockout mouse model is relatively easy. However, genetic studies using this type of model may have inherent limitations. First, for a gene that is widely expressed, pleiotropic effects from its deletion in all tissues can obscure the cell type–specific gene functions. Second, an early onset lethality or gross abnormality of a mutant will prevent its application for studying gene function at adult stages or during aging conditions.

Cre/loxP-mediated conditional knockout models can circumvent these difficulties. Cre can delete the flanked gene sequence between two loxP sites through DNA recombination(Sauer & Henderson, 1988). Built on this principle, more sophisticated models of hormone-sensitive or tetracycline-inducible conditional knockouts were developed that allowed precise temporal control of gene disruption(Danielian et al., 1998; Feil et al., 2009; Jaisser, 2000; Schonig et al., 2002). These models have afforded valuable opportunities to interrogate the context-dependent gene function, thus providing clinically relevant information to treat genetic disease. The Cre/loxP system requires the creation of a conditional allele for the gene of interest. Although many tissue-specific/hormone-inducible Cre-expressing mouse strains are readily available,

generation of the loxP-flanked (floxed) alleles is challenging and labor-intensive due to the lack of an efficient method for their generation(Bouabe & Okkenhaug, 2013; Lewandoski, 2002; Skarnes et al., 2011).

The common approach for generating floxed alleles was established in the 1980s (Capecchi, 1989; Limonta et al., 1995; Mansour et al., 1988; Riele et al., 1992; Skarnes, 2015; Thomas & Capecchi, 1987b; Zijlstra et al., 1989). It utilizes homologous recombination in embryonic stem cells and requires technically challenging embryo-manipulation procedures. Such practice is largely restricted to transgenic core facilities, making the approach costly, time-consuming, and lacking in guaranteed success. Although this method has cumulatively created many invaluable mouse models over the past decades(Skarnes et al., 2011), scaling this approach up to functionally characterize the vast majority of the genome, with its rapidly expanding gene list(Chen et al., 2020) and associated genetic elements, is a challenging endeavor. Therefore, an alternative method that is inexpensive and easy to implement is awaited by the mouse genetic research community. Ideally, such methodology can be performed by regular laboratory personnel, for example, graduate students, with necessary technical training. Toward this goal, both the gene targeting strategy and the delivery method should be streamlined.

CRISPR genome-editing technologies have revolutionized genetic studies(Adli, 2018; Aida et al., 2015; Gurumurthy O'Brien, et al., 2019; Hsu et al., 2014; Irion et al., 2014; Jiang & Doudna, 2017; Miura et al., 2018; Platt et al., 2014; Rasys et al., 2019; Square et al., 2015; H. F. Wang et al., 2016; Yuan et al., 2019; Zu et al., 2016). However, successful applications of CRISPR-based mutagenesis have been largely restricted to creation of global loss-of-function models. Compared with random indels, the efficiency of precise editing through homology-mediated repair (HDR) is low(Aird et al., 2018; Doudna & Charpentier, 2014; Jiang &

Marraffini, 2015; Richardson et al., 2016; Zhang et al., 2017). Because the generation of conditional alleles requires simultaneous integration of two loxP sites precisely in the same chromosomal region (*in cis*), the chance of success is significantly lower when compared with other HDR projects.

Single-stranded oligo DNA (ssODNA) that contains homologous sequences flanking the nuclease-induced dsDNA break site emerged as an ideal form of HDR template that delivers higher knock-in efficiency and specificity (Miura et al., 2015; Yoshimi et al., 2016). A recent study of the interactions between the Cas9 protein with its DNA substrate provided a rational to improve the HDR design. Specifically, asymmetric target-strand ssODNs were shown to be highly effective in introducing point mutations (Richardson et al., 2016). Using this type of ssODNA, we previously generated two conditional alleles for the *MymX* gene by microinjection with an overall 12% efficiency(Bi et al., 2018). It should be noted, however, that an independent test of loxP insertions for 30 genes showed a nonsignificant impact of homology arm symmetry on HDR efficiency(Lanza et al., 2018). Reported in this large-scale test, the efficiency of loxP insertion by using short ssODNA, either symmetric or asymmetric designs, is around 9%(Lanza et al., 2018). More recently, utilizing various types of short ssODNA to separately insert loxP sites, extensive efforts from a consortium of core facilities and laboratories reported an overall 1% efficiency on 56 loci(Gurumurthy O'Brien, et al., 2019). These studies revealed large disparities of the gene targeting efficiency through microinjection.

In addition to microinjection, alternative CRISPR delivery methods were reported(Kaneko & Mashimo, 2015; Modzelewski et al., 2018; Ohtsuka et al., 2018; Takahashi et al., 2015b; Teixeira et al., 2018; W. B. Wang et al., 2016). Of special interest, a mouse zygote-stage embryo transfection strategy called improved-Genome editing via Oviductal Nucleic Acids

Delivery (*i*-GONAD) was reported(Ohtsuka et al., 2018). This method delivers a gene editing cocktail into mouse zygotes through oviduct electroporation. Operation of *i*-GONAD is easier than the ES-cell-based approach or microinjection because mouse zygotes no longer need to be individually handled and transferred into pseudopregnant mice(Gurumurthy, Sato, et al., 2019; Ohtsuka et al., 2018), yet the HDR efficiency of *i*-GONAD was comparable to that achieved through microinjection(Ohtsuka et al., 2018). For the creation of conditional alleles, one recent study proposed a two-step *i*-GONAD workflow that sequentially inserts two loxP sites, one at a time(Sato et al., 2020). However, the proof-of-principle test of this approach was not satisfactory, that is, only one loxP was integrated(Sato et al., 2020). Therefore, both the CRISPR targeting strategy and the logistics of *i*-GONAD for creation of conditional alleles require improvement. Here, we aim to develop and test a new approach by integrating a unique design of asymmetric loxP-ssODNA with the *i*-GONAD delivery method to create mouse conditional alleles.

Results

Exploiting the *i*-GONAD method to create a conditional allele: a proof-of-principle test

The principle of HDR template design, major experimental procedures, and milestones for this method are schematized in Figure 2.1A. It involves using two guide RNAs (gRNAs) and two short ssODNs as HDR donors for loxP insertions. Each ssODNA is 161 nt long, composed of 91 nt of the 5′ homology arm from the PAM-proximal side, 34 nt of loxP sequence, and 36 nt of the 3′ homology arm from the PAM-distal side.

We first tested the i-GONAD method by generating a mouse conditional allele for the *Fosl1* (fos-like antigen 1) gene for which the expression at both mRNA and protein

levels was induced during muscle regeneration (Fig. S2.1). The function of the *Fosl1* gene during this biological process remains unknown. Because *Fosl1* global knockout mice die as embryos (Schreiber et al. 2000), studying the postnatal muscle-specific function of this gene requires a conditional allele.

The mouse *Fosl1* gene contains four exons, with the last two being close to each other and representing 64% of the coding sequence including critical domains of the FOSL1 protein (Matsuo et al. 2000). Therefore, deletions of exons 3 and 4 can unequivocally abolish gene function. We designed a pair of gRNAs and the corresponding ssODNs to insert loxP sites flanking these exons (Fig. 2.1B). Different from microinjection, which directly delivers CRISPR components into the zygotes, *i*-GONAD involves a two-step transfer of the gene editing cocktail: first, the cocktail is injected into the lumen of the oviduct, followed by a second step of oviduct electroporation that transfers the cocktail into zygotes (Fig. 2.1A; (Ohtsuka et al., 2018)). Owing to the volume restriction of the oviduct and inevitable dilutions of the gene editing cocktail by the much larger volume of oviduct fluid, we used concentrated Cas9 protein, ssODNs, and gRNAs in molar ratios of 1:6:10, as we previously used in microinjection experiments(Bi et al., 2018).

CD-1 female mice in estrus were mated with C57BL/6J males. We performed i-GONAD on two females that showed copulation plugs. To avoid false detection of loxP sites in scenarios of random ssODNA integration, genotyping primers were designed in the regions outside the homology arms of donors. Successful incorporation of loxP was identified by a 34-base-pair (bp) increase in PCR amplicon size. Our results revealed the simultaneous 5′- and 3′-loxP insertions in one mouse (#2) (Fig. S2.2). We also detected 5′- or 3′-loxP integrations in other mice: #1, #10, #11, #14, #15, and #20 (Fig. S2.2). Because transgenic founders are commonly mosaic, we

tested germline editing of the #2 mouse by breeding it with wild-type (WT) mice. Out of a total of 22 filial 1 (F1) progenies obtained, four showed simultaneous inheritance of 5′- and 3′-loxP sites (Fig. 2.1C). The fidelity of these loxP sites was also validated by sequencing (Fig. 2.1D). Intercrossing of the heterozygous mice generated homozygous Fosl1loxP/loxP mutants at expected Mendelian ratios. These mutants appeared phenotypically normal, indicating that loxP insertions do not alter gene function, a prerequisite for conditional alleles.

More tests of the i-GONAD method to create conditional alleles for another four genes

To our knowledge, the Fosl1loxP allele is the first conditional allele created by the *i*-GONAD protocol in one step, which is easier and faster than two-step approaches. To better evaluate the efficiency, we performed additional tests on four other genes: *Plagl1* (pleiomorphic adenoma gene-like 1), *Ak040954*, *Clcf1* (cardiotrophin-like cytokine factor 1), and *Gm44386*. In addition to having different genomic locations, these genes were chosen because of our research interests, their distinct functions, and patterns of epigenetic regulations (Fig. 2.2A). As such, tests on these loci may demonstrate the broader utility of this method.

We first tested the synergy and editing efficiency of gRNAs in mouse fibroblasts (Fig. S2.3). The gRNA pair that can generate large deletions between the gRNAs was chosen for *i*-GONAD. The loxP sequence contains an 8-bp asymmetric core spacer that defines the orientation of the loxP cassette(Sauer, 1998; Sternberg et al., 1981). Deletion of the flanked sequence requires that the two loxP sites are aligned in the same direction(Guo et al., 1997). We therefore adjusted the orientation of the loxP sequence within the HDR donors when gRNAs targeted opposite DNA strands.

For the *Plagl1* gene, we aimed to generate a conditional allele by flanking the coding exons 5 and 6 with loxP sites (Fig. 2.2B). Four females were used for the *i*-GONAD procedure. Among 28 pups that were born, three (#8, #10, #11) showed simultaneous 5′- and 3′-loxP insertions, and another eight mice showed either 5′- or 3′-loxP insertions (Fig. S2.4A). Among 15 progenies obtained from breeding the #10 founder with C57BL/6J WT mice, eight pups showed successful germline transmission of both loxP sites (Fig. S2.4B). Correct targeting in these mice was also confirmed by sequencing (Fig. 2.2B, boxed panels). Of note, all other progeny showed the insertion of only the 3′-loxP site (Fig. S2.4B). This reveals the mosaicism of genome editing.

The long noncoding gene *Ak040954* contains two exons. We targeted the major exon 2 which represents 91% of the transcript (Fig. 2.2C). Three female mice were used for *i*-GONAD. Among 11 mice that were born, two pups (#5, #7) showed simultaneous 5′- and 3′-loxP insertions, whereas another two pups (#8, #9) showed only 5′-loxP insertions (Fig. S2.4C). Among nine progenies obtained from breeding of #5 founder with C57BL/6J WT, three pups showed successful germline transmissions of floxed alleles that contained both the 5′- and 3′-loxP sites (Fig. S2.4D). The fidelity of loxP sequences was validated by sequencing (Fig. 2.2C, boxed panels). We also observed the inheritance of other types of mutations, showing up as >34 bp insertions (#2, #7) (Fig. S2.4D), which mirrored the genotype of their F0 parent (Fig. S2.4C).

The *Clcf1* gene contains three exons that together encode a 225-amino acid cytokine. We generated a conditional knockout allele by targeting exon 3 (Fig. 2.2D) that encodes the majority of the protein. Among eight pups produced, one mouse (#2) showed simultaneous 5′- and 3′-loxP insertions, and another two mice (#1, #4) showed either 3′- or 5′-loxP insertion, respectively (Fig. S2.4E). Among 13 progenies of the #2 founder, eight mice showed successful germline

transmissions of both 5′- and 3′-loxP insertions (Fig. S2.4F). The fidelity of loxP sites was also confirmed by sequencing (Fig. 2.2D, boxed panels). All other pups showed only 5′-loxP insertions (Fig. S2.4F). This is consistent with the genotype of the F0 founder for which the 5′-loxP insertion was nearly homozygous (Fig. S2.4E).

Using the *i*-GONAD method, we also generated a conditional allele for the *Gm44386* gene, whereby the coding exons were flanked by two loxP sites (Fig. 2.2E). Among nine pups produced, two (#1, #5) showed simultaneous 5′- and 3′-loxP insertions, whereas another two (#3, #9) showed only 3′-loxP insertions (Fig. S2.4G). Successful transmissions of the two loxP sites were also confirmed by PCR (Fig. S2.4H) and sequencing (Fig. 2.2E, boxed panels).

A cloning-based strategy to rapidly identify founders with loxP insertions *in cis*

By Mendel's law of inheritance, the simultaneous transmission of 5′- and 3′-loxP sites into the F1 generation validated loxP insertions in cis for five founders, that is, one for each gene. In addition to these mice, we also obtained other F0 founders that showed both 5′- and 3′-loxP sites. This includes the #5 mouse for the *Gm44386* gene (Fig. S2.4G), the #7 mouse for the *Ak040954* gene (Fig. S2.4C), and the #8 and #11 mice for the Plagl1 gene (Fig. S2.4A). To deconvolute the potential mosaicism in these F0 founders (Fig. 2.3A) and identify more floxed alleles, we devised a cloning-based strategy of genotyping.

As illustrated in Figure 2.3B, long-range genotyping PCR was performed with the forward primer from the 5′ gRNA region (5′F) and the reverse primer from 3′ gRNA region (3′R). Because the sizes of these PCR products were large (Fig. 2.3B), gel electrophoresis cannot reliably identify floxed alleles from others, for example, single loxP, WT, or small indels. We leveraged the principle of molecular cloning to genotype a single DNA molecule amplified by the long-range PCR (Fig. 2.3B). During transformation, the plasmid incompatibility ensures that

each bacterium only maintains one vector that hosts one DNA insert. This provides an opportunity to verify the presence of two loxP sites in a single DNA molecule through genotyping the bacterial colony using 5′F&5′R and 3′F&3′R primers, which give rise to much shorter amplicons that can be analyzed by regular gel electrophoresis (Fig. 2.3B). In rare cases where a competent cell takes more than one vector, such heterogeneity can also be detected by PCR and will be excluded from analyses.

As expected, the separation of long-range PCR products by electrophoresis is poor (green arrows, Fig. 2.3C). To reduce the cloning background, we purified the large amplicons (green boxes, Fig. 2.3C) for ligations. Genotyping results of bacterial colonies for the #5 mouse of the *Gm44386* gene showed only 5′ loxP, whereas the 3′ gRNA region was WT-size (Fig. 2.3D). Mimicking the bacterium genotyping results, the progeny of this mouse only showed 5′ loxP (Fig. S2.4I). Compared with the genotype of this founder (Fig. S2.4G), these observations indicate a mosaicism that possibly includes scenarios #3 and #6 illustrated in Figure 2.3A (lower panel). In comparison, floxed alleles were detected for all other founder mice (Fig. 2.3E–H). As a validation, breeding of the #7 mouse (*Ak040954*) produced F1 progeny that contained both loxP sites (three out of 10 pups). Together, these experiments proved the accuracy of the cloning-based method to identify floxed alleles.

Byproducts of the *i*-GONAD method can serve as global knockout models

The long-range PCR revealed large-deletion alleles from these *i*-GONAD experiments (red arrows, Fig. 2.3C). Indeed, deletions of various sizes were observed for all five genes (Fig. 2.4A-D; Figs. S1.5-S1.7). In total, 20 out of 54 (37%) F0 generation mice showed large deletions. As a consequence, critical exons for these genes were removed as confirmed by sequencing. This includes deletions of 7,489 bp for the *Plagl1* gene (Fig. S2.5C), 3,413 bp for

the *Ak040954* gene (Fig. 2.4E), 3,664 bp for the *Gm44386* gene (Fig. 2.4F), 1,812 bp for the *Fosl1* gene (Fig. S2.6B), and 1755 bp for the *Clcf1* gene (Fig. S2.7B). Note that the amplicons for WT or floxed alleles were too large and thus not detected in these PCR conditions. Collectively, these "byproduct" mutants obtained from loxP projects may serve as global knockout models.

Other types of mutations from the F0 generation included smaller indels produced by either 5′- or 3′-gRNA, for example, mice #15 and #20 for the *Fosl1* gene (Fig. S2.2), and mice #1, #2, #6, and #8 for the *Clcf1* gene (Fig. S2.4E). In scenarios where intron-exon splicing sites were destroyed, abnormal splicing may join incompatible exons, making these mutations potentially useful as knockout or hypomorphic alleles.

Examination of off-target mutagenesis by *i*-GONAD

The high efficiency of *i*-GONAD prompted us to examine the genome editing specificity in F0 founders that contained floxed alleles (Fig. S2.8A). We used the polyacrylamide gel electrophoresis (PAGE) method (Zhu et al., 2014) to quickly and sensitively detect small indels. Among 10 gRNAs, #2 gRNA produced off-target mutagenesis in the predicted site (Fig. S2.8A–C). Coincidently, only this off-target site had identical sequence with the 10-bp PAM-proximal "seed" region of the gRNA (Fig. S2.8A). This aligns with the notion that a single nucleotide mismatch within the PAM-proximal region is not tolerated by the CRISPR-Cas9 (Fortin et al., 2019; Qi et al., 2021). Together, our results showed that genome editing delivered by *i*-GONAD is largely specific, though caution is also warranted when gRNAs with predicted low-specificity were used.

Test of *i*-GONAD on the *Mecp2* gene

We continued to examine whether the short symmetric ssODNA donors can work for *i*-GONAD in generation of conditional alleles. For this purpose, we chose the *Mecp2* (methyl CpG binding protein 2) gene because multiple groups have attempted to insert loxP by microinjecting symmetric ssODNA donors(Gurumurthy O'Brien, et al., 2019; Yang et al., 2013). As such, using the same designs of gRNA and ssODNA, it provides an indirect comparison of *i*-GONAD with the microinjection approach.

Three CD-1 female mice that showed copulation plugs after mating with C57BL/6J males were used for the *i*-GONAD procedure. Embryos at day 12.5 postconception (E12.5) were collected for genotyping analysis. The high efficiency of gRNAs was revealed by big truncations and possible elimination of primer binding sites in multiple samples (#1, #2, #4, #6, #9, #15) (Fig. S2.9A,B). Among 19 total embryos, two showed a 5′-loxP site; four showed a 3′-loxP site, with one embryo (#3) showing both 5′- and 3′-loxP sites. Long-range PCR (Fig. S2.9B) and cloning-based genotyping analysis (Fig. S2.9C,D) confirmed in cis loxP insertions in this sample. These results were consistent with a previous report that the efficiency of loxP insertions in this locus was relatively low(Gurumurthy et al. 2019a).

Repeating *i*-GONAD on *Plagl1* and *Clcf1* genes using C57BL/6J females

i-GONAD can efficiently deliver CRISPR cocktails for a variety of hybrid or inbred mouse strains(Ohtsuka et al., 2018). We used CD-1 females because of their good postsurgery performance and generally large litter size. In our experience, performing *i*-GONAD on CD-1 females is also easier than C57BL/6J females thanks to larger volumes of the oviduct. However, with technical proficiency gained from these practices, we continued to determine whether conditional alleles could also be produced from the inbred C57BL/6J strain.

Plag1 and *Clcf1* genes were selected for these tests. C57BL/6J females that showed copulation plugs after mating with C57BL/6J males were used for *i*-GONAD. As previously observed, the pregnancy rate of C57BL/6J females was low (Ohtsuka et al. 2018). From multiple breeding pairs, only two females produced a total of five embryos for the *Plagl1* experiment, and another two females produced six for the *Clcf1* experiment. Nevertheless, we identified one embryo that showed a floxed allele for each gene (Fig. 2.5A,B), which was also confirmed by analyzing the long-range PCR products (Fig. 2.5C; Fig. S2.10). Together, these results are in agreement with previous observations that inbred strains can be used for genome editing by the *i*-GONAD method (Ohtsuka et al., 2018).

Validation of the *Fosl1* conditional allele

We continued to validate the design and utility of the conditional allele that we generated by *i*-GONAD. Through serial crossing of Fosl1$^{loxP/loxP}$ with Pax7^{CreER} mice (Lepper et al., 2009), a widely used muscle stem cell–specific Cre deleter, we obtained Pax7^{CreER}:Fosl1$^{loxP/loxP}$ conditional knock out mouse model, indicated by Fosl1-cKO. Tamoxifen was administered into adult mutants to activate CreER and thus the removal of exons 3 and 4 of the *Fosl1* gene (Fig. 2.6A). Two days after the last dosage of tamoxifen, muscle tissues were collected for genotyping analyses. As expected, the recombined allele can be specifically detected in muscle samples from Fosl1-cKO but not littermate Fosl1$^{loxP/loxP}$ mice (Fig. 2.6B). Sequencing confirmed the correct recombination between 5′- and 3′-loxP sites that excised the targeted exons and joined intron 2 with the 3′ region of the Fosl1 gene (Fig. 2.6C). Because muscle stem cells account for less than 5% of total nuclei in intact muscle tissues (Snow, 1981), the intact floxed allele was also readily detected in Fosl1-cKO muscle samples (Fig. 2.6B).

We then isolated muscle precursor cells from Fosl1-cKO mouse and confirmed the robust inactivation of *Fosl1* gene detected by qPCR using primers from exon 4 of this gene (Fig. 2.6D). As a negative control, fibroblasts that were also isolated from Fosl1-cKO mouse showed a normal level of expression for the *Fosl1* gene (Fig. 2.6D). We did not examine *Fosl1* gene expression in whole muscle tissues because muscle precursor cells only account for a small portion of the tissue, whereas the remaining cell types ($Pax7^{-}$) also abundantly express the *Fosl1* gene, as shown by single-cell RNA sequencing analyses of muscle tissues (Fig. S2.11)(Schaum et al., 2018) .These results validated the utility of the conditional allele produced by the *i*-GONAD method.

Discussion and future direction

The overall targeting efficiency of producing floxed alleles by *i*-GONAD was 10% (eight out of 76) (Table 2.1). In addition to these desired mutants, the frequency of obtaining F0 mice with either 5′- or 3′-loxP insertion was 28% (21 out of 76). Therefore, the combined loxP-insertion efficiency was 38%, close to the HDR efficiency that was previously reported using the *i*-GONAD method (49%) or through microinjection (52%)(Ohtsuka et al., 2018). In F1 generations, the chance of inheriting two loxP sites (*in cis*) was 37% (32 out of 87 pups) (Table 2.1), indicating efficient germline editing by *i*-GONAD. These tests demonstrate that our approach, using the *i*-GONAD method and the HDR template design, is robust, fast, and efficient for the generation of mouse conditional alleles.

One recent large-scale test of microinjection reported an 11% loxP-insertion efficiency by using asymmetric ssODNs and a 7% efficiency by using symmetric ssODNs(Lanza et al., 2018). Compared with these dual-ssODNA approaches, long ssODNA, composed of loxP–Exon(s)–loxP sequences, was shown to be more efficient in generating floxed alleles(Lanza et

al., 2018; Miura et al., 2018; Miyasaka et al., 2018; Quadros et al., 2017). Because both loxP sites were synthesized in one piece, this predicts simultaneous integrations of two loxP sites. However, technical barriers do exist for the preparations of long ssODNA(Lanza et al., 2018). Depending on the length of the floxed area, production of long ssODNA that meets the required yield, purity, and fidelity by either chemical synthesis or enzymatic reactions is still challenging. For instance, even without considering the homology arms, the floxed regions for our genes measured 2–7 kb. In comparison, the maximum size of ssODNA (megamer) that can be ordered from IDT is 2 kb. Therefore, broader applications of long ssODNA await improvement of DNA synthesis technology.

In comparison with the conventional floxing method, an alternative strategy of conditional gene-inactivation by leveraging the exon-splicing machinery (Guzzardo et al., 2017) could make the use of single-piece ssODNA more realistic. This conditional knockout strategy involves the insertion of a small artificial intron that harbors two loxP sites into a coding exon of the target gene. In the absence of Cre, this foreign sequence can be fully excised by splicing machinery without affecting gene function. In the presence of Cre activity, recombination of loxP sites will destroy the artificial intron which causes translational termination, thus abrogating gene function. It remains to be tested whether the artificial-intron ssODNA can produce higher targeting efficiency when delivered by *i*-GONAD.

In addition to the formats of donors, the HDR efficiency can also be affected by donor concentration at the editing site(Liu et al., 2019). Consistent with this notion, HDR frequency was improved when ssODNA was chemically linked to Cas9 protein(Aird et al., 2018; Ling et al., 2020; Ma et al., 2017). In a simpler form, one can test whether the more stable ssODNA, improved by chemical modifications, can enhance *i*-GONAD efficiency. Other methods to

improve HDR frequency include chemical inhibition of the nonhomologous end-joining pathway (Maruyama et al., 2015), engineering of Cas9 protein (Charpentier et al., 2018; Jayavaradhan et al., 2019), and the timing of gene targeting in S/G2 phases of the cell-cycle (Lin et al., 2014). The *i*-GONAD procedure is performed around 4:00 p.m. of the day when the vaginal plug is observed(Gurumurthy, Sato, et al., 2019; Ohtsuka et al., 2018). This marks approximately 16 hpf, a stage when zygotes transit from the S to the G2 phase of the first cell-cycle(Howlett & Bolton, 1985). In comparison, microinjection or ex vivo zygote electroporation was commonly performed at an earlier time that corresponds to 10–12 hpi (Lanza et al., 2018; Teixeira et al., 2018). The timing differences of these CRISPR delivery methods may affect the efficiency of loxP insertions.

One limitation of the current study is the relatively smaller number of genes tested, as compared with the larger-scale microinjection experiments (Gurumurthy, Sato, et al., 2019; Lanza et al., 2018) or multicenter consortium studies (Gurumurthy et al. 2019a). Because we do not have access to microinjection core or *ex vivo* zygote electroporation setups, we cannot directly compare the performance of these delivery methods. However, the initial report of *i*-GONAD confirmed that its HDR efficiency was comparable with that achieved through microinjection(Ohtsuka et al., 2018) . Similarly, the 10% efficiency that we observed for loxP insertions by *i*-GONAD was also comparable with that from microinjection (11%–12%) (Bi et al., 2018; Lanza et al., 2018), though locus-to-locus variability was observed. For instance, the efficiency of creating a floxed allele for the *Fosl1* gene is 5% (one out 20) versus 18% (two out 11) for the *Ak040954* gene (Table 2.1). This could be caused by different levels of chromatin accessibility, a major determinant of Cas9 binding and activity(Chari et al., 2015; Wu et al.,

2014). Nevertheless, successful delivery of CRISPR reagents is required but certainly cannot guarantee the same editing efficiency for different loci.

To provide an indirect comparison with the microinjection method, we repeated *i*-GONAD on the *Mecp2* gene. We selected this locus because it was previously tested by the microinjection method, though a large discrepancy of targeting efficiency, ranging from 0% to 16%, was reported(Gurumurthy O'Brien, et al., 2019; Yang et al., 2013). The *i*-GONAD efficiency of producing a floxed allele for this locus is 5%. Of note, the gRNAs did show high editing activity in producing null alleles. Therefore, *i*-GONAD is a reliable method to deliver the CRISPR cocktail into zygotes, and the efficiency of producing conditional alleles can vary largely at different loci.

We referred to our previous experience of microinjection(Bi et al., 2018)for the molar ratios of Cas9, gRNA, and ssODNA. It remains unknown whether other concentrations of these reagents could enhance the success rate of *i*-GONAD. Although *i*-GONAD does not require direct handling of the mouse embryo, its success depends on many factors. First, similar to microinjection, *i*-GONAD requires steady hand-control of the microcapillary needle for oviduct injection. Second, a thorough understanding of the mouse reproductive system is essential. In our experience, oviduct injections visualized by dye solution have afforded valuable training opportunities. In addition, we recommend testing gRNAs in cultured mouse cells, for example, fibroblasts, before applying them for *i*-GONAD. Last, one should monitor the off-target mutations in picked founders, especially when the predicted off-target site is located near the gene of interest. In summary, our study provides a complete gene targeting workflow to create, analyze, and authenticate conditional alleles. This may promote gene function studies in vivo by providing an inexpensive alternative to generate custom mouse models.

Methods

Oviduct electroporation by the *i*-GONAD protocol

All animal procedures were approved by the Institutional Animal Care and Use Committee (IACUC) at the University of Georgia. Mouse oviduct electroporation was performed as previously reported(Ohtsuka et al., 2018). Briefly, 6- to 10-wk-old CD-1 or C57BL/6J female mice were mated with C57BL/6J stud males the day before electroporation. The copulated female mice were used for surgery to expose the oviduct. CRISPR gene editing cocktails were freshly assembled and contained 6 μM Cas9 protein (IDT 1081058, Lot # 0000405530), 30 μM gRNA (Alt-R crRNA annealed with tracrRNA, IDT 1072534, Lot # 0000403961), and 18 μM ssODNA (IDT Ultramer DNA Oligo, standard desalting). This cocktail was delivered into the oviduct through microcapillary injection. Oviduct electroporation was performed using a CUY21EDIT II electroporator with the following protocol: Pd A: 100 mA, Pd on: 5 msec, Pd off: 50 msec, three cycles, decay 10%. The sequences for gRNA and ssODNA are provided in Supplemental Materials.

Mouse genotyping analysis

Genotyping PCR was performed using genomic DNA extracted from the toe clipping with the primers listed in Supplemental Materials. For Sanger sequencing, PCR products were first gel-purified and cloned into the pCRII Topo vector (Thermo Fisher Scientific K460001) and sequenced with T7 or SP6 primers. Long-range PCR was performed using LongAmp Hot Start Taq 2X Master Mix (NEB M0533S) to examine genomic DNA that was purified by a Monarch Genomic DNA Purification kit (NEB T3010). The large amplicons were gel-purified and cloned into the pCR-XL-2-TOPO vector (Thermo Fisher Scientific K8050-10). The top off-targeting sites were predicted by Cas-OFFinder (Bae et al., 2014).

Tamoxifen and muscle injury

Tamoxifen (Sigma-Aldrich T5648) was dissolved in ethanol (10 mg/mL). This stock solution was diluted in sesame oil (Sigma-Aldrich S3547) with a ratio of 1:9 before injection. Two milligrams of tamoxifen were administered by intraperitoneal injection. Muscle injury was induced by injecting 1.2% barium chloride (50 μL) into the tibialis anterior muscle.

gRNA and ssODNA sequences

Fosl1 5' gRNA: CCGGACGCTTGTCATCTCAT.

Fosl1 3' gRNA: AGAGGGTCGCCCCATTCTTC.

Fosl1 5' ssODNA:

AGGAAGATCAAAGTTTACAGAGAGGGAAAGCATTTCAGGAAAGAAACCAGCAGTA

AAGCTAGGTGTGTGTGAGCTGGAAATGTCACCAATGATAACTTCGTATAGCATACAT

TATACGAAGTTATAGATGACAAGCGTCCGGTACAGAGAAGCAACTGTGG.

Fosl1 3' ssODNA:

ACCATTTGGAACAGGAGTTCCAGGTTCCAGTCTCAGCATTGACCTTGAAGAAACTAC

CATATGTTTTTGGACTTCCATATTCTCACCTGAAATAACTTCGTATAGCATACATTAT

ACGAAGTTATGAATGGGGCGACCCTCTGCTCTTCCTTGTCTCCTAT.

Plagl1 5' gRNA: GATTGCAGGCTTGAATACGG.

Plagl1 3' gRNA: ATGGAACCATCTATGAGACC.

Plagl1 5' ssODNA:

CTGGGTATCTGCAGAGAGAAGAGGAACAGATTTCTCACATCAGCTATTGGAAAACT

GTATCCCCCCACCAGCACCAGCATCAGCACCACCGATAACTTCGTATAATGTATGCT

ATACGAAGTTATTATTCAAGCCTGCAATCAGTATATTCTTTTAAGAGG.

Plagl1 3’ ssODNA:

ATCTCAGAGCAGTGAATTTGATCCCGTGAGGCTATCTTGCTGCTTCATTGTCTACTCT

AGGTCAGGTCAACTGTGTCTTATGGGCCCTGGTATAACTTCGTATAATGTATGCTAT

ACGAAGTTATCTCATAGATGGTTCCATAGTGCAAGGTTTCCCCATT.

Ak040954 5’ gRNA: ACCCTTATAAAATAACCTCG.

Ak040954 3’ gRNA: GTATCTGGCGATGTGTTTAG.

Ak040954 5’ ssODNA:

CAAACTCTTGCCTGCTGGGTCCCCAGCAAGCCTTACAGTCCTGATGTCTGCTCTAAC

ACATTTGCACTCCACCTCTGGTTCCACACCTCTAATAACTTCGTATAGCATACATTAT

ACGAAGTTATAACACATCGCCAGATACCCAAAGTCATCAGTGAACA.

Ak040954 3’ ssODNA:

TGTTTTTCTTTATGCATCTCAAAGGATCCTGTACTGCTTTCAAAGGAACCACTGCACC

ACACGGTTCCTGTCTTCCTGTCTTTCTCCACGAATAACTTCGTATAATGTATGCTATA

CGAAGTTATGGTTATTTTATAAGGGTAAAGCTCAGGTCTTACTTA.

Clcf1 5’ gRNA: GTCAGCACGTCCCACCCGAG.

Clcf1 3’ gRNA: GTACACAGGCCTTGGAGTAC.

Clcf1 5’ ssODNA:

ATCATTTGCATGGAGGAGACAGGTGAAGCAGTGGGGTGATGAGTTCTCCTATGGAG

AAGTGCAGAGAGAGAAAACCACGAAGGAGCCACTCATAACTTCGTATAATGTATGC

TATACGAAGTTATGGGTGGGACGTGCTGACTGTCTGGGTGGAGAATGCC.

Clcf1 3’ ssODNA:

AAACACACACAGCTATCTGGGAGGACCAAGGCATAGTGGGTGTGGCAAGGGAGTGG

ATGGGTTGCTCCAGGGCCAGCAGTAAGAGCCTGTAATAACTTCGTATAATGTATGCT

ATACGAAGTTATCTCCAAGGCCTGTGTACCTCTATGGTATAAAGAGAC.

Gm44386 5’ gRNA: CACCCTCAAACTTGATACAT.

Gm44386 3’ gRNA: GACCACAATGCAATTTACAT.

Gm44386 5’ ssODNA:

TCAAAGCAATTACTATATTAATTATTACTATATTATCACCAAAGGGGTCAGGACCCA

AAGGTTGAGAACCCCTGTTCTGGGTCCTCCTATGATAACTTCGTATAATGTATGCTAT

ACGAAGTTATTATCAAGTTTGAGGGTGGCTTGGGCTACATGAGACT.

Gm44386 3’ ssODNA:

CATCATGAGTTCCAAGCCAGCCTGGACAGAAGGAGCCCCTGTTAGAGATGTAGAGC

CATGCAAGCATGAAGACCTGAGTTTATAACCCATGATAACTTCGTATAGCATACATT

ATACGAAGTTATTAAATTGCATTGTGGTCAGGCAGTGGTGGCACATGC.

Mouse genotyping primer sequences

Gene	Primer name		Sequence (5'–3')	Expected amplicon size
Fosl1	5' *loxP*	Forward	TCCACAGATGAGGAGGCTGA	WT 392 bp, *loxP* 426 bp
		Reverse	TGGGCTGATCTAGGTTGGGA	
	3' *loxP*	Forward	AGAAGCGCTTAGCTTCAGGG	WT 317 bp, *loxP* 351 bp
		Reverse	TGCTTGCACTCCAGAGCATT	
	Long-range PCR		5' *loxP*-F + 3' *loxP*-R	WT 2,115 bp
Plagl1	5' *loxP*	Forward	AGAAAGGGAGGATGGGTTGC	WT 278 bp, *loxP* 312 bp
		Reverse	TGAGGAACTGCTGTGCCATT	
	3' *loxP*	Forward	GGGTTGAAGCCAGTGACAGT	WT 200 bp, *loxP* 234 bp
		Reverse	TTTGGGGAGACTGCCTTTCC	
	Long-range PCR-F		GCAACTAGACTCCATGTCCCC	WT 8,441 bp
	Long-range PCR-R		AGTTGTGCTTGGTGCTGAGT	
Ak040954	5' *loxP*	Forward	CTCCCTCTTCCCTGACCAGA	WT 327 bp, *loxP* 361 bp
		Reverse	TTGCCCTCCACTGATTGTCC	
	3' *loxP*	Forward	GGCCACAGTTCTGCTGGTAT	WT 357 bp, *loxP* 391 bp
		Reverse	CAGGCCTCTCTTTGTCCTGG	
	Long-range PCR		5' *loxP*-F + 3' *loxP*-R	WT 3,755 bp
Clcf1	5' *loxP*	Forward	CTACCTCTCCAGCCTGGTCT	WT 355 bp, *loxP* 389 bp
		Reverse	AGTCAGGCTCGTTGAAAGGG	
	3' *loxP*	Forward	ACCCTAACCCTACCTGCCAT	WT 188 bp, *loxP* 222 bp
		Reverse	CCAGAGGCAAGGAAGACTGG	
	Long-range PCR		5' *loxP*-F + 3' *loxP*-R	WT 1,977 bp
Gm44386	5' *loxP*	Forward	GGAACAGGCTGTCACAGGAG	WT 397 bp, *loxP* 431 bp
		Reverse	GAAGCTGGAGATCAGAAGGCA	
	3' *loxP*	Forward	AGGAGCCCCTGTTAGAGATGT	WT 381 bp, *loxP* 415 bp
		Reverse	GTGTGGGGATATGCTGTCTGA	
	Long-range PCR		5' *loxP*-F + 3' *loxP*-R	WT 4,122 bp
Mecp2	5' *loxP*	Forward	CCCAGCTTGACCCAAGGATA	WT 287 bp, *loxP* 327 bp
		Reverse	GGCTGAAGGTTGTAGTGGCT	
	3' *loxP*	Forward	AGGTGGGTAGGAAGGCTAGG	WT 218 bp, *loxP* 258 bp
		Reverse	CTCCTCTGTACTCCCTGGCT	
	Long-range PCR		5' *loxP*-F + 3' *loxP*-R	WT 773 bp
Pax7^{CreER}	10221-*Pax7*^{CE}		ACTAGGCTCCACTCTGTCCTTC	WT 724 bp, *Pax7*^{CreER} 231 bp
	10222-*Pax7*^{CE}		GCAGATGTAGGGACATTCCAGTG	

Genotyping primers were designed to detect indels in predicted off-targeting sites. The primer sequences are listed in the table below.

Target gene	Off-target of gRNA	Sequence (5'–3')	WT size (bp)
Fosl1	#1	CGCTCACTTGGAGAAATGCC	370
		TGACAACATAGAACTGTGTAGGTTT	
	#2	CCAGCCTGTTTCTTTCCCCA	270
		GGTCATCTTCTGCCCCTGAC	
Plagl1	#3	AGCCCCATACAAACATCGGG	388
		ACCTTGCACTCTGTCTACGC	
	#4	ACAGAATGCATCAAGTGCTATG	369
		GTTCCTCAGATGCTGTGCCT	
Ak040954	#5	ACAGAGAGCTCAGGCATTGG	117
		TCACCGAGGTAACTTTGCCC	
	#6	CTACCCTGTGTCCCAAGCTG	206
		GCTTGAGTCCAAGACCAGCA	
Clcf1	#7	TGGGAAGTTAAGTTCGCGGG	293
		TACAGACCTCCGAACGTCCA	
	#8	TGGGGTACATTGCTGGTCAC	249
		AGCAAATGCAGGCTGAGCTA	
Gm44386	#9	ACACTATGGGGCACTGAAGC	282
		ATGCTAATGCCTGTCGTGCT	
	#10	CATTGGCACCCTTGTTGGTG	108
		GCTTACAGATGTAGCACTGGC	

Cell cultures and transfection

10T1/2 fibroblasts were maintained in 10% FBS with 1% penicillin/streptomycin in DMEM. Lentiviruses expressing Cas9 and gRNA were packed by co-transfections of pLenti-V2 (a gift from Feng Zhang, Addgene, 1000000052) with psPAX2 and pMD2.G plasmids into Lenti-X 293T cells (Takara Bio, 632180). Two days after infection, genomic DNA was extracted for genotyping. Primary myoblasts were isolated from adult muscle tissues by enzymatic digestions as previously described(Bi et al., 2016). Pre-plating was performed to enrich myoblast and separate fibroblasts. To activate CreER, 2 μM 4-hydroxytamoxifen (Cayman Chemical, 14854) was added to cell culture for 48 hrs before collecting RNA for gene expression analysis.

Quantitative real-time PCR (qPCR)

Total RNA was extracted from mouse tissue or cells with TRIzol (Invitrogen). cDNA was synthesized using iScriptTM Reverse Transcription Supermix (Bio-Rad, 1708841). Gene expression was assessed using standard qPCR approaches with KAPA SYBR FAST qPCR

Master Mix (KK4605). Analysis was performed on a QuantStudio 3 PCR System (Thermo Fisher Scientific) with the following primers:

Fosl1-F1: 5'- ATGTACCGAGACTACGGGGAA -3' (in exon1), Fosl1-R1: 5'- CTGCTGCTGTCGATGCTTG -3' (in exon2). This pair of primers was used to generate Supplemental Fig. S2.1A.

Fosl1-F2: 5'- CCAGGACCCGTACTTGAACC-3' (in exon4), Fosl1-R2: 5'- AGGAGTGTAGGAGAGCCCAG-3' (in exon4). This pair of primers was used to generate Fig. 2,6D.

18s-F: 5'- ACCGCAGCTAGGAATAATGGA -3',

18s-R: 5'- GCCTCAGTTCCGAAAACCA -3'.

The $2^{\Delta\Delta Ct}$ method was used to analyze the relative changes in gene expression normalized against 18s rRNA expression.

Western blotting analysis

Protein was isolated from tissues using RIPA buffer (Sigma-Aldrich, R0278). Protein concentrations were determined using BCA Protein Assay Reagent (Thermo Fisher Scientific, 23225), followed by measurement with NanoDrop. Protein samples were mixed with 4X Laemmli sample buffer (Bio-Rad, 161- 0747) and 20-40 μg protein was loaded and separated by SDS-PAGE gel electrophoresis. The proteins were transferred to a polyvinylidene fluoride (PVDF) membrane (Millipore), blocked in 5% fat-free milk for 1 hour at room temperature, and then incubated with the following primary antibodies diluted in 5% milk overnight at 4°C: Gapdh (Thermo Fisher Scientific, MA5-15738), Myomaker (customized, mouse monoclonal), Fosl1 (Santa Cruz Biotechnology, sc-28310). The HRP-conjugated secondary antibodies: Donkey anti-sheep IgG-HRP (Santa Cruz Biotechnology, sc-2473), Goat Anti-Mouse IgG

(H+L)-HRP Conjugate (Bio-Rad, 170-6516) and Goat Anti-Rabbit IgG (H + L)-HRP Conjugate (Bio-Rad, 170-6515) were diluted at 1:5,000. Immunodetection was performed using Western Blotting Luminol Reagent (Santa Cruz Biotechnology, sc2048).

Figures and tables

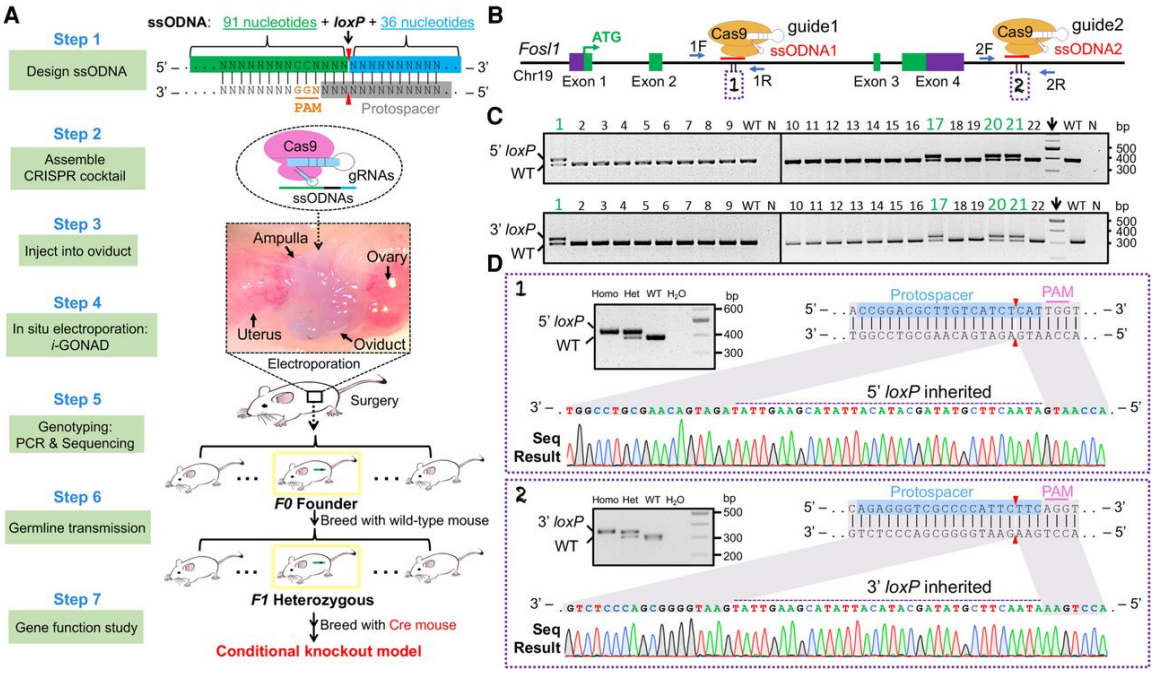

Figure 2.1: Generation of a conditional allele by *i*-GONAD: design and a proof-of-principle test. (A) Schematic illustration of the strategy to generate a conditional allele by *i*-GONAD. The necropsy image was taken to show the anatomical location of the oviduct with a blue ink indicator. (B) Fosl1 gene structure and relative positions of ssODNA, gRNA, and genotyping primer. (ssODNA) Single-stranded oligo DNA. (C) Fosl1 genotyping results for the F1 generation. Top row detects 5′-loxP insertion by primer pair 1F&1R; bottom row detects 3′-loxP insertion by primer pair 2F&2R; 5′-loxP band size is 426 bp; 3′-loxP is 351 bp. Mouse that inherited both 5′- and 3′-loxP is highlighted in green. (Arrow) DNA marker lane, (N) negative control of PCR (water). (D) Validations of loxP sites by Sanger sequencing.

A

Gene	Gene locus[1]	Molecular type[2]	Expression[3]	Imprinted
Plagl1	Chr10: 13,090,788–13,131,694	Transcription factor	Endocardial cell	Yes
Ak040954	Chr12: 32,751,319–32,770,956	Unknown	Unknown	N/A
Clcf1	Chr19: 4,214,238–4,223,490	Cytokine	Satellite cell	N/A
Gm44386	Chr6: 86,513,891–86,516,273	lncRNA	Unknown	N/A

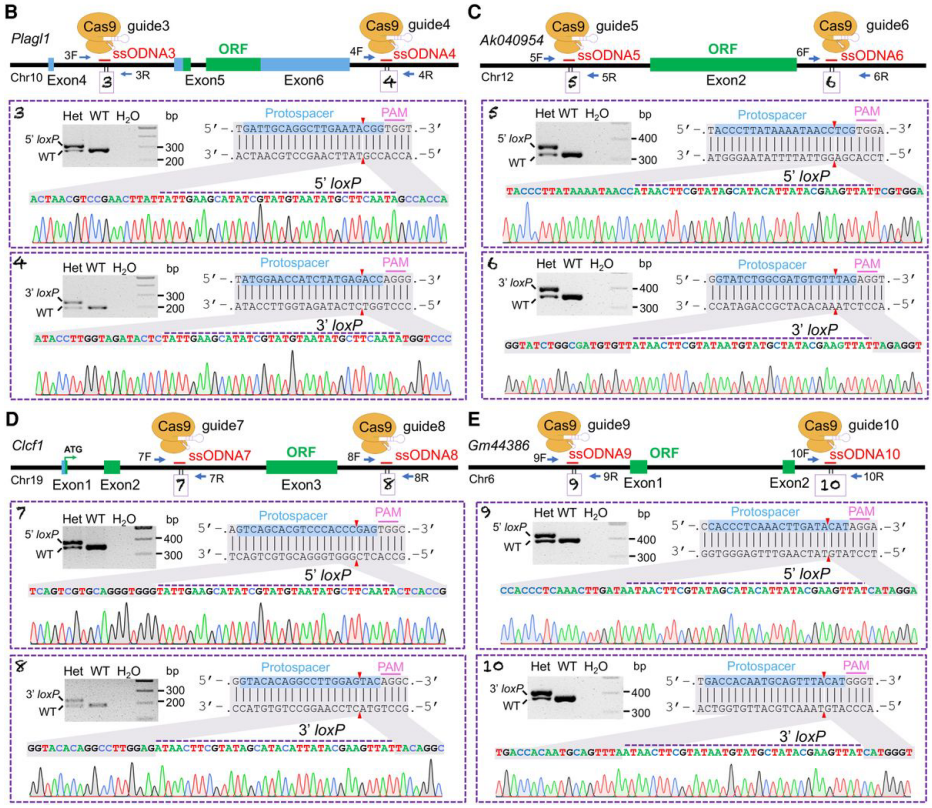

Figure 2.2: Generation of conditional alleles for another four genes by the *i*-GONAD method. (A) Gene information: [1]coordinates as of mouse GRCm38/mm10 genome assembly; [2]NCBI annotation; [3]query of Tabula Muris single-cell RNA sequencing data. (N/A) Data not available. (B–E) Gene structures and relative positions of ssODNA, gRNA, and genotyping primer for Plagl1 (B), Ak040954 (C), Clcf1 (D), and Gm44386 (E) genes. For Plagl1, 5′- and 3′-loxP bands are 312 bp and 234 bp; for Ak040954, 5′- and 3′-loxP bands are 361 bp and 391 bp; for Clcf1, 5′- and 3′-loxP bands are 389 bp and 222 bp; for Gm44386, 5′- and 3′-loxP bands are 431 bp and 415 bp. Boxed panels showed sequencing verifications of loxP sites in F1 generations. (Het) Heterozygous.

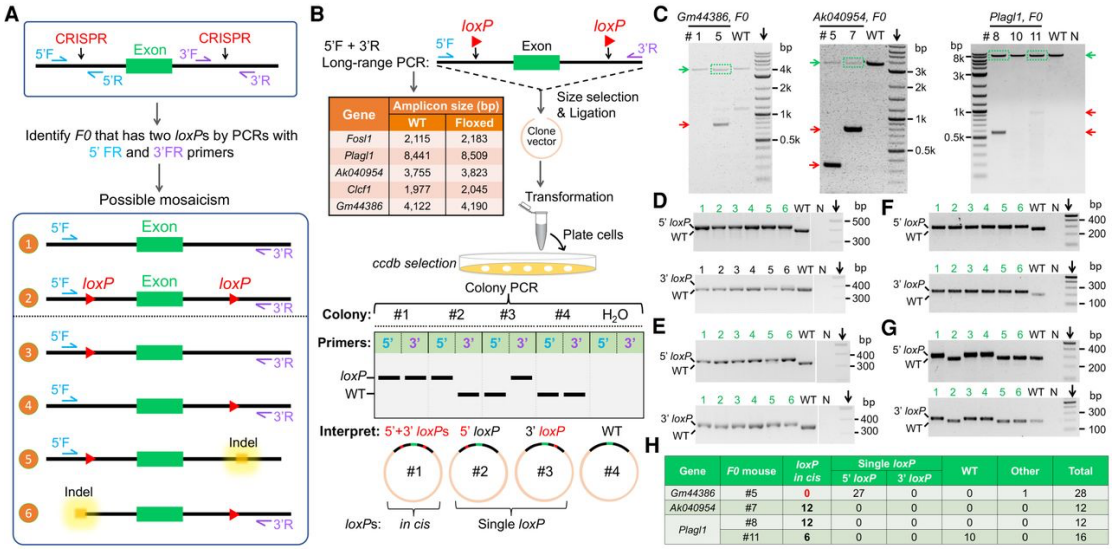

Figure 2.3: Validations of floxed alleles by long-range genotyping PCR. (A) Illustration of the potential mosaicism of F0 founders. Although founders with 5′- and 3′-loxP insertions can be separately identified by genotyping PCR using 5′F + 5′R and 3′F + 3′R primers, this cannot distinguish whether loxP insertions are in cis or in trans. (B) Schematic to show the design and major steps of genotyping strategy. (C) DNA electrophoresis results of long-range PCR. The DNA bands enclosed in the green box were purified and cloned into vectors. (D–G) Representative genotyping results of bacterial colonies from cloning of the purified long-range PCR products for founder #5 of the Gm44386 gene (D), founder #7 for the Ak040954 gene (E), and founder #8 (F) and #11 (G) for the Plagl1 gene. (H) Summary of bacterial colony genotyping results.

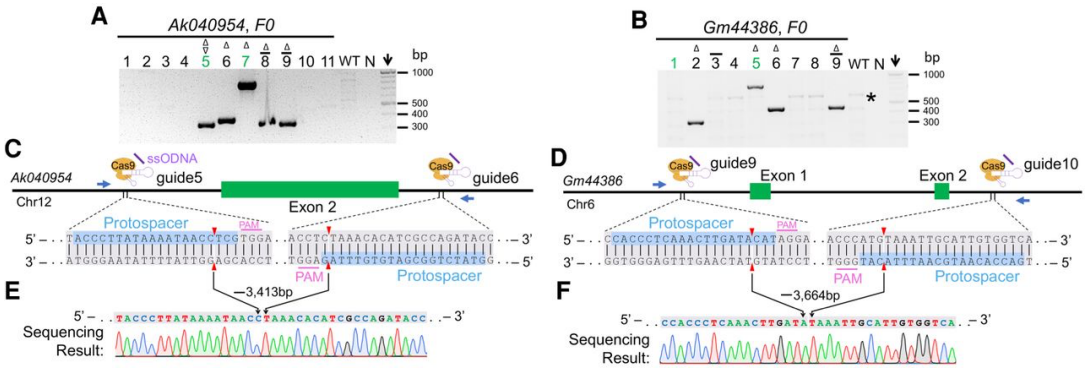

Figure 2.4: Null alleles of *Ak040954* and *Gm44386* genes generated by the *i*-GONAD method. (A,B) Genotyping results of Ak040954 (A) and Gm44386 (B) for the F0 generation using primer pairs shown in C and D. The mice #5 to #9 in A and mice #2, #5, #6, and #9 in B showed large deletions. The star in B indicates a faint, nonspecific band. Note that WT or floxed alleles are too large to be detected in current PCR conditions. (C,D) Gene structures and positions of gRNA and genotyping primers for Ak040954 (C) and Gm44386 (D) genes. (E,F) Sanger sequencing results of founder #9 and #6 as shown in A and B, respectively. For all panels: (WT) wild-type, (N) negative control (water), green ID highlights founders with floxed alleles, (arrow) DNA marker lane, mice with single-side loxP integration are indicated by a bar over the ID, (Δ) deletions, (▿) large insertions.

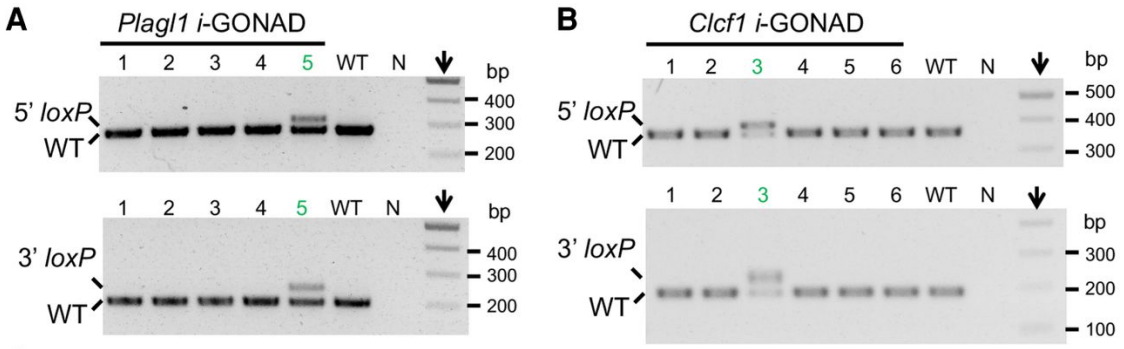

C

Gene Symbol	F0 founder	loxP in cis	Single loxP		WT	Other	Total
			5' loxP	3' loxP			
Plagl1	#5	**7**	1	2	5	1	16
Clcf1	#3	**5**	0	0	10	1	16

Figure 2.5: Testing *i*-GONAD for generation of conditional alleles using C57BL/6J mice.

(A) Plagl1 genotyping results of E12.5 embryos. For the 5′ gRNA region, WT band is 278 bp, loxP band is 312 bp; for the 3′ gRNA region, WT band is 200 bp, loxP band is 234 bp. (B) Clcf1 genotyping results for E12.5 embryos. For the 5′ gRNA region, WT band is 355 bp, loxP band is 389 bp; for the 3′ gRNA region, WT band is 188 bp, loxP band is 222 bp. (C) Summary of bacteria colony genotyping results shown in Figure S2.10C,D.

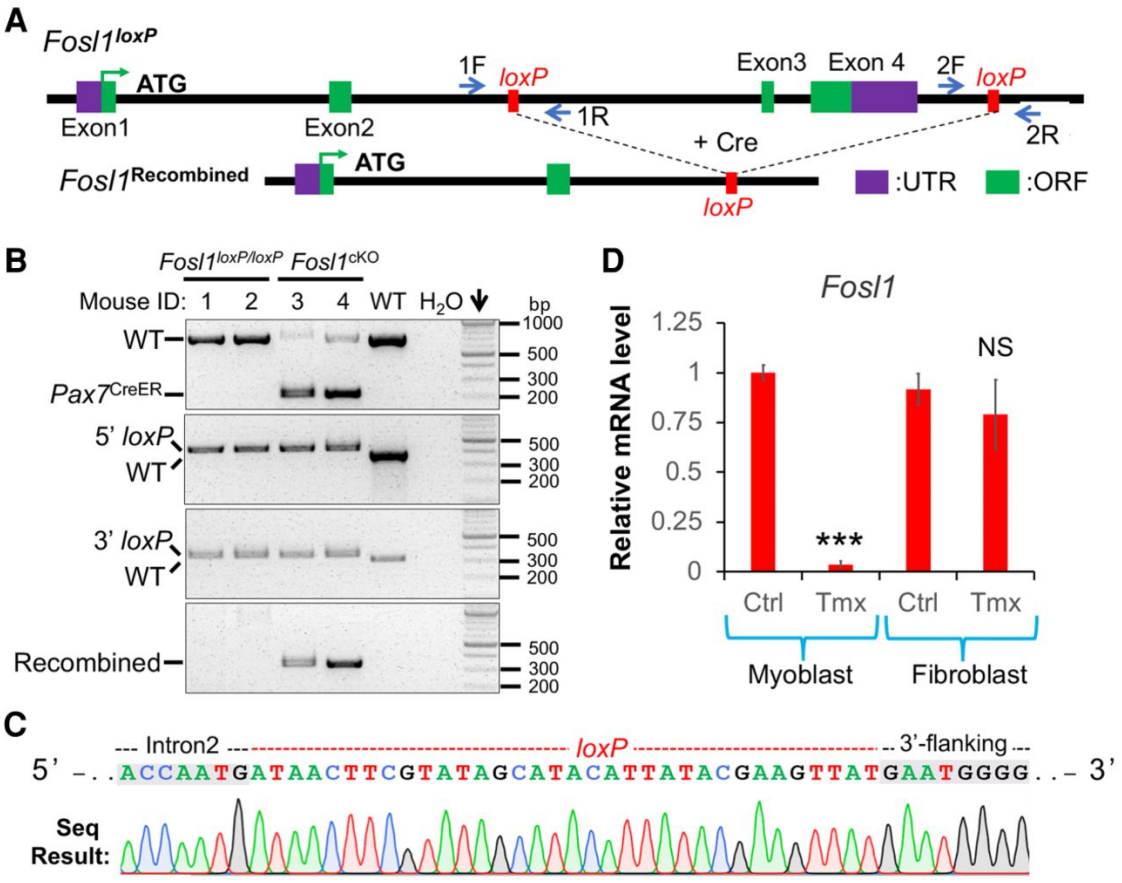

Figure 2.6: Successful recombination of the Fosl1 floxed allele mediated by Cre. (A) Gene structures of the Fosl1loxP and recombined alleles following Cre-mediated DNA recombination. (B) Genotyping results of adult muscle tissues from Fosl1loxP/loxP and littermate Fosl1cKO mice. 5′- and 3′-loxP were detected by primers 1F + 1R and 2F + 2R, respectively. The floxed allele was detected by primers 1F + 2R. (C) Sanger sequencing result that validated DNA recombination in Fosl1cKO muscle sample. (D) qPCR that measured Fosl1 expression in myoblasts and fibroblasts isolated from the Fosl1cKO mice. qPCR primers are located in exon 4 which is floxed. (Ctrl) Vehicle control, (Tmx) 4-OH tamoxifen. (***) $P < 0.001$, (NS) not significant. Data are mean ± SEM.

Supplemental Figures

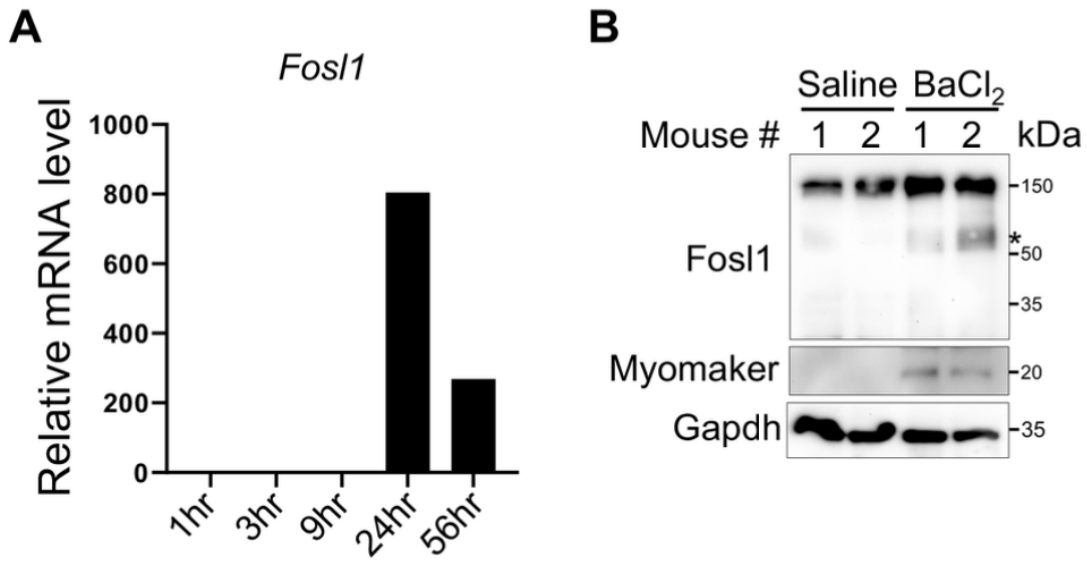

Figure S2.1: Induction of Fosl1 expression in muscle tissue following BaCl2 induced injury.

(A) qPCR measurements of Fosl1 mRNA levels at different hours (hr) following muscle injury.

(B) Western blotting results of muscle tissues at 48 hrs post injury, * highlights the specific band. Myomaker blot serves as a positive control of injury response.

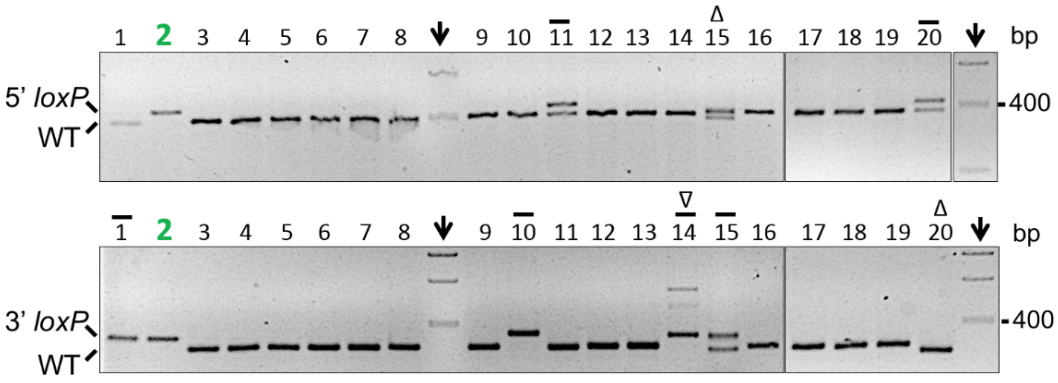

Figure S2.2: Fosl1 genotyping results of the F0 generation. Detection of 5'–loxP (top row) and 3'–loxP (bottom row) insertions using primer pairs 1F&1R and 2F&2R shown in Fig. 2.2B. 5'– and 3'–loxP band sizes are 426 bp and 351 bp, respectively. #2 founder mouse that showed simultaneous 5'– and 3'–loxP insertions is highlighted in green; arrow, DNA marker lane; mouse with single loxP integration is indicated with a bar on top of ID; Δ, deletions; ▿, large insertions.

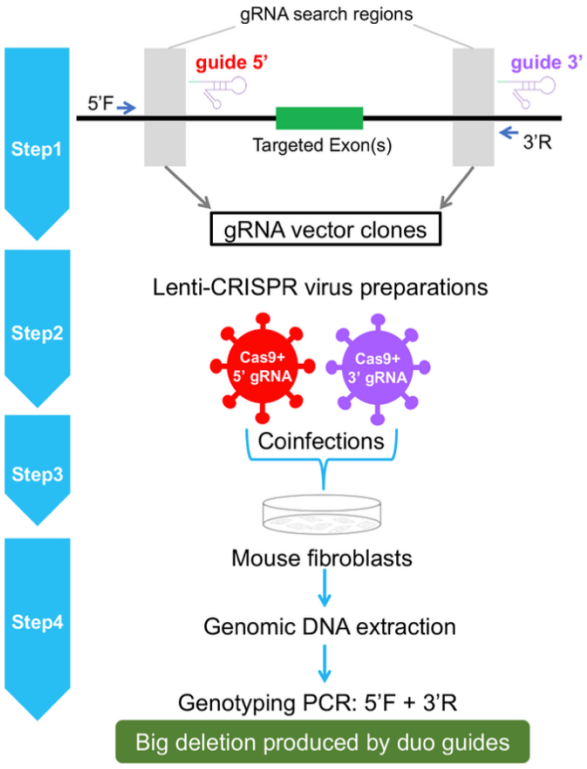

Figure S2.3: A workflow to test gRNA editing efficiency in mouse fibroblasts. Candidate gRNAs with high on-target scores and low risk of off-targeting were cloned into lenti- CRISPR vectors. Efficiency of each gRNA pair (one gRNA from each intron) was tested in fibroblasts. Two days after infections, genotyping PCR was performed with primers 5'F + 3'R. The gRNA pair that can efficiently generate large truncations were chosen for in vivo *i*-GONAD experiments for loxP insertions.

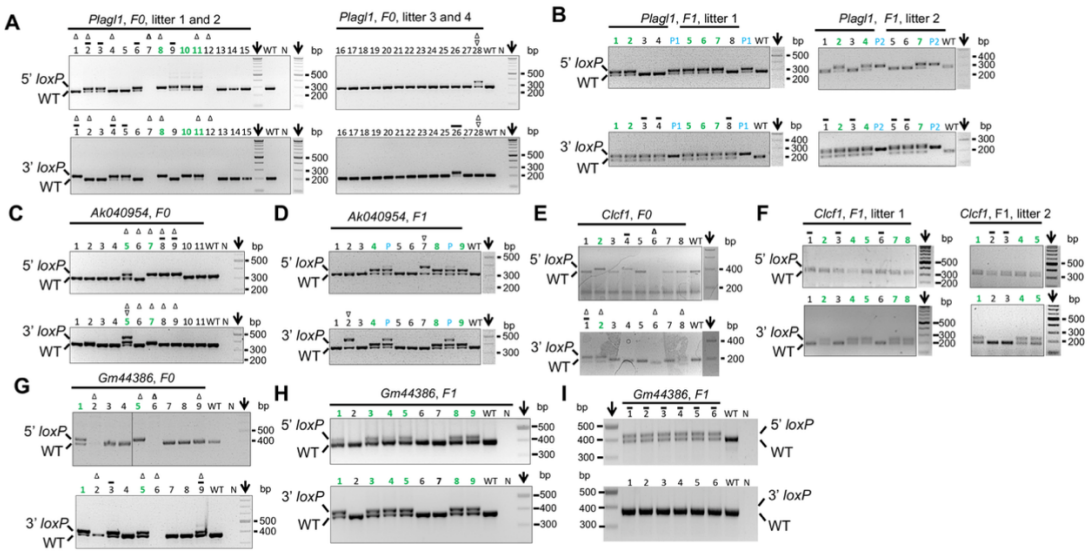

Figure S2.4: Genotyping results of F0 and F1 generations. (A) Plagl1 genotyping results of F0 generation. The 5'– and 3'–loxP band sizes are 312 bp and 234 bp, respectively. (B) Plagl1 genotyping results of F1 generation from breeding of #10 mouse in A. P1: positive control (founder mouse #10); P2: positive control (founder mouse #8). (C) Ak040954 genotyping results of F0 generation. 5'– and 3'–loxP band sizes are 361 bp and 391 bp, respectively. (D) Ak040954 genotyping results of F1 generation from breeding of #5 founder mouse in C. P: positive control (founder mouse #5). (E) Clcf1 genotyping result of F0 generation. 5'– and 3'–loxP bands are 389 bp and 222 bp, respectively. (F) Clcf1 genotyping results of F1 generation from breeding of #2 founder mouse in E. (G) Gm44386 genotyping results for F0 generation. 5'– and 3'–loxP bands are 431 bp and 415 bp, respectively. (H,I) Gm44386 genotyping results for F1 generation from breeding of #1 founder (H) and #5 founder (I). For all panels, N: negative control (water); green ID highlight mice that showed simultaneous 5'– and 3'–loxP insertions; arrow, DNA marker lane; mouse with single-side loxP is indicated with a bar on top of ID; Δ, deletions; ▿, big insertions.

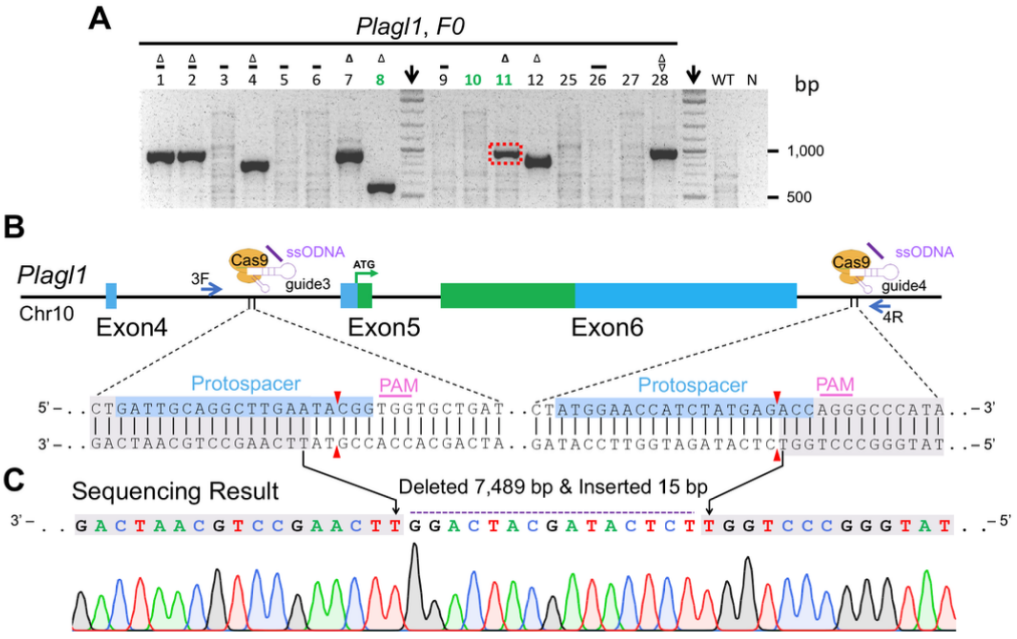

Figure S2.5: Deletions of exons 5 and 6 of Plagl1 gene using *i*-GONAD method. (A) Plagl1 genotyping of F0 generation using primers shown in B. Note that WT and floxed alleles are too large thus not detected in current PCR condition. Mice #1, #2, #4, #7, #8, #11, #12, #28 showed specific bands of large deletions. WT: wild-type; N: negative control (water); green ID highlight founders that showed simultaneous 5'– and 3'–loxP insertions; arrow, DNA marker lane; mouse with single-side loxP integration is indicated with a bar on top of ID; Δ, deletions; , large insertions. (B) Plagl1 gene structure. (C) Sanger sequencing result for the null allele shown in A (red box).

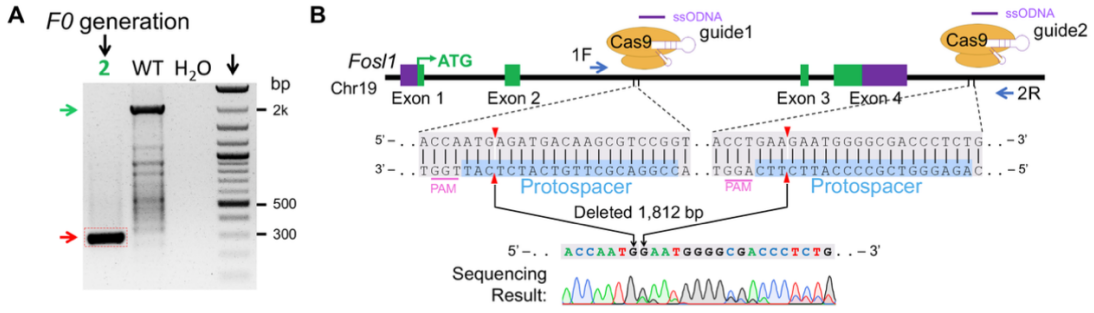

Figure S2.6: Deletions of exons 3 and 4 of Fosl1 gene by *i*-GONAD method. (A) Fosl1 genotyping of F0 generation using primers shown in B. WT allele is 2,115 bp (green arrow). Note the absence of the WT and loxP bands for #2 sample could be caused by biased amplification of the smaller truncated allele (red arrow). (B) Fosl1 gene structure. Sanger sequencing result for the null allele shown in A (red box).

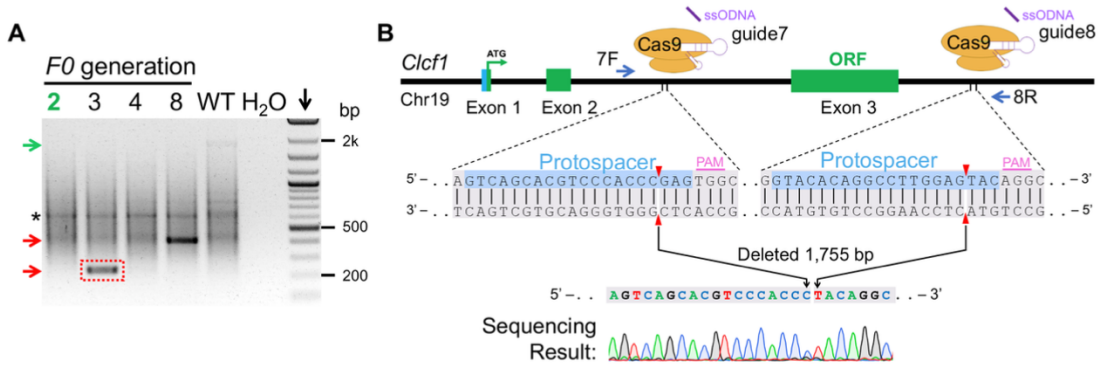

Figure S2.7: Deletion of exon 3 of *Clcf1* gene using the *i*-GONAD method. (A) Clcf1 genotyping of F0 generation using primers shown in B. WT band should be 1,977 bp (green arrow). Red arrows point to the PCR amplifications of null alleles. Note that current PCR condition is not suitable to detect large-sized WT or floxed alleles. (B) Clcf1 gene structure. Sanger sequencing results for the null allele shown in A (red box).

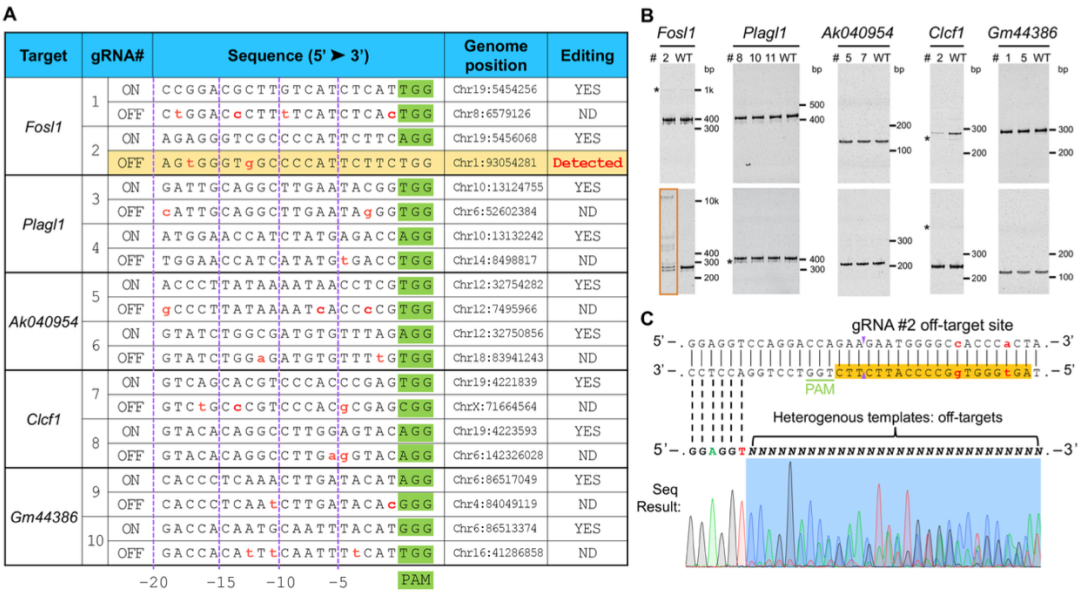

Figure S2.8: Examining off-targeting from *i*-GONAD experiments. (A) Information about top-predicted off-targeting sites for gRNAs used to produce floxed alleles. ND: not detected. Mismatches were highlighted in red. Genome positions are coordinates of mouse GRCm38/mm10. (B) Polyacrylamide gel electrophoresis results for examinations of off-target editing. Top panels are predicted off-sites for 5' gRNAs; lower panels are predicted off-sites for 3' gRNAs. Founder mice that contained floxed alleles were selected for off-targeting evaluations. Asterisks highlight the DNA species that universally appeared in all samples including WT (a mixture of C57BL/6J and CD-1 genomic DNA, as a control of any artifact due to single nucleotide polymorphism). (C) Sanger sequencing result of the off-target region for gRNA #2.

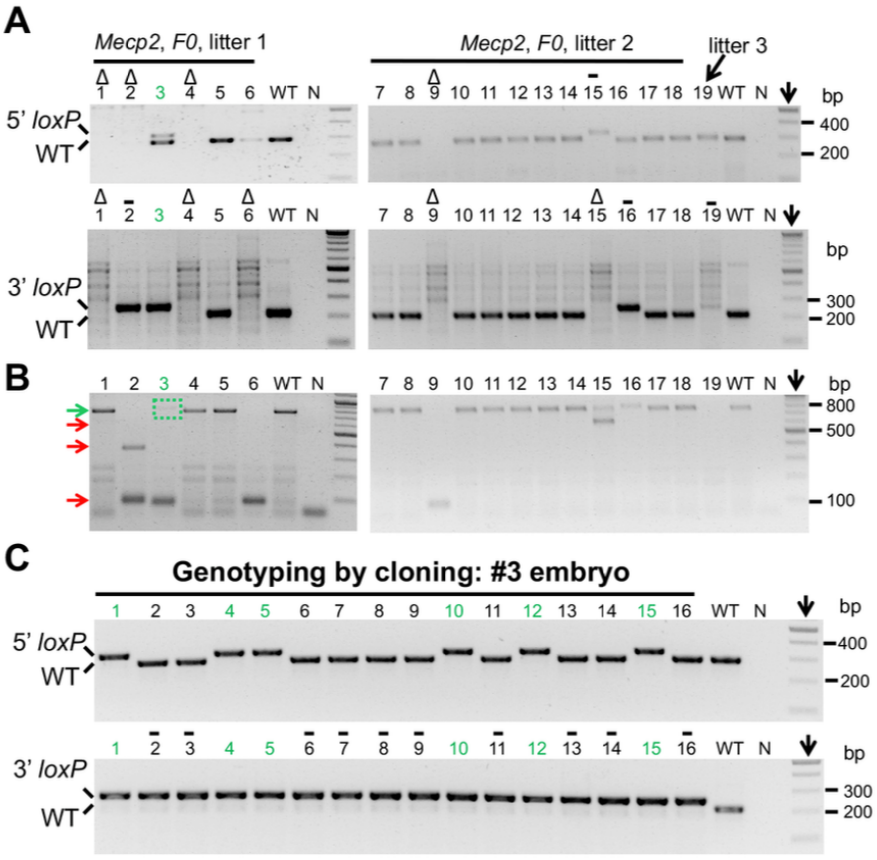

Gene Name	F0 founder	loxP in cis	Single loxP		WT	Other	Total
			5' loxP	3' loxP			
Mecp2	#3	**6**	0	10	0	0	16

Figure S2.9: Test of *i*-GONAD on *Mecp2* gene by using symmetric ssODNs. (A) Mecp2 genotyping results of E12.5 mouse embryos. Top panels: 5' gRNA region (WT band is 287 bp, loxP band is 327 bp). Lower panels: 3' gRNA region (WT band is 218 bp, loxP band is 258 bp). Note only embryo #3 was positive for both 5'– and 3'–loxP. (B) Long-range genotyping PCR results. WT band is 773 bp, floxed-allele band is 853 bp. Green arrow points to the region of WT and floxed-allele amplicons. Red arrows point to amplicons of null alleles. Note the weak band enclosed by the green box appeared slightly larger than WT. (C) Genotyping results of bacterial colonies from cloning of the purified long-range PCR products (green box in B) for embryo #3. (D) Summary of bacterial colony genotyping results.

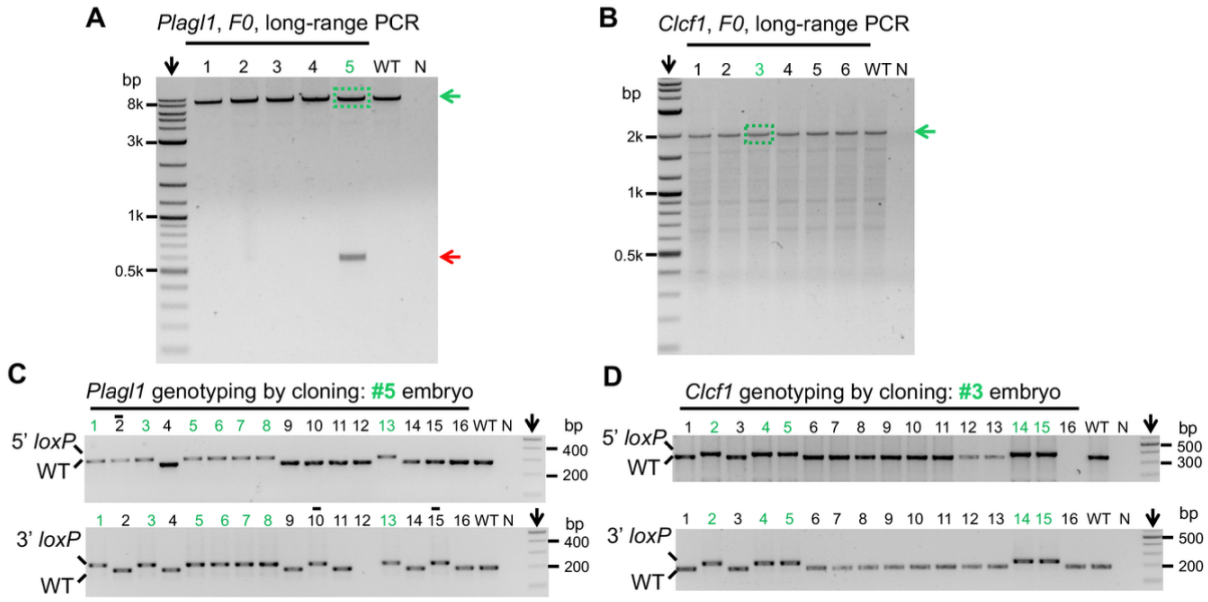

Figure S2.10: Genotyping analyses of conditional alleles produced from C57BL/6J mice.

(A) Long-range genotyping PCR results for Plagl1 gene (WT band is 8,441 bp, floxed-allele band is 8,509 bp). Red arrow points to one null allele. (B) Long-range genotyping PCR results for Clcf1 gene (WT band is 1,977 bp, floxed-allele band is 2,045 bp). (C,D) Genotyping results of bacterial colonies from cloning of the purified long-range PCR products enclosed by green boxes in A and B.

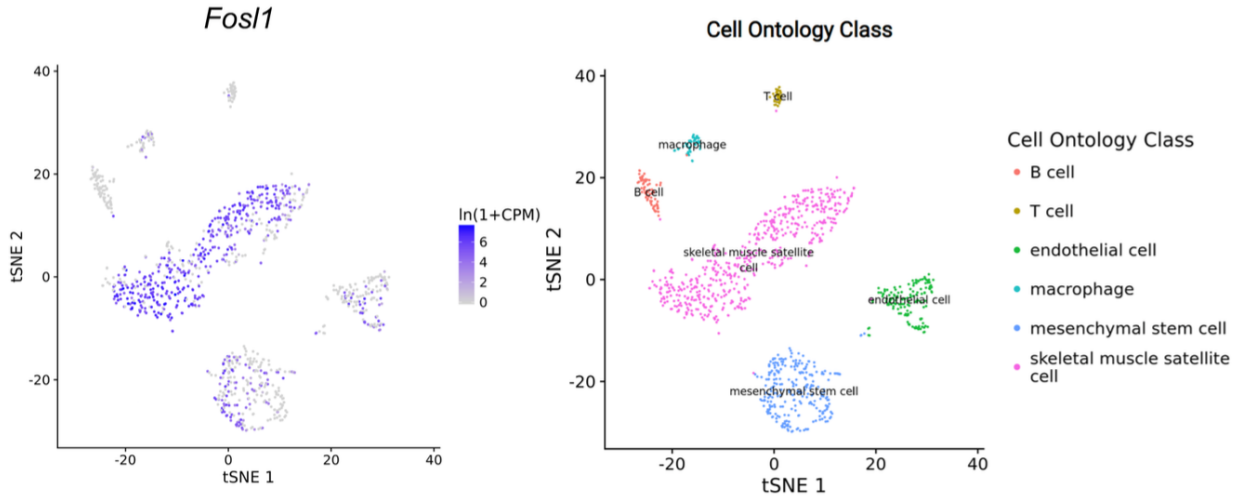

Figure S2.11: Expression of Fosl1 gene in various cell types within mouse muscle tissue.

Fosl1 expression data in single-cell RNA sequencing dataset of adult mouse muscles(Schaum et al., 2018). Note that in addition to myoblasts (labelled as satellite cell), Fosl1 expression was also detected in fibroblasts (labelled as mesenchymal stem cell), endothelial cells and macrophages.

Table 2.1 Summary of *loxP* integration efficiency

	F0 generation				*F1* generation			
Gene	Only 5′ *loxP*	Only 3′ *loxP*	Two *loxPs*	# Genotyped	Only 5′ *loxP*	Only 3′ *loxP*	Two *loxPs*	# Genotyped
Fosl1	2	4	1	20	0	0	4	22
Plagl1	4	4	3	28	0	7	8	15
Ak040954	2	0	2	11	0	0	6	19
Clcf1	1	1	1	8	5	0	8	13
Gm44386	1	2	1	9	3	4	6	18
Totals	10 (13.2%)	11 (14.5%)	8 (10.5%)	76	8 (9.2%)	11 (12.6%)	32 (36.8%)	87

Table 2.1: Summary of *loxP* integration efficiency.

CHAPTER 3

FOSL1 IS REQUIRED FOR SKELETAL MUSCLE REGENRATION

Introduction

Muscle stem cells, also known as satellite cells (SCs), are a crucial component of skeletal muscle tissue involved in maintaining muscle homeostasis and facilitating regeneration (Lepper et al., 2011; Mauro, 1961; Sambasivan et al., 2011; Seale et al., 2000). During periods of muscle quiescence, SCs reside beneath the basal lamina of muscle fibers and express the Pax7 transcription factor, which marks their quiescent state(Mauro, 1961; Seale et al., 2000).
In response to muscle damage or exercise-induced stress, SCs undergo activation, characterized by the expression of myogenic determination factor 1 (MyoD1), and transition from a quiescent to a proliferative state(Zammit et al., 2004). Activated SCs, referred to as myoblasts, then engage in a series of processes that contribute to muscle regeneration. They undergo proliferative expansion, generating a pool of myogenic precursor cells, and subsequently differentiate into myotubes, which fuse with existing muscle fibers or with each other to repair damaged muscle(Lepper et al., 2011; Sambasivan et al., 2011).

The progression of SCs through different stages of the myogenic lineage is tightly regulated by a complex interplay of intrinsic and extrinsic factors (Rocheteau et al., 2012; Rodgers et al., 2014). Disturbances in these regulatory mechanisms can lead to muscle wasting conditions, including muscular dystrophy, cachexia, and sarcopenia (Chakkalakal & Brack, 2012; Dumon et al., 2015). Therefore, understanding the molecular basis of SC activation and

differentiation is essential for developing strategies to enhance their regenerative potential (Rocheteau et al., 2012; Rodgers et al., 2014).

Of note, the technical procedure of isolating SCs from muscle tissues poses challenges due to the potential disruption of their quiescent state and can lead to accidental activation of SCs using the conventional tissue dissociation methods (Cerletti et al., 2008; Montarras et al., 2005; Sacco et al., 2008; Sherwood et al., 2004).To avoid this caveat and maintain the real quiescence state of the isolated SCs, researchers have explored pre-fixation of muscle tissue with paraformaldehyde (PFA) before the enzymatic digestion of muscle tissues. The pre-digestion fixation preserves the quiescent state of SCs (Machado et al., 2017; van den Brink et al., 2017; van Velthoven et al., 2017).

While the function of several AP-1 family transcription factors (Atf3, Fos) during muscle regeneration has been reported (Almada et al., 2021)(Zhang et al., 2022, bioRxiv), largely remains unknown is the function of Fosl1 gene. Recent studies have noted strong induction of Fosl1 gene in SCs when they transit from quiescent state to activation state (Machado et al., 2017; van den Brink et al., 2017; van Velthoven et al., 2017). Further investigation into the function of *Fosl1* gene and its downstream target genes could provide valuable insights into the regenerative activities of SCs. In this study, we uncovered the function of Fosl1 in SC activation and muscle regeneration. Compared with the quiescent SCs, the expression of *Fosl1* is rapidly induced in activated SCs. Specific knockout *Fosl1* gene from SCs causes drastic muscle regeneration defect post muscle injury, and repetitive muscle injuries ultimately results in the complete loss of regeneration in Fosl1 mutant mice. Our RNA-seq analysis of the injured muscle tissue demonstrate that in the Fosl1 conditional knockout group, the expression of muscle stem cell markers such as *Pax7* and myogenic differentiation markers including *MyoD1, Myf5, MymK*,

and *MymX* genes are significantly down-regulated. At the cellular level, deletion of Fosl1 from freshly isolated SC leads to SC activation defect and failure of cell cycle entry. By contrast, deletion of Fosl1 gene from post-activation SCs of mice has neglectable effect for SC proliferation. Consistently, in immortalized human myoblasts, CRISPR knockout of *Fosl1* does not affect the proliferation and normal myogenic differentiation and fusion program. Conversely, over-expression of *Fosl1* also does not affect proliferation or differentiation of the immortalized human myoblasts. Together, our results suggest that *Fosl1* plays a crucial role for the early activation of muscle stem cells and is not essential for cell proliferation at a later stage.

Results

Fosl1 expression is promptly induced during early SC activation and myoblast proliferation but not in the differentiated myofiber.

Previous studies have indicated that *Fosl1* is expressed in various cell types within mouse muscle tissue, including satellite cells, fibroblasts, endothelial cells, and macrophages (Schaum et al., 2018; Shang et al., 2021). Our previous work demonstrated that Fosl1's expression, both at the mRNA and protein levels, is induced by muscle injury(Shang et al., 2021). In order to examine the expression pattern of *Fosl1* during satellite cell (SC) activation, we fixed the skeletal muscle tissues of wildtype C57BL/6 mice using PFA by following an established protocol (Machado et al., 2021). Quiescent satellite cells (QSC) were then isolated by enzymatic dissociation of muscle tissues followed by SCs purification using MACS sorting (Fig. 3.1A). In parallel, we also isolated SCs from non-fixed muscle tissues (freshly isolated satellite cells, FISC), which were then cultured for 24 hours, 48 hours, and 72 hours before being fixed and processed for immunostaining of Fosl1, MyoD and Pax7 proteins (Fig. 3.1A). Interestingly, Fosl1 protein was initially not detected in QSCs and can be detected in FISCs and ASCs. The

induction of Fosl1 expression in FISCs preceded that of MyoD. This expression pattern for Fosl1 and MyoD aligns well with the mRNA expression levels of these genes detected by single-nucleus RNA-sequencing (Fig. S3.1).

The co-culture of SCs with the myofiber represents a key *ex vivo* model to study the early-stage activations of SCs. Thus, we also examined the expression pattern of Fosl1 in SCs cultured on single myofibers. Our results revealed that Fosl1 was exclusively expressed in ASCs and its expression level gradually increased with SC activation (Fig. 3.1C). It is noteworthy that the FISCs (Fig. 3.1A) may differ from SCs attached to freshly isolated myofibers (0 hours, Fig. 3.1C) because the isolation of FISCs requires harsher enzyme digestion condition may have activated SCs.

Through gene set enrichment analysis (GSEA) of a published scRNA-seq dataset, we found that Fosl1 expression is positively correlated with SC activation markers and negatively correlated with SC quiescence markers (Fig. S3.2C). This analysis utilized differentially expressed genes obtained from Fosl1+ SC population (Fosl1 CPM greater than 6) compared to Fosl1- SC population (Fosl1 CPM of zero) (Fig. S3.2B).

We then checked the expression of *Fosl1* gene in the different time points of myogenic differentiation by Western blot and qPCR analysis. Interestingly, Fosl1 expression can be detected in proliferating human myoblasts but dramatically decreased in differentiating muscle cells (Fig. 3.1D). This result is consistent with our differentiation time-course RNA-seq result of the human myoblast (Fig. 3.1E and G). Similar expression changes were observed for mouse myogenic C2C12 cell line (Fig. 3.1F). In addition to Fosl1, our RNA-seq analysis also revealed the expression changes of other AP-1 family proteins along the human myogenic differentiation (Fig. 3.1E). In summary, our findings demonstrate that Fosl1 is rapidly induced during early SC

activation and maintains expression throughout myoblast proliferation until myoblast differentiation. This suggests that Fosl1 may play a crucial role in SC activation and myoblast proliferation.

Fosl1 gene is indispensable for injury-induced muscle regeneration.

Because Fosl1 global knockout mice die as embryos, we generated satellite cell specific Fosl1 knockout mouse model(Shang et al., 2021). Specifically, the $Fosl1^{loxP/loxP}$ mice were bred with $Pax7^{CreERT2/+}$ mice and the progenies were intercrossed to conditional knockout (cKO) mice ($Fosl1^{loxP/loxP}$ -$Pax7^{CreERT2/+}$ genotype) and the control mice ($Fosl1^{loxP/loxP}$ - $Pax7^{+/+}$ genotype) (Fig. 3.2A). To induce the knockout of Fosl1 in satellite cells (SCs), tamoxifen (TMX) was administered five times every other day by intraperitoneal injections, followed by a 14-day TMX diet (Fig. 3.2B). We then assessed muscle regeneration phenotype of control and knockout (cKO) mice at day 5 post injury (5 dpi) and day 14 post injury (14 dpi) of tibialis anterior muscle (TA). We also assessed the regeneration potential of SCs by repetitive injuries (Fig. 3.2B).

H&E staining of muscle cross-sections of the 5 dpi TAs revealed a lack of regenerating fibers in cKO mice, while they were abundantly present in control mice. Additionally, cKO TAs exhibited a greater infiltration of immune cells and adipose tissue compared to control TAs (Fig. 3.2C). There were no significant differences in TA muscle weight and cross-sectional area (CSA) between cKO and control mice, although there was a trend suggesting that the CSA of cKO TAs might be smaller than that of control TAs (Fig. 3.2E, left). At 14 dpi, both cKO and control TAs had largely completed the regeneration process, but adipose tissue remained in some regions of cKO TAs (Fig. 3.2D). Muscle weight and CSA of cKO TAs were smaller compared to control TAs (Fig. 3.2E, left). The muscle regeneration defect was more pronounced in the cKO mice when they are challenged by a second time injury. In this case, we did not observe any

regenerating muscle fibers in the cKO muscle tissues at 5 dpi (Fig. 3.2F) and 14 dpi (Fig. 3.2G). Consistently, the muscle weight and the CSA were both significantly reduced in cKO group compared with WT group (Fig. 3.2H).

It is worth noting that there were no significant differences in body weight among genotypes in both regeneration schemes, suggesting that the loss of Fosl1 in SCs does not result in global muscle mass changes but is limited to the specific muscle tissue undergoing regeneration. Overall, these findings demonstrate the essential role of Fosl1 in proper muscle regeneration, particularly under conditions of repetitive injuries.

FOSL1 is not required for human myoblast proliferation and differentiation.

To understand the mechanism for the regeneration defect upon Fosl1 deletion, we performed loss-of-function study and generated human FOSL1-KO myoblast through CRISPR-Cas9-mediated genome editing (Fig. 3.3A). Briefly, the expression of Cas9 and three guide RNAs targeting the exon2 of human FOSL1 gene were delivered by lentiviral infection (Fig. 3.3B). Cells expressing Cas9 protein but without gRNA were regarded as WT control. FOSL1-KO cells were derived from single-cell sorting and clonal expansion culture. Genotyping and Sanger sequencing analysis identified four FOSL1-KO clones that carries different frameshift mutations (Fig. 3.3B). The depletion of FOSL1 protein in the KO clones were verified by immunostaining (Fig. 3.3C).

In all the following assays, the function of *Fosl1* was assayed by comparing the FOSL-KO cells with or without re-expression of *Fosl1* delivered by retroviral infections: FOSL1-KO cells + empty retrovirus (**KO** myoblast); FOSL1-KO cells + retrovirus expressing mouse Fosl1 ORF (**control** myoblast). This rescue group represents an isogenic condition which serves as a more rigorous control compared with parental cell line because the clonally derived KO cells

could potentially harbor undetected spontaneous mutations arised through the lengthy period of clonal expansion (Fig. 3.3A).

Using the KO cell lines, we first examined whether the loss of FOSL1 could affect human myoblast proliferation. Control and KO myoblasts were cultured in the growth medium supplemented with 5-ethynyl-2′-deoxyuridine (EdU) for 48h (Fig. 3.3D) and 72h (Fig. 3.3E). Quantifications of the EdU positive cells did not show any difference between the two groups (Fig. 3.3I), indicating that *FOSL1* is not required for human myoblast proliferation.

Our previous gene expression data showed that Fosl1 abruptly downregulated upon myogenic differentiation in both mouse and human myoblasts (Fig. 3.1F, 3.1G). To evaluate whether FOSL1 is required for human myoblast differentiation, we switched the culture medium to differentiation medium for four days. Before myogenic induction, the control and KO myoblasts showed similar expression levels of MYOD1, a master regulator of myogenic differentiation (Fig. 3.3F, Fig. 3.3J). After myogenic induction, the control and KO myoblasts also showed comparable expression levels of MYOG, a key transcriptional factor mediating the myogenic activity downstream of MYOD1 (Fig. 3.3G, Fig. 3.3J). The immunostaining of Myosin also showed no difference of myotube formation measured by differentiation index and fusion index (Fig. 3.3H, Fig. 3.3K). Collectively, genetic deletion of FOSL1 does not affect the proliferation, differentiation, or fusion of human myoblast.

Fosl1 is required for early activation of satellite cells post injury.

Fosl1 gene is not expressed in quiescent SCs (Fig. 3.1B, 3.1C). Indeed, deletion of Fosl1 did not affect the numbers of SCs marked by Pax7 immunostaining (Fig. 3.4A). Given the tight correlation of Fosl1 expression and the SCs activation, we then investigated whether Fosl1 is required for breaking the quiescent state and enter the cell-cycle. To address this, we isolated and

cultured single myofibers, where the SCs remain attached, from control and Fosl1-cKO mice in suspension with EdU for 60 hours. As expected, the mitogen enriched culture medium stimulated the SCs activation and the EdU incorporation for the control group (Fig. 3.4B, 3.4C). In comparison, majority of SCs from the of Fosl1-cKO group remained EdU– in the same culture condition. As a result, the total numbers of Pax7+ cells (Fig. 3.4B), the EdU+ cells (Fig. 3.4D) and the ratio of EdU+ (normalized to Pax7, Fig. 3.4E) were significantly reduced in Fosl1-cKO compared with control group. Together, these results indicate that Fosl1 is required for prompt activation and proliferation of SCs.

Deletion of FOSL1 gene from human myoblast did not affect the cell proliferation. We wonder whether this result can be reproduced in mouse myoblasts. Toward this goal, we added the 4-OH TMX to the culture medium of the freshly isolated Fosl1-cKO myoblasts. Prior to the cell isolation, these Fosl1-cKO mice did not receive TMX treatment. By this TMX treatment scheme (Fig. 3.4J), the isolated SCs from both control and Fosl1-cKO mice should normally express Fosl1 gene while the deletion of Fosl1 can be specifically induced in Fosl1 cKO mice precisely after the SCs activation. Indeed, the immunostaining validated the depletion Fosl1 expression in Fosl1-cKO mice after 4-OH TMX treatment (Fig. 3.4F, 3.4G). Concomitantly, a Cre-dependent sfGFP reporter of the Fosl1-cKO (genotype: $Pax7^{CreERT2/+}$ - $Fosl1^{loxP/loxP}$ - ROSA26Sor$^{tm5(CAG-Sun1/sfGFP)Nat}$) also showed prompt induction of sfGFP expression (Fig. 3.4F, 6H). As expected, EdU incorporation assay using the KO-authenticated myoblasts did not show any difference between the 4-OH TMX treatment group and the vehicle control group (Fig. 3.4I–K). Together, these results suggest that Fosl1 is only required for the stem cell activation and dispensable for the proliferation of stem cells post the activation.

Loss of Fosl1 from satellite cells caused drastic reductions of myogenic gene expression during muscle regeneration.

To gain more insights to the cellular and molecular changes in the Fosl1-cKO mice that lead to the drastic regeneration phenotype, we measured the gene expression changes in muscles at three-day post injury (3 dpi), the peak stage of muscle regeneration (Fig. 3.5A). Our muscle injury protocol involves the intramuscular injection of $BaCl_2$ and local accumulation of the myofiber-damaging compound often causes uneven damage and regeneration responses within the same pieces of muscle tissue. To reliably mark the $BaCl_2$ affected area, we performed intraperitoneal injection of evans blue dye (EBD) the day before injury. The EBD will label the dead myofibers and excluded by live cells. By this indicator, we can faithfully dissect the muscle tissues equally affected by injuries in both genotypes (Fig. 3.5A).

RNA was extracted from the dissected muscle tissues of four groups: control-injured (WTI), control-Noninjured (WTN), Fosl1-cKO-injured (KOI) and Fosl1-cKO-Noninjured (KON), each group has at least four mice. RNA samples were then reverse transcribed to generate cDNA for gene expression measurements. First, our qPCR analysis showed significant inductions of expressions for SC marker gene (*Pax7*), myogenic differentiation regulator (*MyoD*), and muscle fusion proteins (*MymK*, *MymX*) in the WT-injured group compared with the WT non-injured group (Fig. 3.5B–E). However, these injury-induced changes were largely blunted in the Fosl1-cKO group.

To gain a global view of the transcriptome changes, we performed the RNA-seq analysis using the same batch of RNA samples generated from above. Principal component analysis (PCA) was conducted to assess the within/between group variations (Fig. S3.5A-D) and revealed high similarities for samples from the same biological groups. Moreover, clear separation was

observed between the WTI versus KOI samples (Fig. S3.5A), WTN versus WTI samples (Fig. S3.5B) and KON versus KOI samples (Fig. S3.5C), but not between the WTN versus KON samples. The PCA analysis not only revealed the large changes between the two genotypes in the injury context (Fig. S3.5A), but also suggests loss of *Fosl1* in SC did not cause major transcriptional difference for the non-injured muscles where SCs remain quiescent (Fig. S3.5D). Differential gene expression analysis showed 345 genes with a fold change > 2 and p value < 0.01 for the injured *Fosl1* cKO muscles, compared with injured WT muscles (Fig. 3.5I). Majority of these genes were actually decreased in cKO group. Among the top ranked genes, expressions for *Pax7*, *MyoD*, *MyoG*, *Myomixer*, *Myomaker* were dramatically downregulated in KOI sample (Fig. 3.5F, 3.5J), which are consistent with our qPCR results (Fig. 3.5B–E). Gene ontology (GO) analysis for the genes that are significantly downregulated in KOI samples (versus WTI samples) showed highly significant enrichment for pathways related to "muscle structure development", "skeletal muscle contraction" , "skeletal muscle cell differentiation" and "tissue morphogenesis" (Fig. 3.5G, upper part and Fig. S3.5G). Genes that are upregulated in KOI samples showed significant enrichment for pathways in "neutrophil chemotaxis" , "peptidyl-amino acid modification" and "lipid and atherosclerosis", likely due to the neutrophil and adipocyte infiltrations in the KOI samples as shown by the histology analysis (Fig. 3.2C). Furthermore, the DE genes that are downregulated in KOI samples were also identified in PaGenBase and TRRUST ontology catteries. The enrichment results showed that these genes were specifically originated from C2C12 cells (an immortalized mouse myoblast cell line) and mainly regulated by *Pax3*, *MyoD* and *Myf5* (Fig. S3.5H), which indicates vast majority of the cells in injured muscle at 3 d.p.i are newly formed myoblast as a consequence of SC activation, which is lacked in KOI samples. Gene set enrichment analysis (GSEA) was also performed to

identify the key biological process in KOI samples. As expected, MyoD target genes are enriched in injured-control sample, suggesting the failure of *MyoD* induction in KOI samples (Fig. 3.5H). Meanwhile, we noticed the terms including "Myc targets" and "E2F targets" were also enriched, this indicates the cell proliferating activities were abundant in WTI samples but not in KOI samples (Fig. S3.5E-F). Lastly, by performing protein-protein interaction analysis carried out with STRING (physical score > 0.132) and BioGrid databases, we noticed the resultant physical interaction networks included "cell-cell junction and adhesion", "regulation of actin cytoskeleton", "muscle contraction" as well as "MAPK signaling pathway", which might be the upstream regulator of Fosl1 in SC activation (Fig. S3.5G-J). Collectively, our data demonstrates that during the early stages of muscle regeneration, the loss of Fosl1 leads to a decrease in the satellite cell (SC) pool due to the inability of SCs to activate. Consequently, the reduction of regenerating SCs caused significant defect in myoblast differentiation and regeneration in the KOI group compared with WTI group.

Discussion and Future direction

In this study, we investigated the role of Fosl1 in muscle regeneration. We observed that *Fosl1* expression is rapidly induced in activated muscle satellite cells, maintained in proliferating myoblasts and promptly decreased upon myogenic differentiation. Furthermore, repetitive muscle injury led to a complete loss of regeneration in muscle tissues where *Fosl1* was specifically deleted in SCs. At the cellular level, deletion of *Fosl1* in quiescent SCs impaired their activation and prevented entry into the cell cycle. In contrast, deletion of *Fosl1* gene in the post-activation SCs had negligible effects on cell proliferation. Moreover, the proliferation, differentiation, and fusion of human myoblasts were not affected by either Fosl1 knockout or overexpression. These results indicate a narrow window of Fosl1 function for the SCs activation

post injury, while *Fosl1* is not required for muscle stem cell proliferation post activation. Our RNA-seq analysis of injured muscle tissue revealed that the conditional knockout of *Fosl1* resulted in significant downregulation of muscle stem cell markers, including *Pax7*, myogenic differentiation markers including *MyoD1, Myf5, MyoG, MymK, MymX* genes, as well as cell-cycle related genes. These findings suggest that blockade of SC activation by *Fosl1* deletion has a profound effect on the subsequent steps of muscle regenerations *in vivo*.

Currently, the precise molecular mechanism by which Fosl1 activates SCs remains unknown. One tempting hypothesis is that, during muscle regeneration, the expression of MyoD in activated SC is controlled by Fosl1. In support of this hypothesis, earlier works identified AP-1 binding sites in the promoter regions of MyoD gene (Pedrazaalva et al., 1994). One future direction could ascertain this binding by performing Cut&Run analysis. Furthermore, sequencing analysis of the Fosl1 binding regions in the SCs could offer unbiased view of the downstream targets of Fosl1. One could also examine the 3D genome structure changes upon deletion of Fosl1 gene by performing the newest technology HiCAR(Wei et al., 2022) to analyze looping and chromatin accessibility changes simultaneously.

Although our RNA-seq analysis revealed profound changes of muscle tissues upon Fosl1 deletion, more accurate changes in SCs would need detailed profiling by single-cell/nucleus RNA-seq analysis. Recent advances in the epigenetic analysis comparing the quiescent SC with activated SCs revealed that the H3 lysin4 trimethylation (H3K3me3) marks were increased globally and the H3 lysine 27 acetylation (H3K27ac) marks were decreased (Machado et al., 2017). Interestingly, *Fosl1* was specially noted as an example gene to gain such H3K4me3 marks in activated SCs.

As another Fos family member, Fos, was noted to be instantly induced in isolated SC from 15 min to 2 h time window after the start of the enzymatic tissue disassociation procedure, where *Fosl1* began expression after 1h disassociation (Almada et al., 2021; Machado et al., 2021). Even though *Fos* was recently demonstrated to be essential for SC activation (Almada et al., 2021) during muscle regeneration, the regeneration phenotypes of Fos-cKO are much milder comparing to our Fosl1-cKO results (Fig. 3.2C-H). This suggests that Fosl1 might play a more vital role in controlling SC activation during muscle regeneration. Regardless, the early cues that activates AP-1 family gene expressions remain unknown. In SC, the signaling cascade by p38a/b MAPK/ERK might induce the expression of both Fos (Machado et al., 2017) and Fosl1 genes because treating SCs with ERK inhibitor can impede SC activation accompanied by reduced Fosl1 expression (Machado et al., 2021). Another key question concerns whether Fosl1 induces SCs activation by itself alone or by forming a conventional AP-1 heterodimer complex. If the latter is true, which of the three Jun family members, Jun, JunB and JunD, would be the real partner of Fosl1 in carrying out the hypothesized function.

Induction of *Fos* and *Fosl1* transcription appeared to be following earlier events that mediate SC activation. This includes the signaling transduction triggered by cytoskeleton rearrangements. In particular, recent studies by multiple groups reported the key role of the cellular projections in maintaining the quiescence of SCs. Upon injury or tissue dissociation, such cellular projection structures will quickly retract and trigger the Rac-to-Rho GTPase switch (Kann et al., 2022). From this context, Fosl1 might function as downstream mediator of mechanosensing pathway that regulate cell cycle reentry of SCs.

Methods

Animals

Fosl1$^{loxP/loxP}$ mice generated from our previous study (Shang et al., 2021) at the University of Georgia. Pax7$^{CreERT2(Fan)}$ mice were from The Jackson Laboratory (Stock 012476). ROSA26Sor$^{tm5(CAG-Sun1/sfGFP)Nat}$ mice were from The Jackson Laboratory (Stock 021039).

Tamoxifen, muscle injury and histology

Tamoxifen (Sigma-Aldrich T5648) was dissolved in ethanol (10 mg/mL). This stock solution was diluted in sesame oil (Sigma-Aldrich S3547) with a ratio of 1:9 before injection. Two milligrams of tamoxifen were administered by intraperitoneal injection. Muscle injury was induced by injecting 1.2% barium chloride (50 μL) into the tibialis anterior or gastroceus muscle. Evans Blue Dye (EBD) was resolved in ultrapure water to 10 mg/mL and intraperitoneally injected as 2.5 μL/g body weight of mice which were euthanized 24 hours later and TA muscles were harvested, weighed and embedded in OCT cooled by liquid nitrogen. Cryosectioning was performed and muscle samples were cross-sectioned as 10 μm thickness.

Single myofiber isolation and immunostaining

Single myofibers were isolated from the extensor digitorum longus (EDL) muscle by digestion with 0.2% collagenase A (Sigma) in DMEM at 37°C for 2 hours with gently hand-shaking every 20 minutes. After digestion, EDL muscle was gently titrated by different pore-sized glass pipettes. Freshly isolated single fibers could be either immediately fixed or cultured in DMEM supplied with 15% FBA and 1% chicken embryo extract (CEE). Single fibers were fixed in 4% PFA for 10 min, washed in 100 mM glycine three times each 10 min, followed by PBS wash for three times and blocking for 1 hr at room temperature. The primary antibody was incubated at 4°C for overnight. Fluorescence secondary antibody was diluted and incubated at

room temperature for 1 hr. Images were taken with a BioTek Lionheat Microscope System or Olympus FV1200 Confocal Laser Scanning Microscope.

Satellite cell isolation and culture

Entire hindlimb muscles from mice were collected and washed by PBS. Then the muscles were minced and digested with warm freshly isolated satellite cells (FISC) digestion medium (collagenase II and dispase B in DMEM) for 90~120 min in 37°C at 90 rpm, the digested muscles were washed and resuspended in cold DMEM and centrifuged at 500g 5min. Then added 1/10 diluted digestion medium in DMEM and digested for 30 min in 37°C at 70 rpm. The suspensions were then passed through a 20 G needle to release myofiber-associated SCs. Mononucleated cells were filtered with a 40-μm cell strainer and sorted by magnetic-activated cell sorting (MACS) according to the manufacture's manuals (Miltenyi Biotec). Briefly, cell pellets were resuspended in FACS buffer and incubated with Satellite Cell Isolation Kit, mouse (Miltenyi Biotec. Stock 130-104-268). Cell suspensions were loaded onto a LD column (Miltenyi Biotec. Stock 130-0420-901) in a magnetic field of a VarioMACS separator (Miltenyi Biotec) and rinsed with FACS buffer. The flow-through from column was collected as FISC, which were then cultured on Matrigel-coated plates in satellite expansion medium (40% Ham's F-10, 40% DMEM, 19% FBS, 1% penicillin/streptomycin).

For the isolation of quiescent satellite cells (QSC), the steps before SC sorting were performed by established protocol (Machado et al., 2021). In brief, entire hindlimb muscles from mice were dissected and collected into ice-old 0.5% PFA (The total dissection time should not exceed 15 minutes). During mincing muscle, add 2-3 drops of ice-old 0.5% PFA per minute on chopped muscles (The total mince time should not exceed 10 minutes). Muscles were collected and gently rotated in ice-old 0.5% PFA at 4°C for 1 hour. Centrifuged at 4°C for 500g 5 minutes,

after discarding the supernatant then washed muscles by ice-old PBS. Then the muscles were collected and suspended in warm QSC digestion medium (collagenase II and dispase B in DMEM) for 90~120 min in 37°C at 90 rpm. All other following steps were same as which were for isolating FISC.

Human myoblast cultures

Human myoblasts (hSkMC-AB1190) were immortalized as we previously described (Mamchaoui et al., 2011). Human myoblasts were cultured in 15% fetal bovine serum (FBS) and 5% Growth Medium Supplement Mix in Skeletal Muscle Cell Basal Medium with 1× GlutaMAX and 1% gentamicin sulfate. Myoblast differentiation medium contains 2% horse serum in DMEM with 1% penicillin-streptomycin. For proliferation assay, the cells were cultured 48 hours or 72 hours with the existence of 0.2 μM EdU. EdU staining was performed by the previous protocol (Salic & Mitchison, 2008).

Quantitative real-time PCR (qPCR)

Total RNA was extracted from mouse tissue or cells using TRIzol (Invitrogen). cDNA was synthesized using iScriptTM Reverse Transcription Supermix (Bio-Rad, 1708841). Gene expression was detected following standard qPCR approaches with KAPA SYBR FAST qPCR Master Mix (KK4605). The Real-time PCR was performed to analyze gene expression changes using QuantStudio 3 Real-Time PCR System (Thermo Fisher Scientific) with SYBR Green Master Mix (Roche) and qPCR primers. The $2^{\Delta\Delta Ct}$ method was used to analyze gene expression after normalization to the expression value of Hprt or 18S rRNA. Primer sequences used in this study are provided below:

Primer for Myod1 qPCR-F: CCACTCCGGGACATAGACTTG

Primer for Myod1 qPCR-R: AAAAGCGCAGGTCTGGTGAG

Primer for Myomixer qPCR-F: CTGAGCTCCCAAGACATGAG

Primer for Myomixer qPCR-R: TGGAGGCCTCTCCAGAAT

Primer for Myomaker qPCR-F: GCCTTTACCACCTTCTCCCC

Primer for Myomaker qPCR-R: GCACAGCACAGACAAACCAG

Primer for 18S qPCR-F: ACCGCAGCTAGGAATAATGGA

Primer for 18S qPCR-R: GCCTCAGTTCCGAAAACCA

Primer for Hprt qPCR-F: GTTGGGCTTACCTCACTGCT

Primer for Hprt qPCR-R: TAATCACGACGCTGGGACTG

Western blotting analysis

Protein was isolated from cells using RIPA buffer (Sigma-Aldrich, R0278). Protein concentrations were determined using BCA Protein Assay Reagent (Thermo Fisher Scientific, 23225), followed by measurement with NanoDrop. Protein samples were mixed with 4X Laemmli sample buffer (Bio-Rad, 161- 0747) and 20-40 μg protein was loaded and separated by SDS-PAGE gel electrophoresis. The proteins were transferred to a polyvinylidene fluoride (PVDF) membrane (Millipore), and then blocked in 5% fat-free milk for 1 hour at room temperature, and then incubated with the following primary antibodies diluted in 5% milk overnight at 4°C: Fosl1 (Santa Cruz Biotechnology, sc-28310) and a-Tubulin (Santa Cruz Biotechnology, sc-8035). This HRP-conjugated secondary antibody was used as 1:5,000 diluted: Goat Anti-Mouse IgG (H+L)-HRP Conjugate (Bio-Rad, 170-6516). Immunodetection was performed using Western Blotting Luminol Reagent (Santa Cruz Biotechnology, sc2048).

Lentivirus preparation and CRISPR-Cas9 knockout experiments in cells

The lentiCRISPR v2-Blast vector used for gene knockout experiments in vitro was a gift from Mohan Babu (Addgene plasmid # 83480). The guide RNAs that target the coding regions

of human FOSL1 gene were individually cloned into the lentiCRISPR v2-Blast vector and verified the correct insert by sanger sequencing. The sequences for gRNA used in this study are provided below:

Human FOSL1 gene gRNA1: CCACTCATGGTGTTGATGCT

Human FOSL1 gene gRNA2: AACCCCGGCCAGGAGTCATC

Human FOSL1 gene gRNA3: CAAGGCCTTCGACGTACCCC

Lentivirus was produced by transfecting Lenti-X 293T cells (Clontech, 632180) using FuGENE6 transfection reagent (Promega, #E2692) with lentiCRISPR v2-Blast, psPAX2 and pMD2.G plasmids. 48 hours after transfection, lentivirus was collected to infect human myoblasts. psPAX2 vector was a gift from Didier Trono (Addgene plasmid # 12260). pMD2.G vector was a gift from Didier Trono (Addgene plasmid # 12259). 3 days after infection, the Blasticytidin (Gibco, A11139-02) was added in 1:1,000 dilution to human myoblast for 5 days. Single clones were isolated from survived cells and expanded culture which were then genotyped by PCR and Sanger sequencing. Genotyping primers are:

Human FOSL1 genotyping primer-F: CCTCAATCCACACGGACCTC

Human FOSL1 genotyping primer-R: CCTTACCCCCTCCTAAGCCT

Retroviral vector preparations and expression

Retroviral expression vector pMXs-Puro (Cell Biolabs, # RTV-012) was used for gene cloning and expression in human myoblasts. The open reading frames (ORF) for live-actin GFP and mouse Fosl1 were cloned into pMXs-Puro vector by In-Fusion cloning. The ORF was mouse Fosl1 was designed to be gRNA insensitive. The successful colonies were Sanger sequencing verified. Two micrograms of retroviral plasmid were transfected into packaging human embryonic kidney (HEK) 293 cells using FuGENE 6 (Promega, #E2692) transfection reagent.

Two days after transfection, virus medium was collected and filtered to infect cells. One day after infection, the cells were switched to growth medium.

Differentiation index and fusion index measurements

Differentiation index was calculated as the percentage of the nuclei number within differentiated cells (MF20+) divided by the total nuclei number in the imaging area. Fusion index was calculated as the nuclei number in only synthesias (≥ 3 nuclei) as a percentage of the total number of nuclei inside muscle cells in the imaging area.

Immunostaining

Cells were fixed in 4% PFA for 10 minutes without light, membrane was permeabilized using 0.5% Triton X-100. Cells are blocked with 5% BSA at room temperature. Primary antibody incubation was performed overnight at 4°C. Immunostaining signal was detected by incubating with fluorophores conjugated secondary antibodies and Hoechst 33342 to visualize nucleus. Fluorescence images were collected using the BioTek Lionheat Microscope System or Olympus FV1200 Confocal Laser Scanning Microscope.

RNA-seq analysis

Total RNA was extracted from mouse tissue or cells using TRIzol (Invitrogen) and shipped to Admerahealth, NJ with dry ice. Released paired-end reads were aligned to mouse reference genome (GRCm38/mm10) using *HISAT2* (Kim et al., 2019). *featureCounts* (Liao et al., 2014) was then used to generated raw counts table which was then used for DE genes analysis by *DESeq2* (Love et al., 2014). DE genes were regarded as which had LogFC >1 and FDR < 0.05. Gene Ontology (GO) analysis was performed by Metascape using DE genes (Dang et al., 2023; Zhou et al., 2019).

Quantification and statistical analysis

Experiments were repeated at least three times. All quantitative results were analyzed with student's t-test with two-tail distribution. Comparisons with p-values < 0.05 were considered significant.

Figures and tables

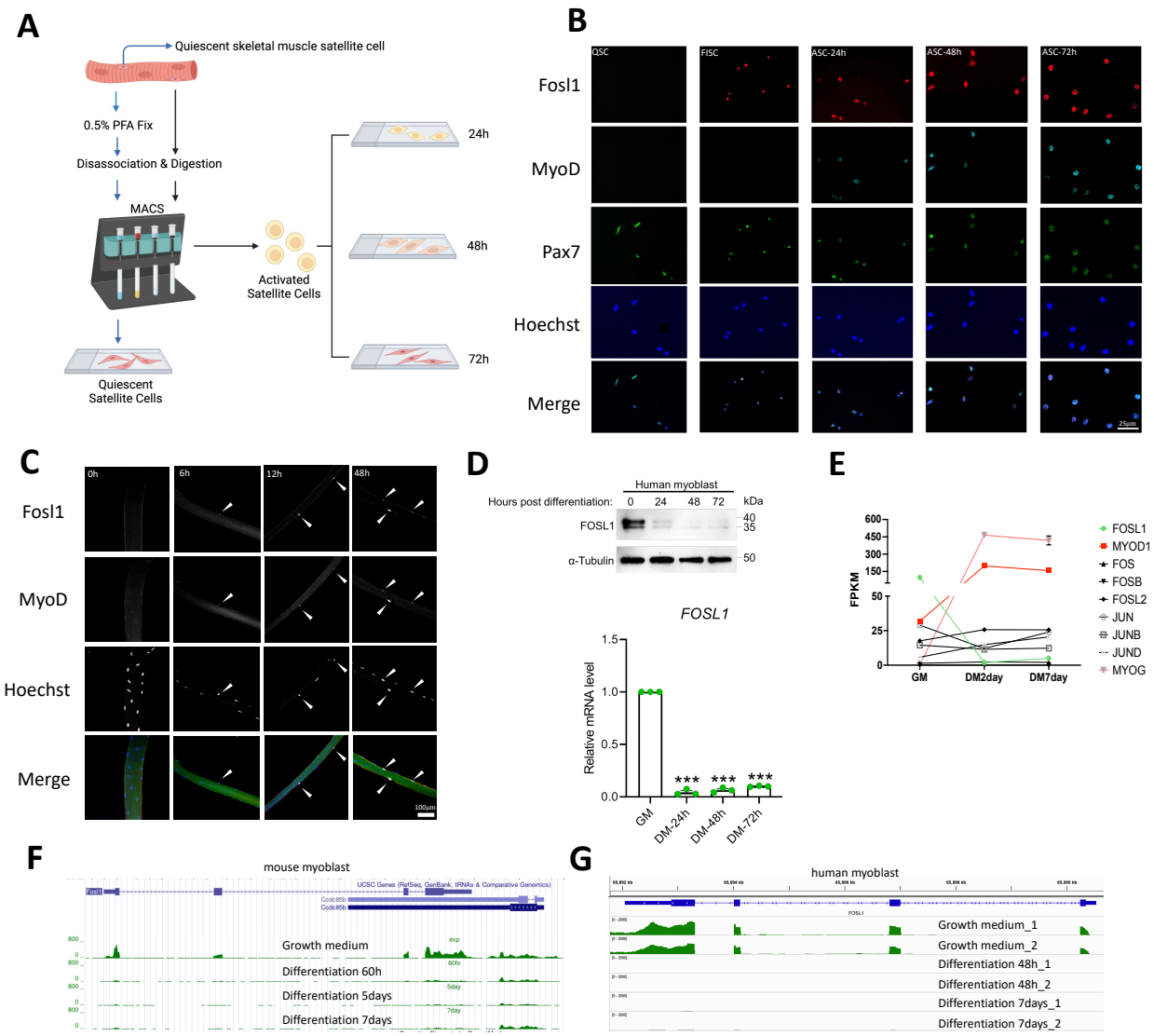

Figure 3.1: Fosl1 is actively induced during early SC activation and myoblast proliferation but not in the differentiated myofiber. (A) The schematic outlines a protocol for isolating quiescent satellite cells (QSC) and freshly isolated satellite cells (FISC) from the muscles of WT mice. In situ fixation was used to preserve the gene expression signatures of the QSCs prior to

disassociation and digestion. The FISCs were then cultured for different time periods (24, 48, and 72 hours) on chamber slide. (B) immunofluorescence (IF) staining was performed to detect the protein expression of Fosl1, MyoD and Pax7 in the SCs from (A). (C) IF staining of Fosl1 and MyoD on single myofibers immediately after isolation or following 6, 12, and 48 hours of culture. (D) Top: Western blots of a-Tubulin and FOSL1 in human myoblasts after 0, 24, 48 and 72 hours of differentiation. Bottom: qPCR analysis of FOSL1 expression FOSL1 in human myoblasts after 0, 24, 48 and 72 hours of differentiation. n = 3. *P < 0.05, **P < 0.01, ***P < 0.001. Data are presented as means ± SEM. DM, differentiation medium. GM, growth medium. (E) FPKM plot of Fos and Jun family members and MyoD and MyoG in human myoblast after 0 hours, 2 days and 7 days of differentiation. (F) RNA sequencing results of Fosl1 during mouse myoblast differentiation (GSE20846). (G) RNA sequencing results of FOSL1 during human myoblast differentiation (Unpublished).

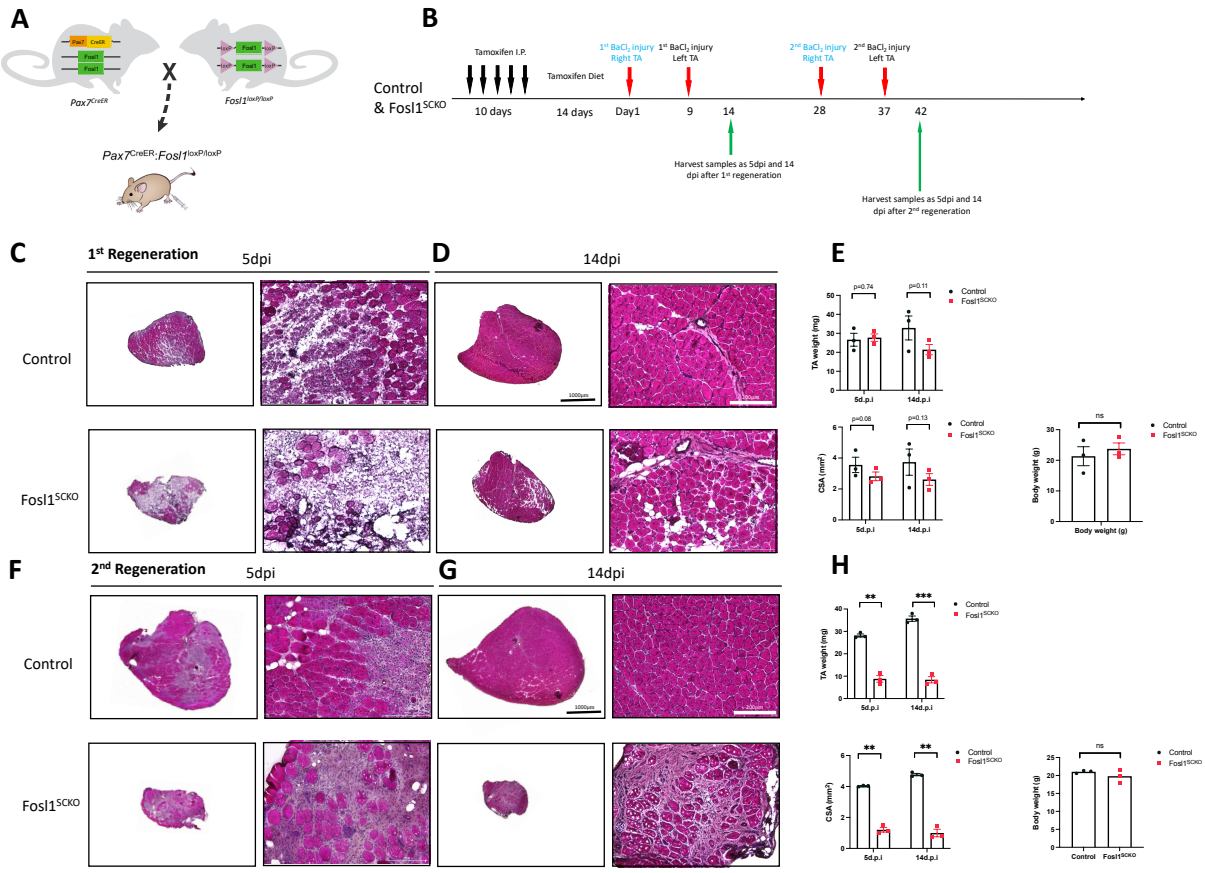

Figure 3.2: Fosl1 is indispensable for injury-induced muscle regeneration. (A) Scheme of breeding to generate Fosl1 conditional knockout in SC. (B) Schematic outlining the strategy of tamoxifen (TMX) and BaCl2 treatment of mice. Control and Fosl1$^{LoxP/LoxP}$ mice were treated with TMX i.p. injection every 2 days over a period of 10 days and then TMX diet were supplied through the whole procedure. (C-D) H&E staining of global and zoom-in views of the TA muscles at 5 and 14 days post the 1st injury, respectively. (E) Quantified results of TA weight, cross-sectional areas (CSA) of TA, and body weight of mice in the 1st regeneration assay. (F-G) H&E staining of global and zoom-in views of the TA muscles at 5 and 14 days post the 2nd injury, respectively. (E) Quantified results of TA weight, cross-sectional areas (CSA) of TA, and body weight of mice in the 2nd regeneration assay.

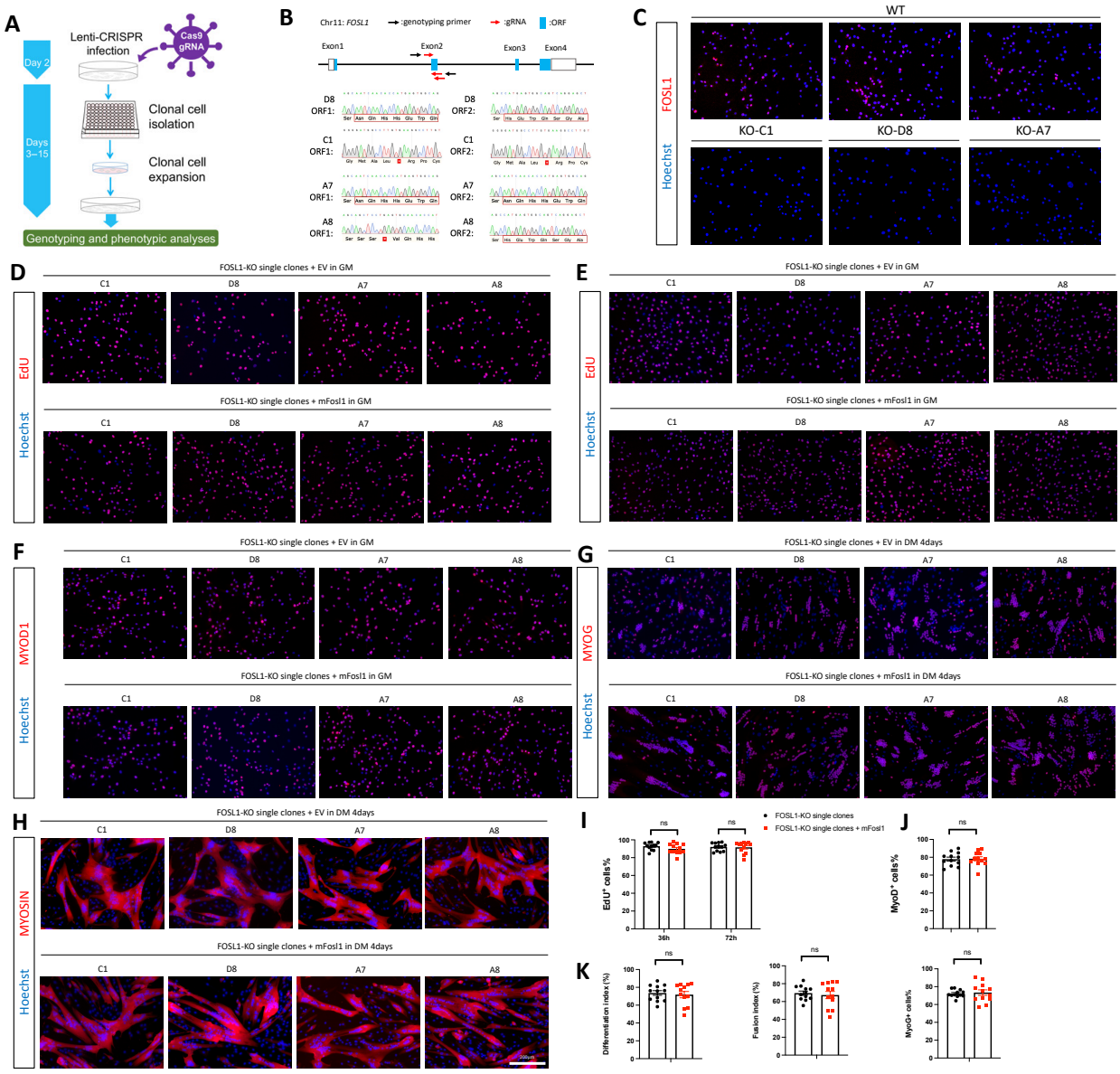

Figure 3.3: Fosl1 is not required for myoblast proliferation or maturation. (A) Scheme of CRISPR approach to generate FOSL1-KO single clones from human myoblasts. (B) Human FOSL1 gene structure including positions of gRNAs and genotyping primers, and sanger sequencing results of four FOSL1-KO single clones. Biallelic deletions of FOSL1 gene were confirmed. The frameshifted codons were in red box. (C) FOSL1 immunostaining result in WT and three of the four FOSL1-KO single clones in growth medium. (D-E) EdU staining results to show the proliferation effect of FOSL1-KO myoblasts by retroviral mouse Fosl1 (mFosl1)

expression in GM for 48h or 72h, respectively. (F) MYOD1 immunostaining results of FOSL1-KO myoblasts by retroviral mouse Fosl1 (mFosl1) expression in GM. (G) MYOG immunostaining results of FOSL1-KO myoblasts by retroviral mouse Fosl1 (mFosl1) expression in DM. Cells were differentiated for 4 days. (H) MYOSIN immunostaining results of FOSL1-KO myoblasts by retroviral mouse Fosl1 (mFosl1) expression in DM. Cells were differentiated for 4 days. (I) Quantification results of EdU+ rates from (D-E). n = 12. *P < 0.05, **P < 0.01, ***P < 0.001. Data are presented as means ± SEM. (J) Quantification results of MYOD+ rates from (F) n = 3. *P < 0.05, **P < 0.01, ***P < 0.001. Data are presented as means ± SEM. (K) Differentiation indexes, fusion indexes and MYOG+ rates from (G-H). n = 3. *P < 0.05, **P < 0.01, ***P < 0.001. Data are presented as means ± SEM.

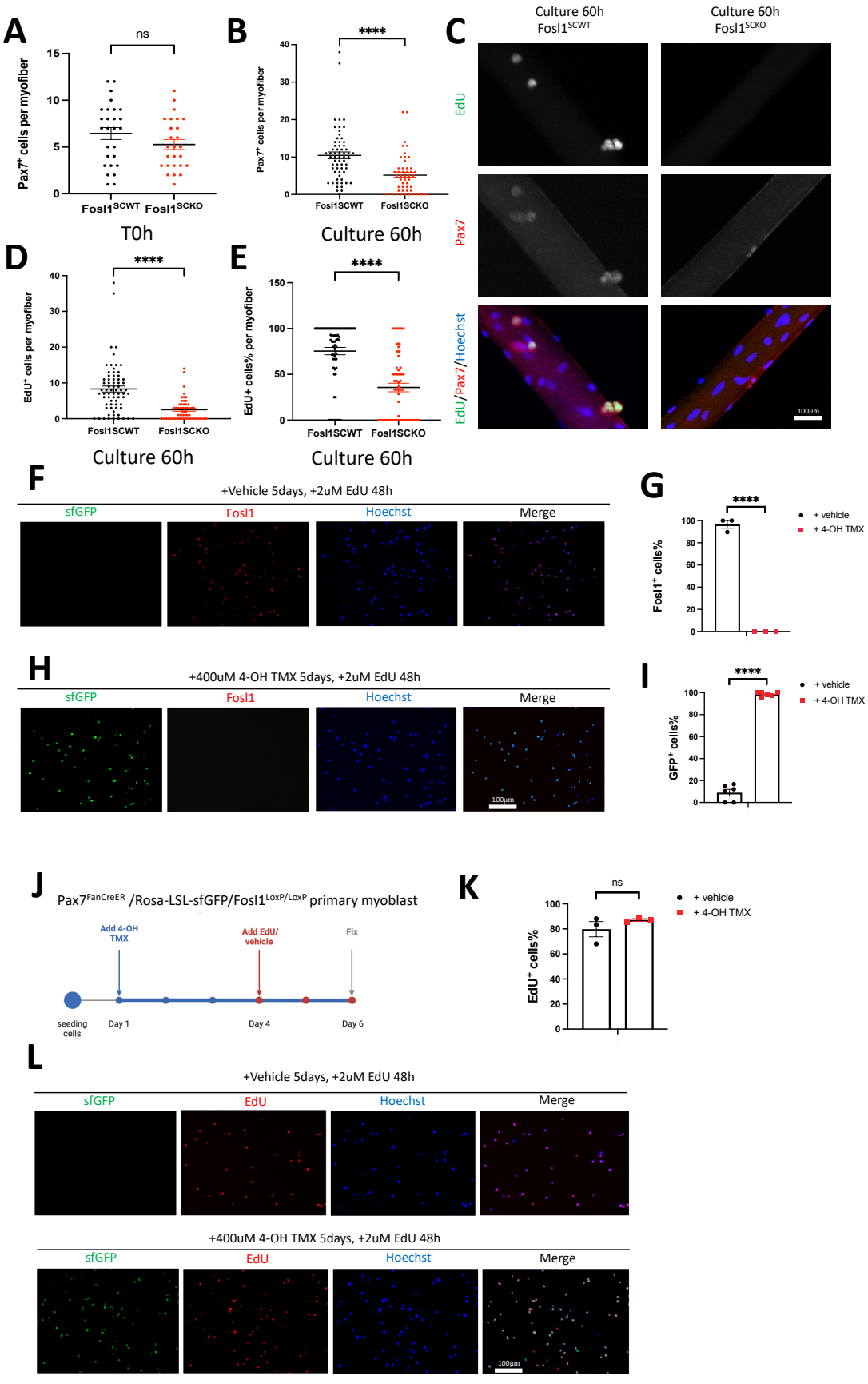
A
ns
Pax7+ cells per myofiber
Fosl1SCWT
Fosl1SCKO
T0h
B
****
Pax7+ cells per myofiber
Culture 60h
C
Culture 60h Fosl1SCWT
Culture 60h Fosl1SCKO
EdU
Pax7
EdU/Pax7/Hoechst
100μm
D
****
EdU+ cells per myofiber
Culture 60h
E
****
EdU+ cells% per myofiber
Culture 60h
F
+Vehicle 5days, +2uM EdU 48h
sfGFP
Fosl1
Hoechst
Merge
G
****
Fosl1+ cells%
+ vehicle
+ 4-OH TMX
H
+400uM 4-OH TMX 5days, +2uM EdU 48h
sfGFP
Fosl1
Hoechst
Merge
100μm
I
****
GFP+ cells%
+ vehicle
+ 4-OH TMX
J
Pax7FanCreER /Rosa-LSL-sfGFP/Fosl1LoxP/LoxP primary myoblast
Add 4-OH TMX
Add EdU/ vehicle
Fix
seeding cells
Day 1
Day 4
Day 6
K
ns
EdU+ cells%
+ vehicle
+ 4-OH TMX
L
+Vehicle 5days, +2uM EdU 48h
sfGFP
EdU
Hoechst
Merge
+400uM 4-OH TMX 5days, +2uM EdU 48h
sfGFP
EdU
Hoechst
Merge
100μm

Figure 3.4: Fosl1 is required for SC activation and proliferation. (A) Quantification of the Pax7+ cells from freshly isolated single myofibers. n = 3 mice per group. (B) Quantification of the Pax7+ cells from isolated single myofibers cultured 60 h. n = 3 mice per group. (C) CLICK staining of EdU and IF staining of Pax7 on control (left) myofiber and Fosl1-cKO myofiber. These fibers were cultured with EdU 60 h post isolation. n = 3 mice per group. (D) Quantification of counting results of EdU+ cells on myofibers from (C). n = 3 mice per group. (E) Quantification of percentage of EdU+ over Pax7+ cells on myofibers from (C). n = 3 mice per group. (F) IF staining of Fosl1 (red) and imaging of sfGFP (green) in primary myoblast cultured with vehicle and EdU as illustrated in (J). (G) Quantification of percentage of Fosl1+ cells in cells from (F) and (H). n = 2 mice per group. (H) IF staining of Fosl1 (red) and imaging of sfGFP (green) in primary myoblast cultured with 4-OH TMX and EdU as illustrated in (J). (I) Quantification of percentage of GFP+ cells in cells from (F), (H) and (L). n = 2 mice per group. (J) A schematic for cell treatment procedure to examine the proliferation of activated SCs (primary myoblasts) after Fosl1 knockout in vitro. SCs were isolated from $Pax7^{FanCreER}$ /Rosa-LSL-sfGFP/$Fosl1^{LoxP/LoxP}$ mice. 24 h after seeding cells, 4-OH TMX or vehicle was added. 3 days later, EdU was added for 48 h before fixation. (K) Quantification of percentage of EdU+ cells from (L). n = 2 mice per group. (L) CLICK staining of EdU (red) and imaging of sfGFP (green) in primary myoblast cultured with 4-OH TMX and EdU as illustrated in (J). All bar graphs are presented as means ± SEM. *P < 0.05, **P < 0.01, ***P < 0.001.

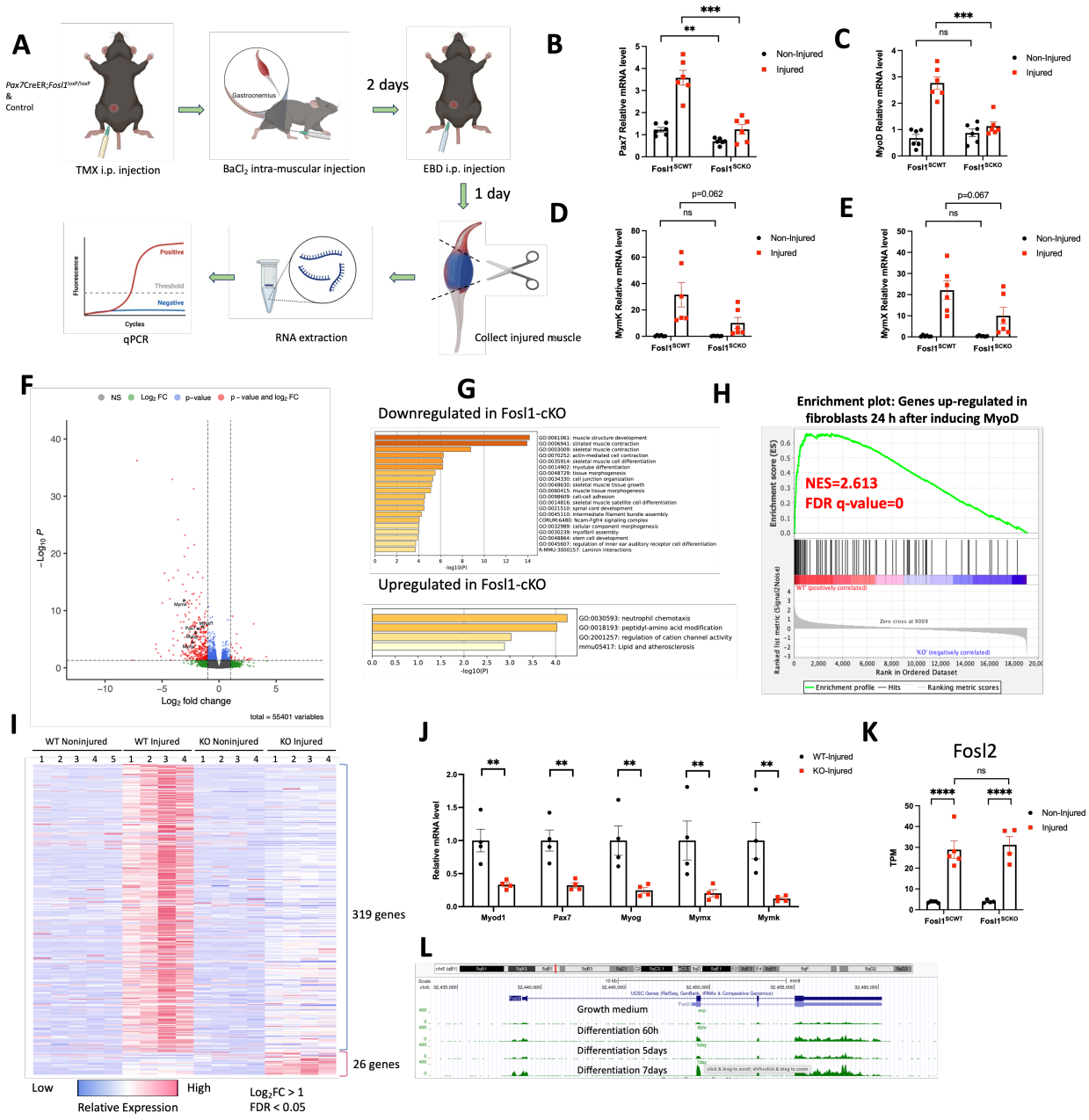

Figure 3.5: Loss of Fosl1 caused SC pool reduction and resulted in myoblast differentiation defect during early muscle regeneration. (A) A scheme of harvesting injured muscle for qPCR. Control and Fosl1$^{LoxP/LoxP}$ mice were treated with TMX i.p. injection every 2 days over a period of 10 days and BaCl2 was injected into gastroceus. 2 days later Evans Blue Dye (EBD) was i.p. injected and 1 day later injured muscle was collected with the indication of EBD. Non-injured muscle was collected at corresponding position. RNA was extracted from muscle

samples for qPCR analysis. (B-E) qPCR results of Pax7 (B), MyoD (C), Myomaker (MymK) (D) and Myomixer (MymX) (E). n = 6 mice per group. (F) Volcano plot of differentially expressed (DE) genes from the RNA-seq analysis. Dot lines are p-value threshold <= 0.05 and fold change >= 1. MymK, MymX, MyoD1, Pax7 and MyoG are pointed by arrows. (G) Gene Ontology (GO) analysis results of 319 DE genes downregulated in Fosl1-cKO samples (top) and 26 DE genes upregulated in Fosl1-cKO samples (bottom). (H) GSEA plot of genes downregulated in Fosl1-cKO samples with genes upregulated in fibroblast 24 h after inducing MyoD. (I) Heatmap indicating expression levels (Log2(TPM)) of DE genes across WTN, WTI, KOI, and KON samples from RNA-seq. (J) Expression levels (TPM) of MyoD1, Pax7, MyoG, MymK and MymX from RNA-seq. (K) Expression levels (TPM) of Fosl2 from RNA-seq. (L) RNA sequencing results of Fosl2 during mouse myoblast differentiation (GSE20846).

Supplemental Figures

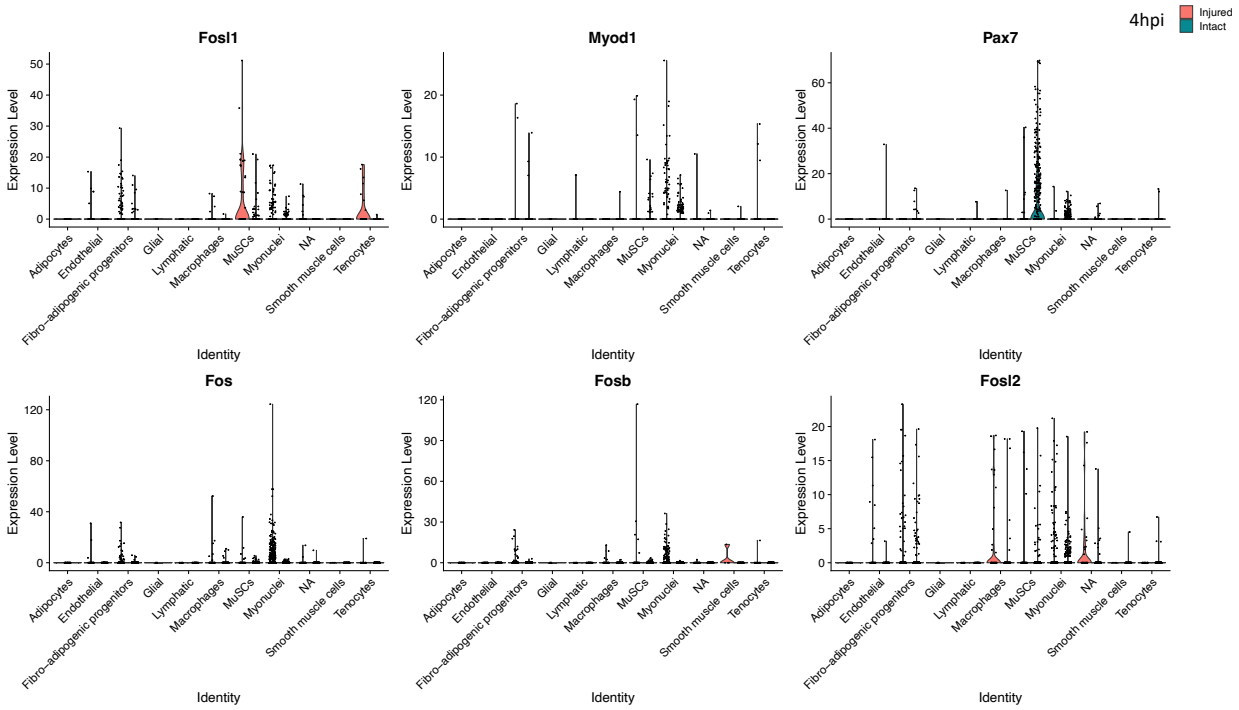

Figure S3.1: Fosl1 is actively induced during early muscle regeneration. Expression pattern of Pax7, Myf5 and Fos family members in different populations inferred from single nucleus RNA-seq results from 4 h.p.i muscle and intact muscle (GSE163856).

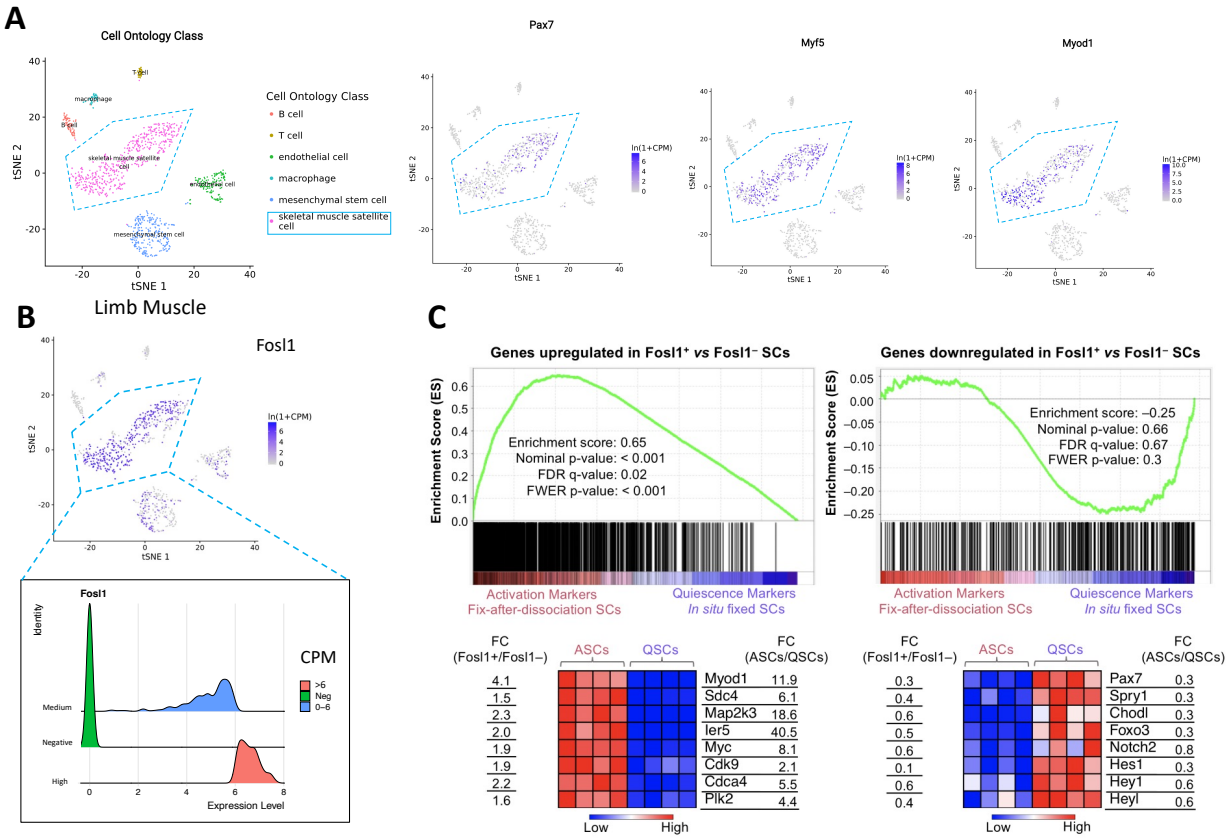

Figure S3.2: Fosl1 is actively induced during early SC activation. (A) Cell clustering result of limb muscle and the expression pattern of Pax7, Myf5 and Myod1 shown in dot plot adopted from Tabula muris database. Blue box: Skeletal muscle satellite cell population. (B) Expression pattern of Fosl1 shown in dot plot (top) in Skeletal muscle satellite cell population from (A) that was further subset by expression level of Fosl1 shown in ridge plot (bottom). (C) GSEA results of genes upregulated in Fosl1+ (CPM>6) versus Fosl1– (CPM=0) satellite cells and heatmap (left); GSEA results of genes downregulated in Fosl1+ (CPM>6) versus Fosl1– (CPM=0) satellite cells and heatmap (right).

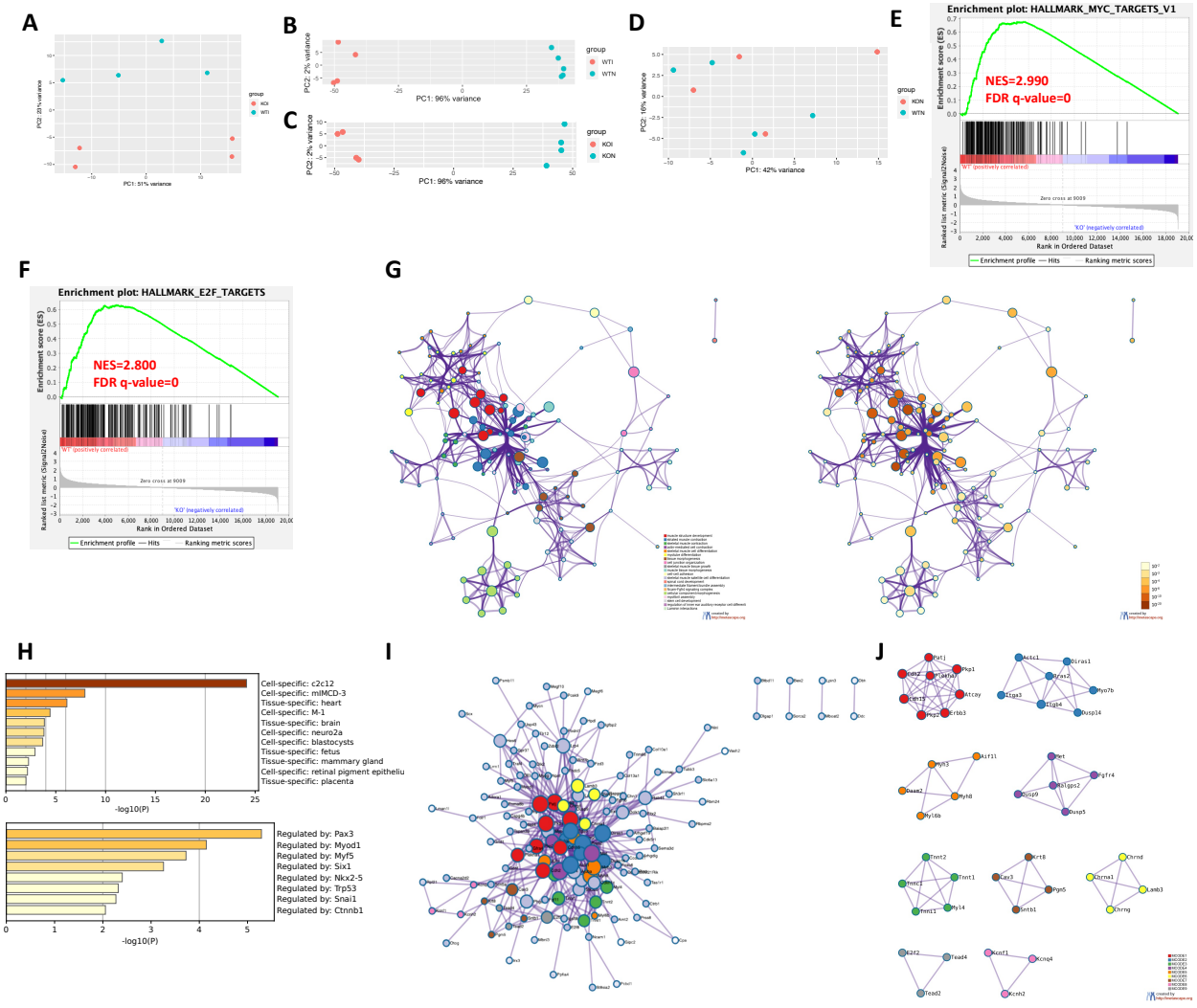

Figure S3.5: Loss of Fosl1 induced early muscle regeneration defect by affecting numerous cellular procedures and signaling pathways. (A-D) PCA results of KOI vs WTI samples (A), WTI vs WTN sample (B), KOI vs KON samples (C), and KON vs WTN samples (D). (E) GSEA plot of genes downregulated in Fosl1-cKO samples with Myc targets. (F) GSEA plot of genes downregulated in Fosl1-cKO samples with E2F targets. (G) Network of enriched terms from genes downregulated in Fosl1-cKO samples. Left: colored by cluster ID, where nodes and circles that share the same cluster ID are close to each other; Right: colored by p-value, where terms include more genes tend to have more significant p-value. (H) Summary of enrichment analysis

in PaGenBase (top) and TRRUST (bottom). (I-J) Protein-protein interaction network (I) and MCODE components (J) identified from the genes downregulated in Fosl1-cKO samples.

CHAPTER 4

SUMMARY AND CONCLUSIONS

Muscle satellite cells are multipotent stem cells located between the sarcolemma (muscle fiber membrane) and the basement membrane of skeletal muscles. Their primary functions are to facilitate muscle growth, maintenance, and repair. Satellite cells are generally quiescent in healthy adult muscle tissue but can be activated in response to muscle injury or certain stimuli. Once activated, they undergo a process of proliferation, differentiation, and fusion to contribute to muscle regeneration. During myogenesis, satellite cells play a critical role in muscle development and growth. These cells have the ability to self-renew, giving rise to a pool of undifferentiated cells that can differentiate into myoblasts. Myoblasts are the precursors of muscle fibers and eventually fuse together to form new muscle tissue. By participating in myogenesis, satellite cells contribute to the increase in muscle mass and the repair of damaged muscle fibers.

When skeletal muscles are injured or subjected to exercise-induced stress, satellite cells become activated and undergo a series of steps to regenerate the damaged tissue. Upon activation, satellite cells enter the cell cycle, proliferate, and generate a population of myoblasts. These myoblasts subsequently differentiate into myocytes, which fuse together and form new muscle fibers to replace the damaged ones. The regenerative capacity of satellite cells is crucial for muscle repair and functional recovery following injury. Satellite cells also play a significant role in muscle diseases, including muscular dystrophies and age-related muscle decline. In conditions like Duchenne muscular dystrophy, the absence or dysfunction of dystrophin protein

leads to continuous muscle fiber damage, triggering chronic activation and depletion of satellite cells. This impaired satellite cell function contributes to the progressive muscle degeneration observed in these diseases. Understanding the mechanisms that regulate satellite cell function is crucial for developing therapeutic strategies to enhance muscle regeneration and combat muscle diseases.

To facilitate the studies of SC in vivo, we reported a novel approach based on *i*-GONAD method to efficiently generate mouse loxP alleles in a convenient and economic manner. To insert loxP sequences by CRISPR/Cas9, the HDR donors, each ssODNA is novelly designed with three main components: (1) 5' Homology Arm: This portion of the ssODNA is 91 nucleotides long and shares sequence similarity with the region immediately adjacent to the desired insertion site, specifically from the PAM (Protospacer Adjacent Motif)-proximal side. The homology arm helps promote the annealing and alignment of the donor DNA with the target site. (2) loxP Sequence: The loxP sequence, which is 34 nucleotides in length, is included in the ssODNA. loxP is a specific DNA sequence recognized by the Cre recombinase enzyme, and its presence allows for conditional DNA recombination events. (3) 3' Homology Arm: This part of the ssODNA spans 36 nucleotides and shares sequence similarity with the region adjacent to the desired insertion site, but from the PAM-distal side. Like the 5' homology arm, the 3' homology arm facilitates the alignment and annealing of the donor DNA with the target site.

By testing our method on five genes, the *i*-GONAD method, combined with HDR template design, proved to be robust, fast, and efficient for generating mouse conditional alleles. The overall targeting efficiency, as indicated in Table 1, was 10% (8 out of 76) for producing floxed alleles. Additionally, the frequency of obtaining F0 mice with either 5'- or 3'-loxP insertion was 28% (21 out of 76), resulting in a combined loxP-insertion efficiency of 38%. In the F1

generations, there was a 37% chance (32 out of 87 pups) of inheriting two loxP sites (*in cis*), indicating efficient germline editing by *i*-GONAD. These results further demonstrate the reliability and effectiveness of the *i*-GONAD method and HDR template design in generating mouse conditional alleles.

Among those five genes we successfully targeted, *Fosl1* was selected because of special interest. We observed that the expression of Fosl1 is rapidly induced in proliferating myoblasts and activated SC. Through specific knockout of Fosl1 in SC by our generated Fosl1$^{loxP/loxP}$ mice, we observed a clear defect in muscle regeneration following initial muscle injury, and repetitive muscle injury resulted in complete loss of regeneration. Deletion of Fosl1 from quiescent SC impaired their activation and prevented entry into the cell cycle. However, loss of Fosl1 in post-activation SC had minimal effects on SC proliferation. Interestingly, the knockout of Fosl1 did not affect the proliferation, differentiation, or fusion of immortalized human myoblasts. Similarly, overexpression of Fosl1 in human myoblasts did not alter these cellular processes. To gain further insights, we performed RNA-seq analysis using injured muscle tissue. In the Fosl1 conditional knockout group, we observed significant downregulation of muscle stem cell markers such as *Pax7* and myogenic differentiation markers including *MyoD1*, *Myf5*, *MymK*, and *MymX* genes. These findings suggest that *Fosl1* plays a critical role in maintaining the activation and/or proliferation of muscle stem cells *in vivo*. Overall, our current data highlights the importance of Fosl1 in SC activation and muscle regeneration. These findings contribute to our understanding of the molecular mechanisms involved in muscle regeneration and provide valuable insights for potential therapeutic strategies targeting muscle stem cells. To uncover the exact mechanisms resulted by loss of Fosl1 in SC during early muscle regeneration, we have harvested the 24 h.p.i muscle sample from Fosl1-cKO and control mice and are currently

working on optimizing the nucleus extraction protocol for snRNA-seq. We aim to recapitulate and identify the cell populations involved in early regenerating muscle and analyze the transcriptional differences in SC population from Fosl1-cKO and control mice.

REFERENCES

Adli, M. (2018). The CRISPR tool kit for genome editing and beyond. *Nature Communications*, *9*. https://doi.org/ARTN 1911
10.1038/s41467-018-04252-2

Aida, T., Chiyo, K., Usami, T., Ishikubo, H., Imahashi, R., Wada, Y., Tanaka, K. F., Sakuma, T., Yamamoto, T., & Tanaka, K. (2015). Cloning-free CRISPR/Cas system facilitates functional cassette knock-in in mice. *Genome Biol*, *16*(1), 87. https://doi.org/10.1186/s13059-015-0653-x

Aird, E. J., Lovendahl, K. N., St Martin, A., Harris, R. S., & Gordon, W. R. (2018). Increasing Cas9-mediated homology-directed repair efficiency through covalent tethering of DNA repair template. *Communications Biology*, *1*. https://doi.org/ARTN 54
10.1038/s42003-018-0054-2

Almada, A. E., Horwitz, N., Price, F. D., Gonzalez, A. E., Ko, M., Bolukbasi, O. V., Messemer, K. A., Chen, S., Sinha, M., Rubin, L. L., & Wagers, A. J. (2021). FOS licenses early events in stem cell activation driving skeletal muscle regeneration. *Cell Reports*, *34*(4). https://doi.org/ARTN 108656
10.1016/j.celrep.2020.108656

Amoasii, L., Long, C. Z., Li, H., Mireault, A. A., Shelton, J. M., Sanchez-Ortiz, E., McAnally, J. R., Bhattacharyya, S., Schmidt, F., Grimm, D., Hauschka, S. D., Bassel-Duby, R., & Olson, E. N. (2017). Single-cut genome editing restores dystrophin expression in a new mouse model of muscular dystrophy. *Science Translational Medicine*, *9*(418). https://doi.org/ARTN eaan8081
10.1126/scitranslmed.aan8081

Andreucci, J. J., Grant, D., Cox, D. M., Tome, L. K., Prywes, R., Goldhamer, D. J., Rodrigues, N., Bedard, P. A., & McDermott, J. C. (2002). Composition and function of AP-1 transcription complexes during muscle cell differentiation. *Journal of Biological Chemistry*, *277*(19), 16426-16432. https://doi.org/10.1074/jbc.M110891200

Bae, S., Park, J., & Kim, J. S. (2014). Cas-OFFinder: a fast and versatile algorithm that searches for potential off-target sites of Cas9 RNA-guided endonucleases. *Bioinformatics*, *30*(10), 1473-1475. https://doi.org/10.1093/bioinformatics/btu048

Bengal, E., Ransone, L., Scharfmann, R., Dwarki, V. J., Tapscott, S. J., Weintraub, H., & Verma, I. M. (1992). Functional Antagonism between C-Jun and Myod Proteins - a Direct Physical Association. *Cell*, *68*(3), 507-519. https://doi.org/Doi 10.1016/0092-8674(92)90187-H

Bentzinger, C. F., von Maltzahn, J., Dumont, N. A., Stark, D. A., Wang, Y. X., Nhan, K., Frenette, J., Cornelison, D. D. W., & Rudnicki, M. A. (2014). Wnt7a stimulates myogenic stem cell motility and engraftment resulting in improved muscle strength. *Journal of Cell Biology*, *205*(1), 97-111. https://doi.org/10.1083/jcb.201310035

Bi, P., Ramirez-Martinez, A., Li, H., Cannavino, J., McAnally, J. R., Shelton, J. M., Sanchez-Ortiz, E., Bassel-Duby, R., & Olson, E. N. (2017). Control of muscle formation by the

fusogenic micropeptide myomixer. *Science*, *356*(6335), 323-327. https://doi.org/10.1126/science.aam9361

Bi, P. P., McAnally, J. R., Shelton, J. M., Sanchez-Ortiz, E., Bassel-Duby, R., & Olson, E. N. (2018). Fusogenic micropeptide Myomixer is essential for satellite cell fusion and muscle regeneration. *Proceedings of the National Academy of Sciences of the United States of America*, *115*(15), 3864-3869. https://doi.org/10.1073/pnas.1800052115

Bi, P. P., Yue, F., Sato, Y., Wirbisky, S., Liu, W. Y., Shan, T. Z., Wen, Y. F., Zhou, D. G., Freeman, J., & Kuang, S. H. (2016). Stage-specific effects of Notch activation during skeletal myogenesis. *Elife*, *5*. https://doi.org/ARTN e17355 10.7554/eLife.17355

Biressi, S., Molinaro, M., & Cossu, G. (2007). Cellular heterogeneity during vertebrate skeletal muscle development. *Dev Biol*, *308*(2), 281-293. https://doi.org/10.1016/j.ydbio.2007.06.006

Bishop, K. A., Harrington, A., Kouranova, E., Weinstein, E. J., Rosen, C. J., Cui, X., & Liaw, L. (2016). CRISPR/Cas9-Mediated Insertion of loxP Sites in the Mouse Dock7 Gene Provides an Effective Alternative to Use of Targeted Embryonic Stem Cells. *G3 (Bethesda)*, *6*(7), 2051-2061. https://doi.org/10.1534/g3.116.030601

Bouabe, H., & Okkenhaug, K. (2013). Gene Targeting in Mice: A Review. *Virus-Host Interactions: Methods and Protocols*, *1064*, 315-336. https://doi.org/10.1007/978-1-62703-601-6_23

Brack, A. S., Conboy, I. M., Conboy, M. J., Shen, J., & Rando, T. A. (2008). A temporal switch from Notch to Wnt signaling in muscle stem cells is necessary for normal adult myogenesis. *Cell Stem Cell*, *2*(1), 50-59. https://doi.org/10.1016/j.stem.2007.10.006

Bray, S. J. (2016). Notch signalling in context. *Nature Reviews Molecular Cell Biology*, *17*(11), 722-735. https://doi.org/10.1038/nrm.2016.94

Brent, A. E., & Tabin, C. J. (2002). Developmental regulation of somite derivatives: muscle, cartilage and tendon. *Curr Opin Genet Dev*, *12*(5), 548-557. https://doi.org/10.1016/s0959-437x(02)00339-8

Capecchi, M. R. (1989). The new mouse genetics: altering the genome by gene targeting. *Trends Genet*, *5*(3), 70-76. https://doi.org/10.1016/0168-9525(89)90029-2

Cerletti, M., Jurga, S., Witczak, C. A., Hirshman, M. F., Shadrach, J. L., Goodyear, L. J., & Wagers, A. J. (2008). Highly efficient, functional engraftment of skeletal muscle stem cells in dystrophic muscles. *Cell*, *134*(1), 37-47. https://doi.org/10.1016/j.cell.2008.05.049

Chakkalakal, J., & Brack, A. (2012). Extrinsic Regulation of Satellite Cell Function and Muscle Regeneration Capacity during Aging. *J Stem Cell Res Ther*, *Suppl 11*, 001. https://doi.org/10.4172/2157-7633.S11-001

Chalamalasetty, R. B., Dunty, W. C., Jr., Biris, K. K., Ajima, R., Iacovino, M., Beisaw, A., Feigenbaum, L., Chapman, D. L., Yoon, J. K., Kyba, M., & Yamaguchi, T. P. (2011). The Wnt3a/beta-catenin target gene Mesogenin1 controls the segmentation clock by activating a Notch signalling program. *Nat Commun*, *2*, 390. https://doi.org/10.1038/ncomms1381

Charge, S. B., & Rudnicki, M. A. (2004). Cellular and molecular regulation of muscle regeneration. *Physiol Rev*, *84*(1), 209-238. https://doi.org/10.1152/physrev.00019.2003

Chari, R., Mali, P., Moosburner, M., & Church, G. M. (2015). Unraveling CRISPR-Cas9 genome engineering parameters via a library-on-library approach. *Nature Methods*, *12*(9), 823-+. https://doi.org/10.1038/Nmeth.3473

Charpentier, M., Khedher, A. H. Y., Menoret, S., Brion, A., Lamribet, K., Dardillac, E., Boix, C., Perrouault, L., Tesson, L., Geny, S., De Cian, A., Itier, J. M., Anegon, I., Lopez, B., Giovannangeli, C., & Concordet, J. P. (2018). CtIP fusion to Cas9 enhances transgene integration by homology-dependent repair. *Nature Communications*, *9*. https://doi.org/ARTN 1133
10.1038/s41467-018-03475-7

Chen, J., Brunner, A. D., Cogan, J. Z., Nunez, J. K., Fields, A. P., Adamson, B., Itzhak, D. N., Li, J. Y., Mann, M., Leonetti, M. D., & Weissman, J. S. (2020). Pervasive functional translation of noncanonical human open reading frames. *Science*, *367*(6482), 1140-+. https://doi.org/10.1126/science.aay0262

Chen, R., Okeyo-Owuor, T., Patel, R. M., Casey, E. B., Cluster, A. S., Yang, W., & Magee, J. A. (2021). Kmt2c mutations enhance HSC self-renewal capacity and convey a selective advantage after chemotherapy. *Cell Rep*, *34*(7), 108751. https://doi.org/10.1016/j.celrep.2021.108751

Cheon, D. J., & Orsulic, S. (2011). Mouse Models of Cancer. *Annual Review of Pathology: Mechanisms of Disease, Vol 6*, *6*, 95-119. https://doi.org/10.1146/annurev.pathol.3.121806.154244

Clausen, B. E., Burkhardt, C., Reith, W., Renkawitz, R., & Forster, I. (1999). Conditional gene targeting in macrophages and granulocytes using LysMcre mice. *Transgenic Res*, *8*(4), 265-277. https://doi.org/10.1023/a:1008942828960

Collins, C. A., Olsen, I., Zammit, P. S., Heslop, L., Petrie, A., Partridge, T. A., & Morgan, J. E. (2005). Stem cell function, self-renewal, and behavioral heterogeneity of cells from the adult muscle satellite cell niche. *Cell*, *122*(2), 289-301. https://doi.org/DOI 10.1016/j.cell.2005.05.010

Cretoiu, D., Pavelescu, L., Duica, F., Radu, M., Suciu, N., & Cretoiu, S. M. (2018). Myofibers. *Muscle Atrophy*, *1088*, 23-46. https://doi.org/10.1007/978-981-13-1435-3_2

Dang, K., Farooq, H. M. U., Dong, J., Yang, H. J., Kong, Y., Wang, H. P., Jiang, S. F., Gao, Y., & Qian, A. R. (2023). Transcriptomic and proteomic time-course analyses based on Metascape reveal mechanisms against muscle atrophy in hibernating Spermophilus dauricus. *Comparative Biochemistry and Physiology a-Molecular & Integrative Physiology*, *275*. https://doi.org/ARTN 111336
10.1016/j.cbpa.2022.111336

Danielian, P. S., Muccino, D., Rowitch, D. H., Michael, S. K., & McMahon, A. P. (1998). Modification of gene activity in mouse embryos in utero by a tamoxifen-inducible form of Cre recombinase. *Current Biology*, *8*(24), 1323-1326. https://doi.org/Doi 10.1016/S0960-9822(07)00562-3

Dort, J., Fabre, P., Molina, T., & Dumont, N. A. (2019). Macrophages Are Key Regulators of Stem Cells during Skeletal Muscle Regeneration and Diseases. *Stem Cells Int*, *2019*, 4761427. https://doi.org/10.1155/2019/4761427

Doudna, J. A., & Charpentier, E. (2014). Genome editing. The new frontier of genome engineering with CRISPR-Cas9. *Science*, *346*(6213), 1258096. https://doi.org/10.1126/science.1258096

Doyle, A., McGarry, M. P., Lee, N. A., & Lee, J. J. (2012). The construction of transgenic and gene knockout/knockin mouse models of human disease. *Transgenic Res*, *21*(2), 327-349. https://doi.org/10.1007/s11248-011-9537-3

Dumon, N. A., Wang, Y. X., & Rudnicki, M. A. (2015). Intrinsic and extrinsic mechanisms regulating satellite cell function. *Development*, *142*(9), 1572-1581. https://doi.org/10.1242/dev.114223

Eferl, R., & Wagner, E. F. (2003). AP-1: A double-edged sword in tumorigenesis. *Nature Reviews Cancer*, *3*(11), 859-868. https://doi.org/10.1038/nrc1209

Feige, P., Brun, C. E., Ritso, M., & Rudnicki, M. A. (2018). Orienting Muscle Stem Cells for Regeneration in Homeostasis, Aging, and Disease. *Cell Stem Cell*, *23*(5), 653-664. https://doi.org/10.1016/j.stem.2018.10.006

Feil, S., Valtcheva, N., & Feil, R. (2009). Inducible Cre mice. *Virus-Host Interactions: Methods and Protocols*, *530*, 343-363. https://doi.org/10.1007/978-1-59745-471-1_18

Fortin, J. P., Tan, J., Gascoigne, K. E., Haverty, P. M., Forrest, W. F., Costa, M. R., & Martin, S. E. (2019). Multiple-gene targeting and mismatch tolerance can confound analysis of genome-wide pooled CRISPR screens. *Genome Biology*, *20*. https://doi.org/ARTN 21
10.1186/s13059-019-1621-7

Frontera, W. R., & Ochala, J. (2015). Skeletal muscle: a brief review of structure and function. *Calcif Tissue Int*, *96*(3), 183-195. https://doi.org/10.1007/s00223-014-9915-y

Fujii, W., Kawasaki, K., Sugiura, K., & Naito, K. (2013). Efficient generation of large-scale genome-modified mice using gRNA and CAS9 endonuclease. *Nucleic Acids Res*, *41*(20), e187. https://doi.org/10.1093/nar/gkt772

Glover, J. N. M., & Harrison, S. C. (1995). Crystal-Structure of the Heterodimeric Bzip Transcription Factor C-Fos-C-Jun Bound to DNA. *Nature*, *373*(6511), 257-261. https://doi.org/DOI 10.1038/373257a0

Goulding, M. D., Chalepakis, G., Deutsch, U., Erselius, J. R., & Gruss, P. (1991). Pax-3, a novel murine DNA binding protein expressed during early neurogenesis. *EMBO J*, *10*(5), 1135-1147. https://doi.org/10.1002/j.1460-2075.1991.tb08054.x

Guo, F., Gopaul, D. N., & VanDuyne, G. D. (1997). Structure of Cre recombinase complexed with DNA in a site-specific recombination synapse. *Nature*, *389*(6646), 40-46. https://doi.org/Doi 10.1038/37925

Gurumurthy, C. B., & Lloyd, K. C. K. (2019). Generating mouse models for biomedical research: technological advances. *Disease Models & Mechanisms*, *12*(1). https://doi.org/ARTN dmm029462
10.1242/dmm.029462

Gurumurthy, C. B., O'Brien, A. R., Quadros, R. M., Adams, J., Jr., Alcaide, P., Ayabe, S., Ballard, J., Batra, S. K., Beauchamp, M. C., Becker, K. A., Bernas, G., Brough, D., Carrillo-Salinas, F., Chan, W., Chen, H., Dawson, R., DeMambro, V., D'Hont, J., Dibb, K. M., . . . Burgio, G. (2019). Reproducibility of CRISPR-Cas9 methods for generation of conditional mouse alleles: a multi-center evaluation. *Genome Biol*, *20*(1), 171. https://doi.org/10.1186/s13059-019-1776-2

Gurumurthy, C. B., Sato, M., Nakamura, A., Inui, M., Kawano, N., Islam, M. A., Ogiwara, S., Takabayashi, S., Matsuyama, M., Nakagawa, S., Miura, H., & Ohtsuka, M. (2019). Creation of CRISPR-based germline-genome-engineered mice without ex vivo handling of zygotes by i-GONAD. *Nature Protocols*, *14*(8), 2452-2482. https://doi.org/10.1038/s41596-019-0187-x

Guzzardo, P. M., Rashkova, C., dos Santos, R. L., Tehrani, R., Collin, P., & Burckstummer, T. (2017). A small cassette enables conditional gene inactivation by CRISPR/Cas9. *Scientific Reports*, *7*. https://doi.org/ARTN 16770
10.1038/s41598-017-16931-z
Hai, L., Szwarc, M. M., Lanza, D. G., Heaney, J. D., & Lydon, J. P. (2019). Using CRISPR/Cas9 engineering to generate a mouse with a conditional knockout allele for the promyelocytic leukemia zinc finger transcription factor. *Genesis*, *57*(3), e23281. https://doi.org/10.1002/dvg.23281
Hall, B., Limaye, A., & Kulkarni, A. B. (2009). Overview: generation of gene knockout mice. *Curr Protoc Cell Biol*, *Chapter 19*, Unit 19 12 19 12 11-17. https://doi.org/10.1002/0471143030.cb1912s44
Harms, D. W., Quadros, R. M., Seruggia, D., Ohtsuka, M., Takahashi, G., Montoliu, L., & Gurumurthy, C. B. (2014). Mouse Genome Editing Using the CRISPR/Cas System. *Curr Protoc Hum Genet*, *83*, 15 17 11-27. https://doi.org/10.1002/0471142905.hg1507s83
Heckl, D., Kowalczyk, M. S., Yudovich, D., Belizaire, R., Puram, R. V., McConkey, M. E., Thielke, A., Aster, J. C., Regev, A., & Ebert, B. L. (2014). Generation of mouse models of myeloid malignancy with combinatorial genetic lesions using CRISPR-Cas9 genome editing. *Nat Biotechnol*, *32*(9), 941-946. https://doi.org/10.1038/nbt.2951
Howlett, S. K., & Bolton, V. N. (1985). Sequence and regulation of morphological and molecular events during the first cell cycle of mouse embryogenesis. *J Embryol Exp Morphol*, *87*, 175-206. https://www.ncbi.nlm.nih.gov/pubmed/4031752
Hsu, P. D., Lander, E. S., & Zhang, F. (2014). Development and applications of CRISPR-Cas9 for genome engineering. *Cell*, *157*(6), 1262-1278. https://doi.org/10.1016/j.cell.2014.05.010
Hubbard, E. J. (2014). FLP/FRT and Cre/lox recombination technology in C. elegans. *Methods*, *68*(3), 417-424. https://doi.org/10.1016/j.ymeth.2014.05.007
Indra, A. K., Warot, X., Brocard, J., Bornert, J. M., Xiao, J. H., Chambon, P., & Metzger, D. (1999). Temporally-controlled site-specific mutagenesis in the basal layer of the epidermis: comparison of the recombinase activity of the tamoxifen-inducible Cre-ER(T) and Cre-ER(T2) recombinases. *Nucleic Acids Res*, *27*(22), 4324-4327. https://doi.org/10.1093/nar/27.22.4324
Irion, U., Krauss, J., & Nusslein-Volhard, C. (2014). Precise and efficient genome editing in zebrafish using the CRISPR/Cas9 system. *Development*, *141*(24), 4827-4830. https://doi.org/10.1242/dev.115584
Jaisser, F. (2000). Inducible gene expression and gene modification in transgenic mice. *J Am Soc Nephrol*, *11 Suppl 16*, S95-S100. https://www.ncbi.nlm.nih.gov/pubmed/11065338
Jayavaradhan, R., Pillis, D. M., Goodman, M., Zhang, F., Zhang, Y., Andreassen, P. R., & Malik, P. (2019). CRISPR-Cas9 fusion to dominant-negative 53BP1 enhances HDR and inhibits NHEJ specifically at Cas9 target sites. *Nature Communications*, *10*. https://doi.org/ARTN 2866
10.1038/s41467-019-10735-7
Jiang, F. G., & Doudna, J. A. (2017). CRISPR-Cas9 Structures and Mechanisms. *Annual Review of Biophysics, Vol 46*, *46*, 505-529. https://doi.org/10.1146/annurev-biophys-062215-010822

Jiang, W. Y., & Marraffini, L. A. (2015). CRISPR-Cas: New Tools for Genetic Manipulations from Bacterial Immunity Systems. *Annual Review of Microbiology, Vol 69*, *69*, 209-228. https://doi.org/10.1146/annurev-micro-091014-104441

Jochum, W., Passegue, E., & Wagner, E. F. (2001). AP-1 in mouse development and tumorigenesis. *Oncogene*, *20*(19), 2401-2412. https://doi.org/10.1038/sj.onc.1204389

Kaneko, T., & Mashimo, T. (2015). Simple Genome Editing of Rodent Intact Embryos by Electroporation. *PLoS One*, *10*(11). https://doi.org/ARTN e0142755 10.1371/journal.pone.0142755

Kann, A. P., Hung, M., Wang, W., Nguyen, J., Gilbert, P. M., Wu, Z. H., & Krauss, R. S. (2022). An injury-responsive Rac-to-Rho GTPase switch drives activation of muscle stem cells through rapid cytoskeletal remodeling. *Cell Stem Cell*, *29*(6), 933-+. https://doi.org/10.1016/j.stem.2022.04.016

Karimova, M., Abi-Ghanem, J., Berger, N., Surendranath, V., Pisabarro, M. T., & Buchholz, F. (2013). Vika/vox, a novel efficient and specific Cre/loxP-like site-specific recombination system. *Nucleic Acids Res*, *41*(2), e37. https://doi.org/10.1093/nar/gks1037

Kassar-Duchossoy, L., Giacone, E., Gayraud-Morel, B., Jory, A., Gomes, D., & Tajbakhsh, S. (2005). Pax3/Pax7 mark a novel population of primitive myogenic cells during development. *Genes & Development*, *19*(12), 1426-1431. https://doi.org/10.1101/gad.345505

Kim, D., Paggi, J. M., Park, C., Bennett, C., & Salzberg, S. L. (2019). Graph-based genome alignment and genotyping with HISAT2 and HISAT-genotype. *Nature Biotechnology*, *37*(8), 907-+. https://doi.org/10.1038/s41587-019-0201-4

Kim, H., Kim, M., Im, S. K., & Fang, S. (2018). Mouse Cre-LoxP system: general principles to determine tissue-specific roles of target genes. *Lab Anim Res*, *34*(4), 147-159. https://doi.org/10.5625/lar.2018.34.4.147

Kume, T., Jiang, H. Y., Topczewska, J. M., & Hogan, B. L. M. (2001). The murine winged helix transcription factors, Foxc1 and Foxc2, are both required for cardiovascular development and somitogenesis. *Genes & Development*, *15*(18), 2470-2482. https://doi.org/DOI 10.1101/gad.907301

Langer, S. J., Ghafoori, A. P., Byrd, M., & Leinwand, L. (2002). A genetic screen identifies novel non-compatible loxP sites. *Nucleic Acids Res*, *30*(14), 3067-3077. https://doi.org/10.1093/nar/gkf421

Lanza, D. G., Gaspero, A., Lorenzo, I., Liao, L., Zheng, P., Wang, Y., Deng, Y., Cheng, C. H., Zhang, C. S., Seavitt, J. R., DeMayo, F. J., Xu, J. M., Dickinson, M. E., Beaudet, A. L., & Heaney, J. D. (2018). Comparative analysis of single-stranded DNA donors to generate conditional null mouse alleles. *Bmc Biology*, *16*. https://doi.org/ARTN 69 10.1186/s12915-018-0529-0

Latroche, C., Weiss-Gayet, M., Muller, L., Gitiaux, C., Leblanc, P., Liot, S., Ben-Larbi, S., Abou-Khalil, R., Verger, N., Bardot, P., Magnan, M., Chretien, F., Mounier, R., Germain, S., & Chazaud, B. (2017). Coupling between Myogenesis and Angiogenesis during Skeletal Muscle Regeneration Is Stimulated by Restorative Macrophages. *Stem Cell Reports*, *9*(6), 2018-2033. https://doi.org/10.1016/j.stemcr.2017.10.027

Laumonier, T., & Menetrey, J. (2016). Muscle injuries and strategies for improving their repair. *J Exp Orthop*, *3*(1), 15. https://doi.org/10.1186/s40634-016-0051-7

Le Grand, F., Jones, A. E., Seale, V., Scime, A., & Rudnicki, M. A. (2009). Wnt7a Activates the Planar Cell Polarity Pathway to Drive the Symmetric Expansion of Satellite Stem Cells. *Cell Stem Cell*, *4*(6), 535-547. https://doi.org/10.1016/j.stem.2009.03.013

Lepper, C., Conway, S. J., & Fan, C. M. (2009). Adult satellite cells and embryonic muscle progenitors have distinct genetic requirements. *Nature*, *460*(7255), 627-U694. https://doi.org/10.1038/nature08209

Lepper, C., Partridge, T. A., & Fan, C. M. (2011). An absolute requirement for Pax7-positive satellite cells in acute injury-induced skeletal muscle regeneration. *Development*, *138*(17), 3639-3646. https://doi.org/10.1242/dev.067595

Lewandoski, M. (2002). Conditional control of gene expression in the mouse (vol 2, pg 743, 2001). *Nature Reviews Genetics*, *3*(1), 79-79. <Go to ISI>://WOS:000173267200020

Liao, Y., Smyth, G. K., & Shi, W. (2014). featureCounts: an efficient general purpose program for assigning sequence reads to genomic features. *Bioinformatics*, *30*(7), 923-930. https://doi.org/10.1093/bioinformatics/btt656

Limonta, J., Pedraza, A., Rodriguez, A., Freyre, F. M., Barral, A. M., Castro, F. O., Lleonart, R., Gracia, C. A., Gavilondo, J. V., & Delafuente, J. (1995). Production of Active Anti-Cd6 Mouse-Human Chimeric Antibodies in the Milk of Transgenic Mice. *Immunotechnology*, *1*(2), 107-113. https://doi.org/Doi 10.1016/1380-2933(95)00010-0

Lin, S., Staahl, B., Alla, R. K., & Doudna, J. A. (2014). Enhanced homology-directed human genome engineering by controlled timing of CRISPR/Cas9 delivery. *Elife*, *3*. https://doi.org/ARTN e04766
10.7554/eLife.04766

Ling, X. Y., Xie, B. T., Gao, X. Q., Chang, L. Y., Zheng, W., Chen, H. Q., Huang, Y. J., Tan, L. Z., Li, M., & Liu, T. (2020). Improving the efficiency of precise genome editing with site-specific Cas9-oligonucleotide conjugates. *Science Advances*, *6*(15). https://doi.org/ARTN eaaz0051
10.1126/sciadv.aaz0051

Liu, M. J., Rehman, S., Tang, X. D., Gu, K., Fan, Q. L., Chen, D. K., & Ma, W. T. (2019). Methodologies for Improving HDR Efficiency. *Frontiers in Genetics*, *9*. https://doi.org/ARTN 691
10.3389/fgene.2018.00691

Lou, X., Fang, P., Li, S., Hu, R. Y., Kuerner, K. M., Steinbeisser, H., & Ding, X. (2006). Xenopus Tbx6 mediates posterior patterning via activation of Wnt and FGF signalling. *Cell Res*, *16*(9), 771-779. https://doi.org/10.1038/sj.cr.7310093

Love, M. I., Huber, W., & Anders, S. (2014). Moderated estimation of fold change and dispersion for RNA-seq data with DESeq2. *Genome Biology*, *15*(12). https://doi.org/ARTN 550
10.1186/s13059-014-0550-8

Ma, M., Zhuang, F., Hu, X., Wang, B., Wen, X. Z., Ji, J. F., & Xi, J. J. (2017). Efficient generation of mice carrying homozygous double-floxp alleles using the Cas9-Avidin/Biotin-donor DNA system. *Cell Res*, *27*(4), 578-581. https://doi.org/10.1038/cr.2017.29

Machado, L., de Lima, J. E., Fabre, O., Proux, C., Legendre, R., Szegedi, A., Varet, H., Ingerslev, L. R., Barres, R., Relaix, F., & Mourikis, P. (2017). In Situ Fixation Redefines Quiescence and Early Activation of Skeletal Muscle Stem Cells. *Cell Reports*, *21*(7), 1982-1993. https://doi.org/10.1016/j.celrep.2017.10.080

Machado, L., Geara, P., Camps, J., Dos Santos, M., Teixeira-Clerc, F., Van Herck, J., Varet, H., Legendre, R., Pawlotsky, J. M., Sampaolesi, M., Voet, T., Maire, P., Relaix, F., & Mourikis, P. (2021). Tissue damage induces a conserved stress response that initiates quiescent muscle stem cell activation. *Cell Stem Cell*, *28*(6), 1125-+. https://doi.org/10.1016/j.stem.2021.01.017

Maddalo, D., Manchado, E., Concepcion, C. P., Bonetti, C., Vidigal, J. A., Han, Y. C., Ogrodowski, P., Crippa, A., Rekhtman, N., de Stanchina, E., Lowe, S. W., & Ventura, A. (2014). In vivo engineering of oncogenic chromosomal rearrangements with the CRISPR/Cas9 system. *Nature*, *516*(7531), 423-427. https://doi.org/10.1038/nature13902

Mamchaoui, K., Trollet, C., Bigot, A., Negroni, E., Chaouch, S., Wolff, A., Kandalla, P. K., Marie, S., Di Santo, J., St Guily, J. L., Muntoni, F., Kim, J., Philippi, S., Spuler, S., Levy, N., Blumen, S. C., Voit, T., Wright, W. E., Aamiri, A., . . . Mouly, V. (2011). Immortalized pathological human myoblasts: towards a universal tool for the study of neuromuscular disorders. *Skeletal Muscle*, *1*. https://doi.org/Artn 34
10.1186/2044-5040-1-34

Mankoo, B. S., Skuntz, S., Harrigan, I., Grigorieva, E., Candia, A., Wright, C. V. E., Arnheiter, H., & Pachnis, V. (2003). The concerted action of Meox homeobox genes is required upstream of genetic pathways essential for the formation, patterning and differentiation of somites. *Development*, *130*(19), 4655-4664. https://doi.org/10.1242/dev.00687

Mansour, S. L., Thomas, K. R., & Capecchi, M. R. (1988). Disruption of the proto-oncogene int-2 in mouse embryo-derived stem cells: a general strategy for targeting mutations to non-selectable genes. *Nature*, *336*(6197), 348-352. https://doi.org/10.1038/336348a0

Maruyama, T., Dougan, S. K., Truttmann, M. C., Bilate, A. M., Ingram, J. R., & Ploegh, H. L. (2015). Increasing the efficiency of precise genome editing with CRISPR-Cas9 by inhibition of nonhomologous end joining. *Nat Biotechnol*, *33*(5), 538-542. https://doi.org/10.1038/nbt.3190

Mauro, A. (1961). Satellite Cell of Skeletal Muscle Fibers. *Journal of Biophysical and Biochemical Cytology*, *9*(2), 493-&. https://doi.org/DOI 10.1083/jcb.9.2.493

Meinke, G., Bohm, A., Hauber, J., Pisabarro, M. T., & Buchholz, F. (2016). Cre Recombinase and Other Tyrosine Recombinases. *Chem Rev*, *116*(20), 12785-12820. https://doi.org/10.1021/acs.chemrev.6b00077

Merz, K. E., & Thurmond, D. C. (2020). Role of Skeletal Muscle in Insulin Resistance and Glucose Uptake. *Compr Physiol*, *10*(3), 785-809. https://doi.org/10.1002/cphy.c190029

Metzger, D., & Feil, R. (1999). Engineering the mouse genome by site-specific recombination. *Curr Opin Biotechnol*, *10*(5), 470-476. https://doi.org/10.1016/s0958-1669(99)00012-9

Millay, D. P., O'Rourke, J. R., Sutherland, L. B., Bezprozvannaya, S., Shelton, J. M., Bassel-Duby, R., & Olson, E. N. (2013). Myomaker is a membrane activator of myoblast fusion and muscle formation. *Nature*, *499*(7458), 301-+. https://doi.org/10.1038/nature12343

Millay, D. P., Sutherland, L. B., Bassel-Duby, R., & Olson, E. N. (2014). Myomaker is essential for muscle regeneration. *Genes & Development*, *28*(15), 1641-1646. https://doi.org/10.1101/gad.247205.114

Miura, H., Gurumurthy, C. B., Sato, T., Sato, M., & Ohtsuka, M. (2015). CRISPR/Cas9-based generation of knockdown mice by intronic insertion of artificial microRNA using longer single-stranded DNA. *Sci Rep*, *5*, 12799. https://doi.org/10.1038/srep12799

Miura, H., Quadros, R. M., Gurumurthy, C. B., & Ohtsuka, M. (2018). Easi-CRISPR for creating knock-in and conditional knockout mouse models using long ssDNA donors. *Nature Protocols*, *13*(1), 195-215. https://doi.org/10.1038/nprot.2017.153

Miyasaka, Y., Uno, Y., Yoshimi, K., Kunihiro, Y., Yoshimura, T., Tanaka, T., Ishikubo, H., Hiraoka, Y., Takemoto, N., Tanaka, T., Ooguchi, Y., Skehel, P., Aida, T., Takeda, J., & Mashimo, T. (2018). CLICK: one-step generation of conditional knockout mice. *Bmc Genomics*, *19*. https://doi.org/ARTN 318
10.1186/s12864-018-4713-y

Modzelewski, A. J., Chen, S., Willis, B. J., Lloyd, K. C. K., Wood, J. A., & He, L. (2018). Efficient mouse genome engineering by CRISPR-EZ technology. *Nature Protocols*, *13*(6), 1253-1274. https://doi.org/10.1038/nprot.2018.012

Montarras, D., Morgan, J., Collins, C., Relaix, F., Zaffran, S., Cumano, A., Partridge, T., & Buckingham, M. (2005). Direct isolation of satellite cells for skeletal muscle regeneration. *Science*, *309*(5743), 2064-2067. https://doi.org/10.1126/science.1114758

Monvoisin, A., Alva, J. A., Hofmann, J. J., Zovein, A. C., Lane, T. F., & Iruela-Arispe, M. L. (2006). VE-cadherin-CreERT2 transgenic mouse: a model for inducible recombination in the endothelium. *Dev Dyn*, *235*(12), 3413-3422. https://doi.org/10.1002/dvdy.20982

Nagy, A. (2000). Cre recombinase: the universal reagent for genome tailoring. *Genesis*, *26*(2), 99-109. https://www.ncbi.nlm.nih.gov/pubmed/10686599

Nakagawa, Y., Oikawa, F., Mizuno, S., Ohno, H., Yagishita, Y., Satoh, A., Osaki, Y., Takei, K., Kikuchi, T., Han, S. I., Matsuzaka, T., Iwasaki, H., Kobayashi, K., Yatoh, S., Yahagi, N., Isaka, M., Suzuki, H., Sone, H., Takahashi, S., . . . Shimano, H. (2016). Hyperlipidemia and hepatitis in liver-specific CREB3L3 knockout mice generated using a one-step CRISPR/Cas9 system. *Sci Rep*, *6*, 27857. https://doi.org/10.1038/srep27857

Ohtsuka, M., Sato, M., Miura, H., Takabayashi, S., Matsuyama, M., Koyano, T., Arifin, N., Nakamura, S., Wada, K., & Gurumurthy, C. B. (2018). i-GONAD: a robust method for in situ germline genome engineering using CRISPR nucleases. *Genome Biol*, *19*(1), 25. https://doi.org/10.1186/s13059-018-1400-x

Olguin, H. C., & Pisconti, A. (2012). Marking the tempo for myogenesis: Pax7 and the regulation of muscle stem cell fate decisions. *Journal of Cellular and Molecular Medicine*, *16*(5), 1013-1025. https://doi.org/10.1111/j.1582-4934.2011.01348.x

Otto, A., Schmidt, C., & Patel, K. (2006). Pax3 and Pax7 expression and regulation in the avian embryo. *Anat Embryol (Berl)*, *211*(4), 293-310. https://doi.org/10.1007/s00429-006-0083-3

Pan, X., Wan, H., Chia, W., Tong, Y., & Gong, Z. (2005). Demonstration of site-directed recombination in transgenic zebrafish using the Cre/loxP system. *Transgenic Res*, *14*(2), 217-223. https://doi.org/10.1007/s11248-004-5790-z

Pedrazaalva, G., Zingg, J. M., & Jost, J. P. (1994). Ap-1 Binds to a Putative Camp Response Element of the Myod1 Promoter and Negatively Modulates Myod1 Expression in Dividing Myoblasts. *Journal of Biological Chemistry*, *269*(9), 6978-6985. <Go to ISI>://WOS:A1994MZ50300109

Platt, R. J., Chen, S. D., Zhou, Y., Yim, M. J., Swiech, L., Kempton, H. R., Dahlman, J. E., Parnas, O., Eisenhaure, T. M., Jovanovic, M., Graham, D. B., Jhunjhunwala, S., Heidenreich, M., Xavier, R. J., Langer, R., Anderson, D. G., Hacohen, N., Regev, A., Feng, G. P., . . . Zhang, F. (2014). CRISPR-Cas9 Knockin Mice for Genome Editing and Cancer Modeling. *Cell*, *159*(2), 440-455. https://doi.org/10.1016/j.cell.2014.09.014

Pownall, M. E., Gustafsson, M. K., & Emerson, C. P. (2002). Myogenic regulatory factors and the specification of muscle progenitors in vertebrate embryos. *Annual Review of Cell and Developmental Biology*, *18*, 747-783. https://doi.org/10.1146/annurev.cellbio.18.012502.105758

Pu, Q., Patel, K., & Huang, R. (2015). The lateral plate mesoderm: a novel source of skeletal muscle. *Results Probl Cell Differ*, *56*, 143-163. https://doi.org/10.1007/978-3-662-44608-9_7

Qi, L. S., Larson, M. H., Gilbert, L. A., Doudna, J. A., Weissman, J. S., Arkin, A. P., & Lim, W. A. (2021). Repurposing CRISPR as an RNA-guided platform for sequence-specific control of gene expression (vol 152, pg 1173, 2013). *Cell*, *184*(3), 844-844. https://doi.org/10.1016/j.cell.2021.01.019

Qin, W., Kutny, P. M., Maser, R. S., Dion, S. L., Lamont, J. D., Zhang, Y., Perry, G. A., & Wang, H. (2016). Generating Mouse Models Using CRISPR-Cas9-Mediated Genome Editing. *Curr Protoc Mouse Biol*, *6*(1), 39-66. https://doi.org/10.1002/9780470942390.mo150178

Quadros, R. M., Miura, H., Harms, D. W., Akatsuka, H., Sato, T., Aida, T., Redder, R., Richardson, G. P., Inagaki, Y., Sakai, D., Buckley, S. M., Seshacharyulu, P., Batra, S. K., Behlke, M. A., Zeiner, S. A., Jacobi, A. M., Izu, Y., Thoreson, W. B., Urness, L. D., . . . Gurumurthy, C. B. (2017). Easi-CRISPR: a robust method for one-step generation of mice carrying conditional and insertion alleles using long ssDNA donors and CRISPR ribonucleoproteins. *Genome Biology*, *18*. https://doi.org/ARTN 92
10.1186/s13059-017-1220-4

Quinn, M. E., Goh, Q., Kurosaka, M., Gamage, D. G., Petrany, M. J., Prasad, V., & Millay, D. P. (2017). Myomerger induces fusion of non-fusogenic cells and is required for skeletal muscle development. *Nature Communications*, *8*. https://doi.org/ARTN 15665
10.1038/ncomms15665

Rasys, A. M., Park, S., Ball, R. E., Alcala, A. J., Lauderdale, J. D., & Menke, D. B. (2019). CRISPR-Cas9 Gene Editing in Lizards through Microinjection of Unfertilized Oocytes. *Cell Reports*, *28*(9), 2288-+. https://doi.org/10.1016/j.celrep.2019.07.089

Richardson, C. D., Ray, G. J., DeWitt, M. A., Curie, G. L., & Corn, J. E. (2016). Enhancing homology-directed genome editing by catalytically active and inactive CRISPR-Cas9 using asymmetric donor DNA. *Nat Biotechnol*, *34*(3), 339-344. https://doi.org/10.1038/nbt.3481

Riele, H. T., Maandag, E. R., & Berns, A. (1992). Highly Efficient Gene Targeting in Embryonic Stem-Cells through Homologous Recombination with Isogenic DNA Constructs. *Proceedings of the National Academy of Sciences of the United States of America*, *89*(11), 5128-5132. https://doi.org/DOI 10.1073/pnas.89.11.5128

Rocheteau, P., Gayraud-Morel, B., Siegl-Cachedenier, I., Blasco, M. A., & Tajbakhsh, S. (2012). A Subpopulation of Adult Skeletal Muscle Stem Cells Retains All Template DNA Strands after Cell Division. *Cell*, *148*(1-2), 112-125. https://doi.org/10.1016/j.cell.2011.11.049

Rodgers, J. T., King, K. Y., Brett, J. O., Cromie, M. J., Charville, G. W., Maguire, K. K., Brunson, C., Mastey, N., Liu, L., Tsai, C. R., Goodell, M. A., & Rando, T. A. (2014). mTORC1 controls the adaptive transition of quiescent stem cells from G0 to G(Alert). *Nature*, *510*(7505), 393-396. https://doi.org/10.1038/nature13255

Rodriguez-Outeirino, L., Hernandez-Torres, F., Ramirez-de Acuna, F., Matias-Valiente, L., Sanchez-Fernandez, C., Franco, D., & Aranega, A. E. (2021). Muscle Satellite Cell Heterogeneity: Does Embryonic Origin Matter? *Frontiers in Cell and Developmental Biology*, *9*. https://doi.org/ARTN 750534
10.3389/fcell.2021.750534
Rudnicki, M. A., Schnegelsberg, P. N. J., Stead, R. H., Braun, T., Arnold, H. H., & Jaenisch, R. (1993). Myod or Myf-5 Is Required for the Formation of Skeletal-Muscle. *Cell*, *75*(7), 1351-1359. https://doi.org/Doi 10.1016/0092-8674(93)90621-V
Sacco, A., Doyonnas, R., Kraft, P., Vitorovic, S., & Blau, H. M. (2008). Self-renewal and expansion of single transplanted muscle stem cells. *Nature*, *456*(7221), 502-506. https://doi.org/10.1038/nature07384
Salic, A., & Mitchison, T. J. (2008). A chemical method for fast and sensitive detection of DNA synthesis in vivo. *Proceedings of the National Academy of Sciences of the United States of America*, *105*(7), 2415-2420. https://doi.org/10.1073/pnas.0712168105
Sambasivan, R., Yao, R., Kissenpfennig, A., Van Wittenberghe, L., Paldi, A., Gayraud-Morel, B., Guenou, H., Malissen, B., Tajbakhsh, S., & Galy, A. (2011). Pax7-expressing satellite cells are indispensable for adult skeletal muscle regeneration (vol 138, pg 3647, 2011). *Development*, *138*(19), 4333-4333. https://doi.org/10.1242/dev.073601
Sato, M., Miyagasako, R., Takabayashi, S., Ohtsuka, M., Hatada, I., & Horii, T. (2020). Sequential i-GONAD: An Improved In Vivo Technique for CRISPR/Cas9-Based Genetic Manipulations in Mice. *Cells*, *9*(3). https://doi.org/ARTN 546
10.3390/cells9030546
Sauer, B. (1998). Inducible gene targeting in mice using the Cre/lox system. *Methods*, *14*(4), 381-392. https://doi.org/10.1006/meth.1998.0593
Sauer, B., & Henderson, N. (1988). Site-specific DNA recombination in mammalian cells by the Cre recombinase of bacteriophage P1. *Proc Natl Acad Sci U S A*, *85*(14), 5166-5170. https://doi.org/10.1073/pnas.85.14.5166
Schaum, N., Karkanias, J., Neff, N. F., May, A. P., Quake, S. R., Wyss-Coray, T., Darmanis, S., Batson, J., Botvinnik, O., Chen, M. B., Chen, S., Green, F., Jones, R. C., Maynard, A., Penland, L., Pisco, A. O., Sit, R. V., Stanley, G. M., Webber, J. T., . . . Consortium, T. M. (2018). Single-cell transcriptomics of 20 mouse organs creates a Tabula Muris. *Nature*, *562*(7727), 367-+. https://doi.org/10.1038/s41586-018-0590-4
Schmidt, M., Schuler, S. C., Huttner, S. S., von Eyss, B., & von Maltzahn, J. (2019). Adult stem cells at work: regenerating skeletal muscle. *Cell Mol Life Sci*, *76*(13), 2559-2570. https://doi.org/10.1007/s00018-019-03093-6
Schonig, K., Schwenk, F., Rajewsky, K., & Bujard, H. (2002). Stringent doxycycline dependent control of CRE recombinase in vivo. *Nucleic Acids Research*, *30*(23). https://doi.org/ARTN e134
DOI 10.1093/nar/gnf134
Schultz, E., Jaryszak, D. L., & Valliere, C. R. (1985). Response of Satellite Cells to Focal Skeletal-Muscle Injury. *Muscle & Nerve*, *8*(3), 217-222. https://doi.org/DOI 10.1002/mus.880080307
Seale, P., Sabourin, L. A., Girgis-Gabardo, A., Mansouri, A., Gruss, P., & Rudnicki, M. A. (2000). Pax7 is required for the specification of myogenic satellite cells. *Cell*, *102*(6), 777-786. https://doi.org/Doi 10.1016/S0092-8674(00)00066-0

Sentmanat, M. F., White, J. M., Kouranova, E., & Cui, X. (2022). Highly reliable creation of floxed alleles by electroporating single-cell embryos. *BMC Biol*, *20*(1), 31. https://doi.org/10.1186/s12915-021-01223-w

Shang, M., Cappellesso, F., Amorim, R., Serneels, J., Virga, F., Eelen, G., Carobbio, S., Rincon, M. Y., Maechler, P., De Bock, K., Ho, P. C., Sandri, M., Ghesquiere, B., Carmeliet, P., Di Matteo, M., Berardi, E., & Mazzone, M. (2020). Macrophage-derived glutamine boosts satellite cells and muscle regeneration. *Nature*, *587*(7835), 626-631. https://doi.org/10.1038/s41586-020-2857-9

Shang, R., Zhang, H., & Bi, P. (2021). Generation of mouse conditional knockout alleles in one step using the i-GONAD method. *Genome Res*, *31*(1), 121-130. https://doi.org/10.1101/gr.265439.120

Shaulian, E., & Karin, M. (2002). AP-1 as a regulator of cell life and death. *Nature Cell Biology*, *4*(5), E131-E136. https://doi.org/10.1038/ncb0502-e131

Sherwood, R. I., Christensen, J. L., Conboy, I. M., Conboy, M. J., Rando, T. A., Weissman, I. L., & Wagers, A. J. (2004). Isolation of adult mouse myogenic progenitors: Functional heterogeneity of cells within and engrafting skeletal muscle. *Cell*, *119*(4), 543-554. https://doi.org/DOI 10.1016/j.cell.2004.10.021

Siegal, M. L., & Hartl, D. L. (1996). Transgene Coplacement and high efficiency site-specific recombination with the Cre/loxP system in Drosophila. *Genetics*, *144*(2), 715-726. https://doi.org/10.1093/genetics/144.2.715

Skarnes, W. C. (2015). Is mouse embryonic stem cell technology obsolete? *Genome Biology*, *16*. https://doi.org/ARTN 109
10.1186/s13059-015-0673-6

Skarnes, W. C., Rosen, B., West, A. P., Koutsourakis, M., Bushell, W., Iyer, V., Mujica, A. O., Thomas, M., Harrow, J., Cox, T., Jackson, D., Severin, J., Biggs, P., Fu, J., Nefedov, M., de Jong, P. J., Stewart, A. F., & Bradley, A. (2011). A conditional knockout resource for the genome-wide study of mouse gene function. *Nature*, *474*(7351), 337-342. https://doi.org/10.1038/nature10163

Snow, M. H. (1977). Myogenic cell formation in regenerating rat skeletal muscle injured by mincing. II. An autoradiographic study. *Anat Rec*, *188*(2), 201-217. https://doi.org/10.1002/ar.1091880206

Snow, M. H. (1981). Satellite Cell Distribution within the Soleus Muscle of the Adult-Mouse. *Anatomical Record*, *201*(3), 463-469. https://doi.org/DOI 10.1002/ar.1092010303

Square, T., Romasek, M., Jandzik, D., Cattell, M. V., Klymkowsky, M., & Medeiros, D. M. (2015). CRISPR/Cas9-mediated mutagenesis in the sea lamprey Petromyzon marinus: a powerful tool for understanding ancestral gene functions in vertebrates. *Development*, *142*(23), 4180-4187. https://doi.org/10.1242/dev.125609

Sternberg, N., Austin, S., Hamilton, D., & Yarmolinsky, M. (1978). Analysis of bacteriophage P1 immunity by using lambda-P1 recombinants constructed in vitro. *Proc Natl Acad Sci U S A*, *75*(11), 5594-5598. https://doi.org/10.1073/pnas.75.11.5594

Sternberg, N., Hamilton, D., & Hoess, R. (1981). Bacteriophage-P1 Site-Specific Recombination .2. Recombination between Loxp and the Bacterial Chromosome. *Journal of Molecular Biology*, *150*(4), 487-507. https://doi.org/Doi 10.1016/0022-2836(81)90376-4

Stockdale, F. E. (1992). Myogenic cell lineages. *Dev Biol*, *154*(2), 284-298. https://doi.org/10.1016/0012-1606(92)90068-r

Summan, M., Warren, G. L., Mercer, R. R., Chapman, R., Hulderman, T., Van Rooijen, N., & Simeonova, P. P. (2006). Macrophages and skeletal muscle regeneration: a clodronate-containing liposome depletion study. *Am J Physiol Regul Integr Comp Physiol*, *290*(6), R1488-1495. https://doi.org/10.1152/ajpregu.00465.2005

Sun, D. Q., Li, H., & Zolkiewska, A. (2008). The role of Delta-like 1 shedding in muscle cell self-renewal and differentiation. *Journal of Cell Science*, *121*(22), 3815-3823. https://doi.org/10.1242/jcs.035493

Takada, S., Stark, K. L., Shea, M. J., Vassileva, G., McMahon, J. A., & McMahon, A. P. (1994). Wnt-3a regulates somite and tailbud formation in the mouse embryo. *Genes Dev*, *8*(2), 174-189. https://doi.org/10.1101/gad.8.2.174

Takahashi, G., Gurumurthy, C. B., Wada, K., Miura, H., Sato, M., & Ohtsuka, M. (2015a). GONAD: Genome-editing via Oviductal Nucleic Acids Delivery system: a novel microinjection independent genome engineering method in mice. *Sci Rep*, *5*, 11406. https://doi.org/10.1038/srep11406

Takahashi, G., Gurumurthy, C. B., Wada, K., Miura, H., Sato, M., & Ohtsuka, M. (2015b). GONAD: Genome-editing via Oviductal Nucleic Acids Delivery system: a novel microinjection independent genome engineering method in mice. *Scientific Reports*, *5*. https://doi.org/ARTN 11406
10.1038/srep11406

Tani, S., Chung, U. I., Ohba, S., & Hojo, H. (2020). Understanding paraxial mesoderm development and sclerotome specification for skeletal repair. *Exp Mol Med*, *52*(8), 1166-1177. https://doi.org/10.1038/s12276-020-0482-1

Teixeira, M., Py, B. F., Bosc, C., Laubreton, D., Moutin, M. J., Marvel, J., Flamant, F., & Markossian, S. (2018). Electroporation of mice zygotes with dual guide RNA/Cas9 complexes for simple and efficient cloning-free genome editing (vol 8, 2018). *Scientific Reports*, *8*. https://doi.org/ARTN 4679
10.1038/s41598-018-22724-9

Thomas, K. R., & Capecchi, M. R. (1987a). Site-directed mutagenesis by gene targeting in mouse embryo-derived stem cells. *Cell*, *51*(3), 503-512. https://doi.org/10.1016/0092-8674(87)90646-5

Thomas, K. R., & Capecchi, M. R. (1987b). Site-Directed Mutagenesis by Gene Targeting in Mouse Embryo-Derived Stem-Cells. *Cell*, *51*(3), 503-512. https://doi.org/Doi 10.1016/0092-8674(87)90646-5

Tirosh-Finkel, L., Elhanany, H., Rinon, A., & Tzahor, E. (2006). Mesoderm progenitor cells of common origin contribute to the head musculature and the cardiac outflow tract. *Development*, *133*(10), 1943-1953. https://doi.org/10.1242/dev.02365

Turner, D. A., Rue, P., Mackenzie, J. P., Davies, E., & Martinez Arias, A. (2014). Brachyury cooperates with Wnt/beta-catenin signalling to elicit primitive-streak-like behaviour in differentiating mouse embryonic stem cells. *BMC Biol*, *12*, 63. https://doi.org/10.1186/s12915-014-0063-7

van den Brink, S. C., Sage, F., Vertesy, A., Spanjaard, B., Peterson-Maduro, J., Baron, C. S., Robin, C., & van Oudenaarden, A. (2017). Single-cell sequencing reveals dissociation-induced gene expression in tissue subpopulations. *Nature Methods*, *14*(10), 935-936. https://doi.org/10.1038/nmeth.4437

van Velthoven, C. T. J., de Morree, A., Egner, I. M., Brett, J. O., & Rando, T. A. (2017). Transcriptional Profiling of Quiescent Muscle Stem Cells In Vivo. *Cell Reports*, *21*(7), 1994-2004. https://doi.org/10.1016/j.celrep.2017.10.037

von Maltzahn, J., Bentzinger, C. F., & Rudnicki, M. A. (2012). Wnt7a-Fzd7 signalling directly activates the Akt/mTOR anabolic growth pathway in skeletal muscle. *Nature Cell Biology*, *14*(2), 186-191. https://doi.org/10.1038/ncb2404

Wang, H. F., La Russa, M., & Qi, L. S. (2016). CRISPR/Cas9 in Genome Editing and Beyond. *Annual Review of Biochemistry, Vol 85*, *85*, 227-264. https://doi.org/10.1146/annurev-biochem-060815-014607

Wang, H. Y., Yang, H., Shivalila, C. S., Dawlaty, M. M., Cheng, A. W., Zhang, F., & Jaenisch, R. (2013). One-Step Generation of Mice Carrying Mutations in Multiple Genes by CRISPR/Cas-Mediated Genome Engineering. *Cell*, *153*(4), 910-918. https://doi.org/10.1016/j.cell.2013.04.025

Wang, W. B., Kutny, P. M., Byers, S. L., Longstaff, C. J., DaCosta, M. J., Pang, C. H., Zhang, Y. F., Taft, R. A., Buaas, F. W., & Wang, H. Y. (2016). Delivery of Cas9 Protein into Mouse Zygotes through a Series of Electroporation Dramatically Increases the Efficiency of Model Creation. *Journal of Genetics and Genomics*, *43*(5), 319-327. https://doi.org/10.1016/j.jgg.2016.02.004

Wei, X., Xiang, Y., Peters, D. T., Marius, C., Sun, T., Shan, R., Ou, J., Lin, X., Yue, F., Li, W., Southerland, K. W., & Diao, Y. (2022). HiCAR is a robust and sensitive method to analyze open-chromatin-associated genome organization. *Mol Cell*, *82*(6), 1225-1238 e1226. https://doi.org/10.1016/j.molcel.2022.01.023

Wu, X. B., Scott, D. A., Kriz, A. J., Chiu, A. C., Hsu, P. D., Dadon, D. B., Cheng, A. W., Trevino, A. E., Konermann, S., Chen, S. D., Jaenisch, R., Zhang, F., & Sharp, P. A. (2014). Genome-wide binding of the CRISPR endonuclease Cas9 in mammalian cells. *Nature Biotechnology*, *32*(7), 670-+. https://doi.org/10.1038/nbt.2889

Yablonkareuveni, Z., & Rivera, A. J. (1994). Temporal Expression of Regulatory and Structural Muscle Proteins during Myogenesis of Satellite Cells on Isolated Adult-Rat Fibers. *Developmental Biology*, *164*(2), 588-603. https://doi.org/DOI 10.1006/dbio.1994.1226

Yamaguchi, T. P., Harpal, K., Henkemeyer, M., & Rossant, J. (1994). fgfr-1 is required for embryonic growth and mesodermal patterning during mouse gastrulation. *Genes Dev*, *8*(24), 3032-3044. https://doi.org/10.1101/gad.8.24.3032

Yang, H., Wang, H., Shivalila, C. S., Cheng, A. W., Shi, L., & Jaenisch, R. (2013). One-step generation of mice carrying reporter and conditional alleles by CRISPR/Cas-mediated genome engineering. *Cell*, *154*(6), 1370-1379. https://doi.org/10.1016/j.cell.2013.08.022

Yartseva, V., Goldstein, L. D., Rodman, J., Kates, L., Chen, M. Z., Chen, Y. J. J., Foreman, O., Siebel, C. W., Modrusan, Z., Peterson, A. S., & Jovicic, A. (2020). Heterogeneity of Satellite Cells Implicates DELTA1/NOTCH2 Signaling in Self-Renewal. *Cell Reports*, *30*(5), 1491-+. https://doi.org/10.1016/j.celrep.2019.12.100

Yasuhiko, Y., Haraguchi, S., Kitajima, S., Takahashi, Y., Kanno, J., & Saga, Y. (2006). Tbx6-mediated Notch signaling controls somite-specific Mesp2 expression. *Proc Natl Acad Sci U S A*, *103*(10), 3651-3656. https://doi.org/10.1073/pnas.0508238103

Yin, H., Price, F., & Rudnicki, M. A. (2013). Satellite cells and the muscle stem cell niche. *Physiol Rev*, *93*(1), 23-67. https://doi.org/10.1152/physrev.00043.2011

Yoshimi, K., Kunihiro, Y., Kaneko, T., Nagahora, H., Voigt, B., & Mashimo, T. (2016). ssODN-mediated knock-in with CRISPR-Cas for large genomic regions in zygotes. *Nat Commun*, *7*, 10431. https://doi.org/10.1038/ncomms10431

Yuan, T. T., Zhong, Y., Wang, Y. G., Zhang, T., Lu, R., Zhou, M. Y., Lu, Y. Y., Yan, K. N., Chen, Y. J., Hu, Z. H., Liang, J. Y., Fan, J. L., & Cheng, Y. (2019). Generation of hyperlipidemic rabbit models using multiple sgRNAs targeted CRISPR/Cas9 gene editing system. *Lipids in Health and Disease*, *18*. https://doi.org/ARTN 69
10.1186/s12944-019-1013-8

Zammit, P. S., Golding, J. P., Nagata, Y., Hudon, V., Partridge, T. A., & Beauchamp, J. R. (2004). Muscle satellite cells adopt divergent fates: a mechanism for self-renewal? *Journal of Cell Biology*, *166*(3), 347-357. https://doi.org/10.1083/jcb.200312007

Zhang, H. F., Wen, J. F., Bigot, A. N., Chen, J. C., Shang, R. J., Mouly, V., & Bi, P. P. (2020). Human myotube formation is determined by MyoD-Myomixer/Myomaker axis. *Science Advances*, *6*(51). https://doi.org/ARTN eabc4062
10.1126/sciadv.abc4062

Zhang, Q., Vashisht, A. A., O'Rourke, J., Corbel, S. Y., Moran, R., Romero, A., Miraglia, L., Zhang, J., Durrant, E., Schmedt, C., Sampath, S. C., & Sampath, S. C. (2017). The microprotein Minion controls cell fusion and muscle formation. *Nature Communications*, *8*. https://doi.org/ARTN 15664
10.1038/ncomms15664

Zhou, Y. Y., Zhou, B., Pache, L., Chang, M., Khodabakhshi, A. H., Tanaseichuk, O., Benner, C., & Chanda, S. K. (2019). Metascape provides a biologist-oriented resource for the analysis of systems-level datasets. *Nature Communications*, *10*. https://doi.org/ARTN 1523
10.1038/s41467-019-09234-6

Zhu, X. X., Xu, Y. J., Yu, S. S., Lu, L., Ding, M. Q., Cheng, J., Song, G. X., Gao, X., Yao, L. M., Fan, D. D., Meng, S., Zhang, X. W., Hu, S. D., & Tian, Y. (2014). An Efficient Genotyping Method for Genome-modified Animals and Human Cells Generated with CRISPR/Cas9 System. *Scientific Reports*, *4*. https://doi.org/ARTN 6420
10.1038/srep06420

Zijlstra, M., Li, E., Sajjadi, F., Subramani, S., & Jaenisch, R. (1989). Germ-line transmission of a disrupted beta 2-microglobulin gene produced by homologous recombination in embryonic stem cells. *Nature*, *342*(6248), 435-438. https://doi.org/10.1038/342435a0

Zu, Y., Zhang, X. S., Ren, J. F., Dong, X. H., Zhu, Z., Jia, L., Zhang, Q. H., & Li, W. M. (2016). Biallelic editing of a lamprey genome using the CRISPR/Cas9 system. *Scientific Reports*, *6*. https://doi.org/ARTN 23496
10.1038/srep23496